January 2016

Design of Mixed-Solvent Extraction and Size-Exclusion Simulated Moving Bed Chromatography to Recover Valuable Compounds from Electronic Waste

George S. Weeden Jr.
Purdue University

Graduate School Form
30 Updated 12/26/2015

PURDUE UNIVERSITY
GRADUATE SCHOOL
Thesis/Dissertation Acceptance

This is to certify that the thesis/dissertation prepared

By George S. Weeden Jr.

Entitled

Design of Mixed-Solvent Extraction and Size-Exclusion Simulated Moving Bed Chromatography to Recover Valuable Compounds from Electronic Waste

For the degree of Doctor of Philosophy

Is approved by the final examining committee:

Nien-Hwa Linda Wang
Chair

Osman Basaran

Chongli Yuan

Abigail Engelberth

To the best of my knowledge and as understood by the student in the Thesis/Dissertation Agreement, Publication Delay, and Certification Disclaimer (Graduate School Form 32), this thesis/dissertation adheres to the provisions of Purdue University's "Policy of Integrity in Research" and the use of copyright material.

Approved by Major Professor(s): Nien-Hwa Linda Wang

Approved by: John A. Morgan 4/28/2016
Head of the Departmental Graduate Program Date

DESIGN OF MIXED-SOLVENT EXTRACTION AND SIZE-EXCLUSION SIMULATED MOVING BED CHROMATOGRAPHY TO RECOVER VALUABLE COMPOUNDS FROM ELECTRONIC WASTE

A Dissertation

Submitted to the Faculty

of

Purdue University

by

George S. Weeden Jr.

In Partial Fulfillment of the

Requirements for the Degree

of

Doctor of Philosophy

May 2016

Purdue University

West Lafayette, Indiana

ACKNOWLEDGEMENTS

I want to first express my gratitude to Professor N.-H. Linda Wang for her support and guidance throughout all these years of research. I might have the longest retention time in her research group of any student because I joined as a Junior in undergrad. I am extremely grateful that I was able to start my research experience with what ended up being an area that I really enjoy. Over a seven-year period, I have learned more than I could ever express. I am very thankful for her patience with me in my first years of graduate school and for her infectious enthusiasm (and also her amazingly delicious group dinners at her house).

I would also like to thank Professor Osman Basaran (Chemical Engineering), Professor Chongli Yuan (Chemical Engineering), and Professor Abigail Engelberth (Agricultural & Biological Engineering) for serving on my PhD committee and for their valuable comments and suggestions.

I am happy to say that I have greatly enjoyed working in my research group and have to thank previous and current members for all their support throughout the years: Dr. Chim Chin, Dr. Pei-Lun Chung, Dr. Lei Ling, Dr. Hung-Wei Tsui, Dr. Wei Dai, Dr. Nicholas Soepriatna, Hoon Choi, and David Harvey. I would also like to thank Betty Yang from Professor Franses' group for putting up with all of us in our tiny office.

I also have to thank the undergraduate students who helped me perform many of the experiments that make up the core of this dissertation. Mingzhe Chong, Ye Tao, and Gideon R. Liem assisted with extraction experiments and HPLC analyses. Shinae Kim, Matthew Nieves, and Dr. Wei Dai assisted with HPLC analyses and batch column experiments.

I would like to thank SABIC Innovative Plastics (Mt. Vernon, IN) for partially funding my PhD and for the assistance and insights of Dr. Philip Bell, Dr. David Zoller, and Dr. Zheng Liu. I would also like to thank funding sources from Purdue University, including the School of Chemical Engineering and the Hugh and Edna Donnan Dissertation Fellowship. This work was also partially supported by the National Science Foundation (CBET 1403854).

I have really enjoyed my time at Purdue and that is thanks in no small part to all the amazing friends I have made outside my research group. The office I had as a first year graduate student was amazing and I will never forget all the time we spent in there doing homework and just hanging out. Living together after our first year was great and I'll never forget "The Barn" or "The Pile." Thank you Nathan J. "Ninja" Davis, Dan Pohlman, Aditya "Diddy" Baradwaj, John "Jern" Degenstein, Steven Mcleod, Brian "Bgraze" Graeser, and Nathan Nurse.

I would also like to thank my sister, Emily Weeden, for almost always sharing the same taste in movies, TV, and music so we could always talk about entertainment. Obviously none of this would have been possible without my loving parents, George S. Weeden Sr. and JoEllen Weeden. Thank you for always being there for me.

TABLE OF CONTENTS

Page

Page

APPENDICES Page

LIST OF TABLES

Appendix Table Page

LIST OF FIGURES

Figure Page

Figure Page

Figure Page

Appendix Figure

Appendix Figure Page

ABSTRACT

Weeden, George S. Ph.D., Purdue University, May 2016. Design of Mixed-Solvent Extraction and Size-Exclusion Simulated Moving Bed Chromatography to Recover Valuable Compounds from Electronic Waste. Major Professor: N.-H. Linda Wang.

More than one million tons of polycarbonates and over 500,000 tons of flame retardants are consigned to landfills each year in the form of waste electrical and electronic equipment. Electronic waste is the fasting growing waste steam at a rate of 3-5% per year. Two separation processes are developed to efficiently recover these valuable compounds.

The polycarbonates are recovered by sequential, mixed-solvent extraction. The solvent compositions are found using guidelines from Hansen solubility parameters, gradient polymer elution chromatography, and solubility tests. A room-temperature sequential extraction process using acetone and dichloromethane is developed to recover polycarbonates with high yield (>95%) and a similar purity and molecular weight distribution as virgin polycarbonates. The estimated cost of recovery is less than 30% of the cost of producing virgin polycarbonates from petroleum.

One side stream of the extraction process is composed of low molecular weight flame retardants and a polymer, styrene acrylonitrile. Because of the large molecular weight difference, flame retardants can be recovered using a size-exclusion simulated moving bed (SEC-SMB).

While SEC-SMBs are orders of magnitude more efficient than batch chromatography, they are not widely used. One key barrier is the complexity in design and optimization. A four-zone SEC-SMB for a binary separation has seven material properties and 14 design parameters (two yields, five operating parameters, and seven equipment parameters). Previous optimization studies using numerical methods do not guarantee global optima or explicitly express solvent consumption (*D/F*) or sorbent productivity (P_R) as functions of the material properties and design parameters.

The Standing Wave concept is used to develop analytical expressions for *D/F* and P_R as functions of 14 dimensionless groups, which consist of 21 material and design parameters. The resulting Speedy Standing Wave Design (SSWD) solutions are simplified for two limiting cases: diffusion- or dispersion-controlled systems. An example of SEC-SMB for insulin purification is used to illustrate how *D/F* and P_R change with the dimensionless groups. The results show that maximum P_R for both diffusion- and dispersion-controlled systems is mainly determined by yields, equipment parameters, material properties, and two key dimensionless groups: (1) the ratio of step time to diffusion time and (2) the ratio of diffusion time to pressure-limited convection time. A sharp trade off of *D/F* and P_R occurs when the yield is greater than 99%. The column configuration for maximum P_R is analytically related to the diffusivity ratio and the selectivity. Among the material properties, selectivity and particle size have the largest impact on *D/F* and P_R. Particle size and 14 design parameters can be optimized for minimum *D/F*, maximum P_R, or minimum cost.

Using the SSWD, a room-temperature SEC-SMB is developed to recover high-purity (>99%) flame retardants with high yield (>99%). Fourteen decision variables were

optimized to obtain the lowest separation cost. The unit separation cost of the optimized SEC-SMB is less than 10% of the purchase cost of the flame retardants and less than 3% of the unit separation cost of a conventional batch SEC process. Additionally, fast startup methods are developed to reduce SMB start-up time by more than 18 fold.

The polycarbonate extraction and SEC-SMB use 84% less energy, reduce emission by 1-6 tons CO_2 per ton polycarbonates, and could reduce polymer accumulation in landfills and associated environmental hazards.

CHAPTER 1. INTRODUCTION

1.1 Polymer Waste – A Growing Problem

More than 280 million tons of polymers were produced globally in 2012. Less than 50% of the polymers produced were consigned to landfills or recycled [1]. The rest are either in use or scattered over the continents or oceans [2]. Based on the current trends, it was estimated that the planet will hold more than 33 billion tons of polymers by 2050 [1]. In the United States, 39 million tons of plastic solid waste were produced in 2012. Only 7% of the polymers were recycled and 10% were incinerated, while the remaining 83% were stored in landfills [3]. The polymers contain potentially toxic chemicals themselves and they also absorb and concentrate persistent organic pollutants [4]. Degradation of polymers in landfills or in the oceans can release harmful chemicals into the environment, resulting in potentially devastating impact on wildlife and our food supply. These harmful consequences have led some to call for the classification of polymer waste as hazardous waste [1].

To help combat this growing environmental hazard, this work focused on the fastest growing polymer waste stream, electronic waste, which is growing at a rate of 3-5% per year [5–7]. Globally, about 20 to 55 million tons of waste electrical and electronic equipment (WEEE) are generated each year [8,9]. Less than 20% of the wastes are recycled; mostly glass, valuable metals (steel, gold, copper, etc.), and highly toxic metals,

such as cadmium [10,11]. About a third of the waste weight consists of polymeric materials from items such as refrigerators, televisions, computers, monitors, mobile phones, and video game consoles [12,13]. The wastes are an untapped source for recovering valuable polymers and additives, such as polycarbonates (PCs) and organophosphorus flame retardants (FRs), respectively. It is estimated that up to 2.5 million tons of PCs and up to 500,000 tons FRs can potentially be recovered from WEEE each year [6].

1.2 Polycarbonates

Polycarbonates are thermoplastic polymers containing carbonate (-O-(C=O)-O-) groups, which can be easily molded or thermo-formed. They have a high resistance to chemicals, high temperatures, and mechanical impact. They also have high optical quality with good electrical insulating properties. They are widely used in electronic devices, construction materials, data storage (CD's, DVD's, and Blu-Ray Discs), automobiles, airplanes, bullet-resistant windows, corrective lenses, medical devices, and other applications (Figure 1.1). Their bulk cost ranges from $2.50 to $5.00 per kg. They are more expensive than other polymers commonly found in the wastes. Their annual global production is ~3 million tons, and consumes about 24 million barrels of crude oil and 526 trillion BTU's of energy, about the same as the annual electrical energy consumption of New York State [14]. Polycarbonate recycling can help reduce the amount of energy and oil consumed for PC synthesis, the amount of wastes in landfills, and related health or environmental hazards [4,15,16]. Emissions of CO_2 can be reduced by 1 to 6 tons per ton of PCs recycled, compared to the emissions resulting from the production of virgin PCs from crude oil, or from the incineration of polymer waste for fuel [17].

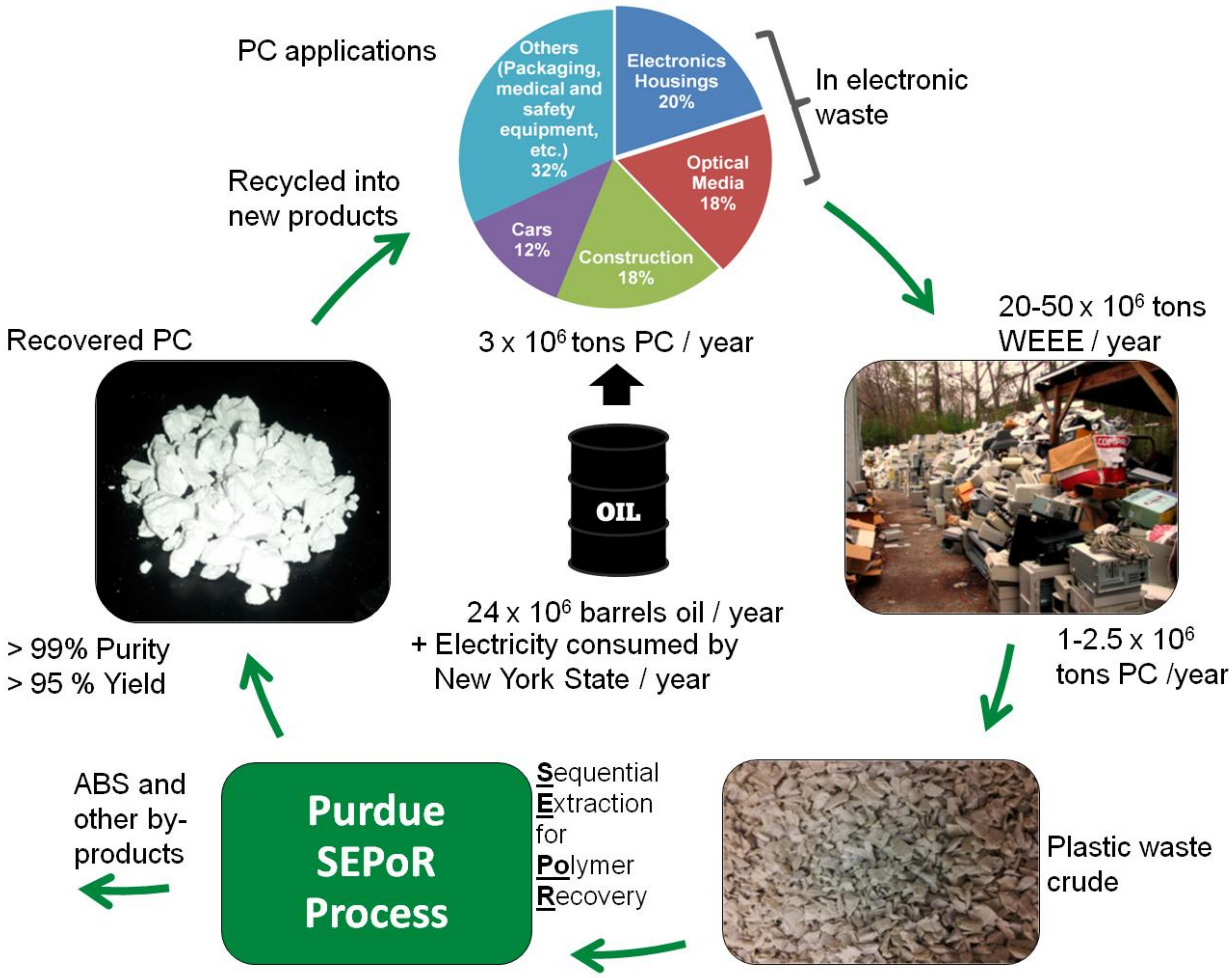

Figure 1.1. Overview of PC applications and recycle process developed at Purdue.

Recovery of high-purity polymers with high yield from a polymer waste can be difficult for various reasons. The wastes are complex mixtures of polymer blends of highly variable compositions. The major components, molecular weights, concentrations, and retail prices of the components in a particular computer housing waste are shown in Figure 1.2. Their densities, electrical properties, and other physical properties of the polymers are quite similar [18]. No solvents have been found for recovering PCs from the polymer waste by selectively dissolving PCs or the other components. The broad and overlapping MW distributions of PCs and the polymer impurities preclude the use of separation techniques

which rely on molecular size differences, such as size-exclusion chromatography, adsorption, membrane separation, ultrafiltration, and ultracentrifugation. Moreover, gel formation or aggregation of the various polymer components in solvents can affect the purity and yield of the PCs recovered, because several components will be extracted together.

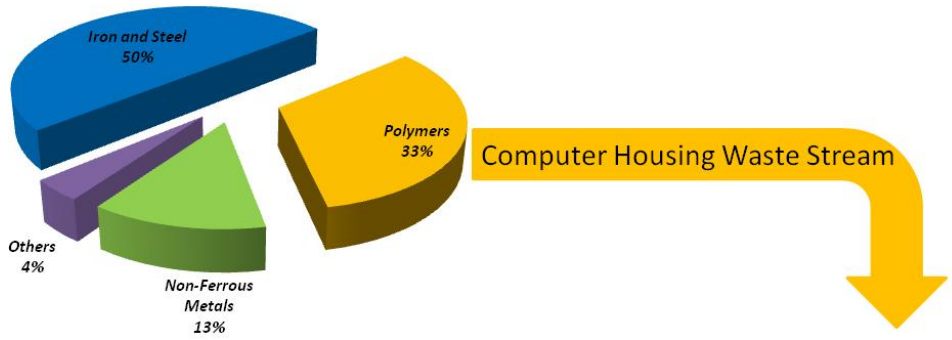

Component	Molecular Weight Range (g/mol)	wt.% in Solid	Bulk Retail Price[a] ($/kg)
Bisphenol A Polycarbonate (PC)	2,000 – 100,000	57.1	2.50 – 5.00
Brominated Bisphenol A Polycarbonate (BrPC)	2,000 – 100,000	2.3	2.50 – 5.00
Resorcinol bis-diphenylphosphate (RDP)	575 – 4,025	6.0	4.00
Bisphenol A bis-diphenylphosphate (BPADP)	693	0.1	3.00
Acrylonitrile-butadiene-styrene (ABS)	20,000 – 500,000	25.0	1.00
Styrene acrylonitrile (SAN)	50,000 – 150,000	9.5	1.00
Polystyrene (PS)[b]	100,000 – 200,000	-	0.85

[a]Costs in May 2014, retrieved from alibaba.com or ICIS.com
[b]Listed for reference. PS is present in other WEEE streams.

Figure 1.2. Main components of particular computer housing waste stream

1.3 Flame Retardants

Flame retardants (FRs) and a polymer, styrene acrylonitrile (SAN), are discharged in a side stream. Recovery of the FRs and SAN from the side stream is economically desirable and beneficial to the environment.

Flame retardants, such as resorcinol bis-diphenylphosphate (RDP) and bisphenol A bis-diphenylphosphate (BPADP), are added to polymers in order to inhibit the spread of flames in case of fire [19,20]. Many flame retardants containing bromine or other halogens are being preplaced by organophosphorus FRs, which are safer and more environmentally benign [21,22]. This work focuses on the recovery of RDP (575–4,025 Da), BPADP (693 Da), and SAN (50,000–150,000 Da) from one of the side streams of the SEPoR process for PC recovery, Figure 1.1.

The FRs are the most valuable components in the polymer wastes by weight. Polymers in WEEE have 10 wt.% or more FRs. More than 500,000 tonnes of FRs potentially could be recovered annually from WEEE. Furthermore, FRs must be removed for recovering high-purity polymers from wastes.

Since the MW of the FRs and SAN differ by two orders of magnitude, size-exclusion chromatography (SEC) is a potential separation technique. SEC has been widely used for analyzing polymer mixtures [23,24]. SEC is a batch chromatography process, which is less efficient than simulated moving-bed (SMB) chromatography for large-scale production. SMB can achieve high product purity without sacrificing product yield. It also requires much less solvent and can have an order of magnitude higher adsorbent productivity. For this reason, this study focuses on developing an economical SMB process based on size exclusion principles (SEC-SMB) for separating the FRs from SAN.

1.4 Size-Exclusion Simulated Moving Bed (SEC-SMB)

Size-exclusion chromatography (SEC) has many important applications. Examples include gel permeation chromatography (GPC), for analysis of protein mixtures or

obtaining molecular weight distributions of polymers [24,25], and purification of proteins, such as human insulin [26]. However, conventional SEC is a batch process and it is less efficient than simulated moving bed (SMB) for large-scale production.

SEC-SMB is a continuous chromatography process. The efficiency of SMB comes from a circular column configuration (a loop) and multiple inlet and outlet ports that divide this loop into various sections (or zones) with different flow rates. Figure 1.3 illustrates a typical 4-zone SMB with two columns per zone (2-2-2-2 configuration).

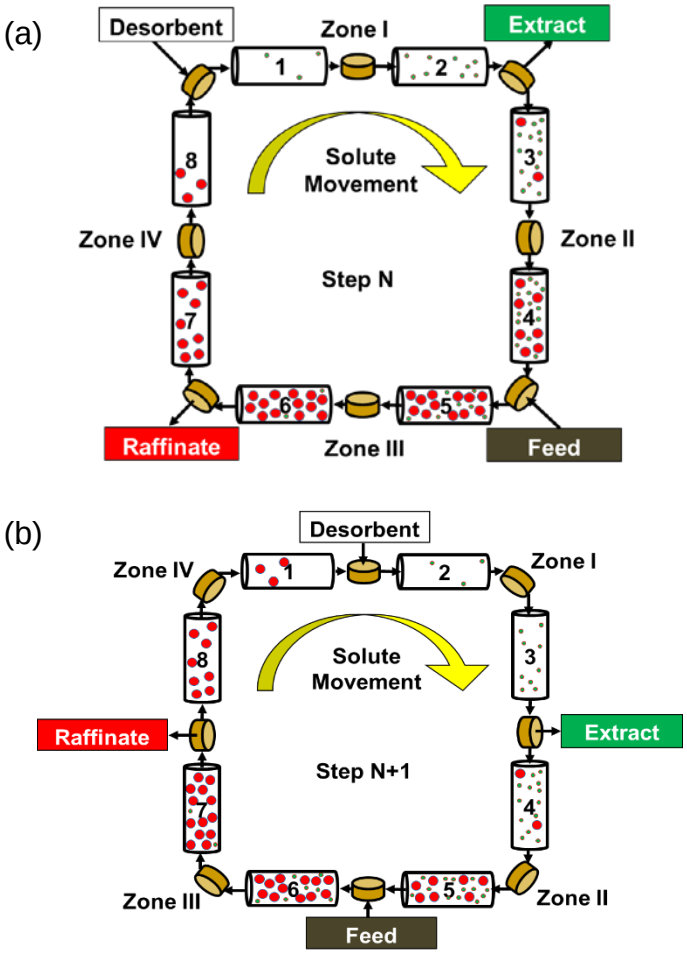

Figure 1.3. Diagram of a four-zone SMB. (a) Step N; (b) step N + 1.

In SMB, the columns are connected in a circular configuration (loop). Inlet and outlet ports divide the loop into different sections (zones) with different flowrates. A typical 4-zone SMB with two columns per zone (2-2-2-2 configuration) is shown in Figure 1.3. The ports are moved periodically to follow the migrating solute bands. The time between port switches is called the switching time, or step time (t_s). The average port velocity (v) is equal to the column length (L_c) divided by the step time. The separation is achieved by containing the solutes in specific zones. As seen in Figure 1.3, the small green component (slow solute) is never present in Zone IV while the large red component (fast solute) is never present in Zone I. By containing the advancing and trailing concentration waves in their respective zones, pure products can be continuously removed.

The objectives of this section are to: (1) estimate the material properties of a selected system (sorbent, solvent, solutes); (2) use the SSWD to design the operating parameters of SEC-SMBs for recovering both FRs and SAN with high purity and high yield; (3) experimentally test the design method and verify the estimated material properties; (4) develop and test fast startup methods to reduce the startup time of SEC-SMB; and (5) investigate the economic feasibility of the SEC-SMBs at large scale.

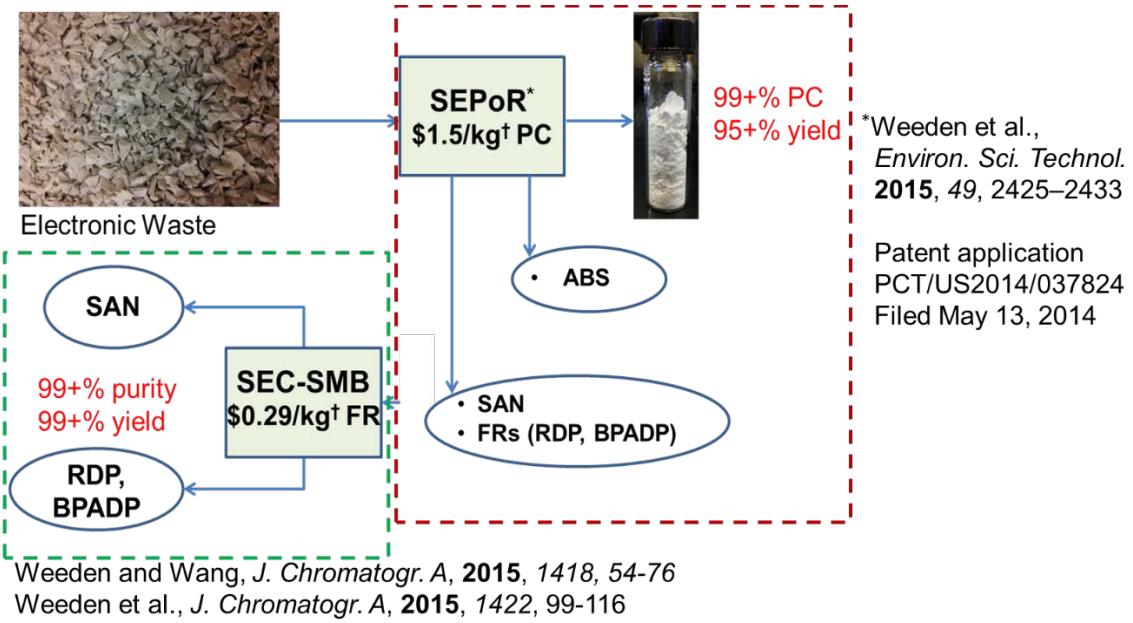

Figure 1.4. Overview of extraction and SMB separation to recover PC, SAN, and FRs from electronic waste.

Size-exclusion simulated moving beds (SEC-SMBs) are more efficient than conventional SEC because only partial separation of solutes in the loop is required to obtain high-purity products with high yield. As a result, a large fraction of the sorbent capacity is utilized and product dilution is reduced. Thus, SMBs consume orders of magnitude less solvent, require an order of magnitude less sorbent, and take up less space than batch operations. Because SMBs are continuous processes, they also require less manpower. These advantages make SMBs economical for large-scale separations.

The SEC-SMB was first introduced by Universal Oil Products (UOP) in 1961 as the Molex® process, which separates linear alkanes from branched alkanes [27,28]. SMBs were later developed for adsorptive systems, such as large-scale hydrocarbon purification and high fructose corn syrup production [29]. SMBs for chiral separations have been

developed since the 1990s [30]. Lab-scale SEC-SMB have been developed for insulin purification [31,32], separation of myoglobin from bovine serum albumin (BSA) [33], lactose removal from human milk [34], and polyethylene glycol (PEG) fractionation by molecular weight (MW) [35].

Even though SMBs have many advantages, they have not been widely used for large-scale production. SMBs have complex transient and cyclic steady-state phenomena. Equipment for SMBs is often more complex and expensive than batch equipment and SMB experiments are costly and time-consuming. The most important barrier is the complexity of the design and optimization of SEC-SMB. A four-zone SEC-SMB for a binary separation has 21 variables, which include seven material properties and 14 design parameters, Figure 1.5.

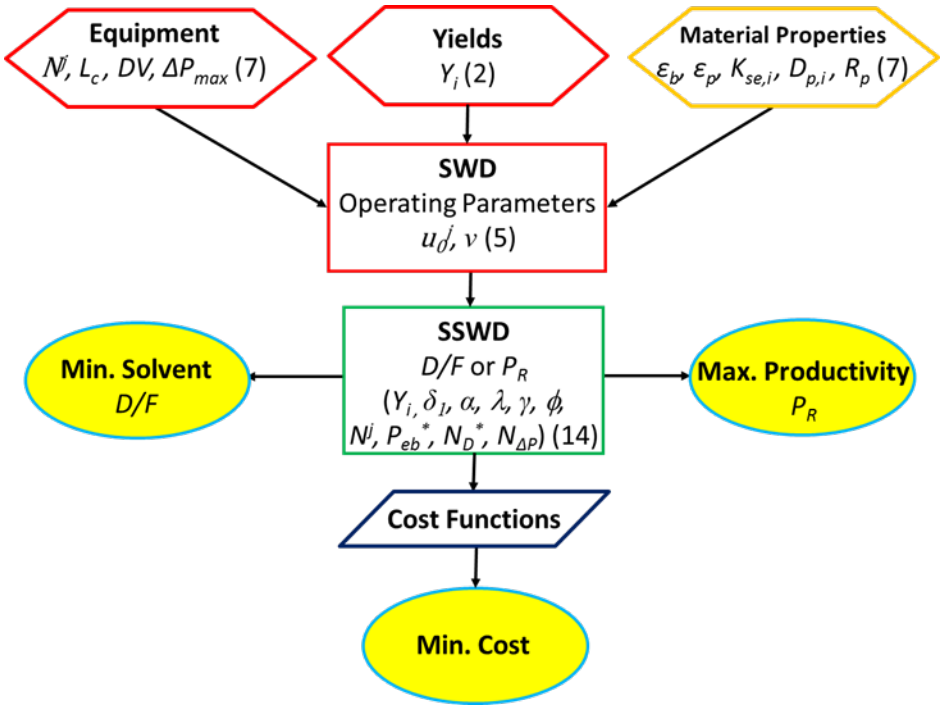

Figure 1.5. Design overview for SEC-SMB separation of two components.

The 14 design parameters include two yield requirements (Y_i), seven equipment parameters, and five operating parameters. The seven material properties are bed void fraction (ε_b), particle porosity (ε_p), two apparent retention factors (δ_i), two intraparticle diffusivities ($D_{p,i}$), and particle size (R_p). The two yield requirements can also be specified as two purities or one yield and one purity. The seven equipment parameters are column length (L_c), dead volume (DV), maximum pressure drop (ΔP_{max}), and the column configuration (the number of columns in each zone, N^j). The five operating parameters are the four zone velocities (u_0^j) and port velocity (ν). Experimental trial and error with 14 design parameters would be extremely costly. Additionally, the seven material properties, including particle size, can be optimized.

SEC-SMB systems can be optimized for maximum productivity, minimum solvent consumption, or minimum cost. Cost optimizations need to incorporate three main costs: equipment cost; solvent cost, which is related to solvent consumption; and sorbent cost, which is related to sorbent productivity. These costs are controlled by the equipment, material properties, and operating parameters.

The objective of this work is to find analytical solutions for the solvent consumption and productivity of SEC-SMB systems as functions of the equipment, material, and operating parameters. These analytical solutions can then be used to understand how solvent consumption and sorbent productivity are affected by the material and design parameters. These solutions can also be used to quickly find the optimal designs for maximum productivity, minimum solvent consumption, or lowest separation cost (with given cost functions). This new method is called the Speedy Standing Wave Design (SSWD) method.

To produce the general analytical solutions, the SWD equations are solved in terms of dimensionless groups. For a binary SEC-SMB separation, combining dimensionless groups with the SWD equations reduces the total number of variables from 21 to 14 (Figure 1.5). The details are shown in Chapter 3. The general solutions are simplified for two limiting cases: diffusion or dispersion controlled systems. The solvent consumption and sorbent productivity results from this new method are compared to those from three SEC-SMB systems in the literature. The effects of the dimensionless groups are explored for the diffusion or dispersion controlled cases using an example from insulin purification.

CHAPTER 2. LITERATURE REVIEW

2.1 Current Polycarbonate Recycling and Flame Retardant Detection

Current bisphenol A polycarbonate (PC) recycling methods are limited to the wastes with high PC contents (>95%) [36], such as CD's and DVD's, and their production rate is limited to less than 1 ton per day [37]. Discs are usually ground up and processed for applications which require lower PC purity. Several methods have been proposed for polycarbonates recycling. In chemical recycling, the polymers are broken down into monomers or other chemicals, which are reused [38]. Pyrolysis, gasification, reactions in supercritical fluids, and other techniques have been proposed [39–43]. These methods are energy intensive. The products would require further separation, additional syntheses, and re-polymerization to produce polycarbonates. Polycarbonates can be recovered from polymer blends by liquid chromatography using solvent gradients [44]. Since large amounts of solvent are required, about 10,000 kg solvent per kg PC recovered, this method is not economical. A single-solvent extraction method for high-PC content wastes, such as CD's and DVD's, has been reported [45].

The existing literature on organophosphorus FRs in polymer wastes focuses on analytical methods for detection [46–49]. Microwave-assisted extraction, combined with gel permeation chromatography and mass spectrometry, was used to detect organophosphorus FRs in biological samples from fish and birds [50]. Solid phase

extraction, combined with reverse phase chromatography, was used to detect FRs in water samples [51]. Pressurized liquid extraction (acetonitrile and water), combined with gas chromatography, was used to analyze sediment samples [52]. No literature has been found for recovering organophosphorus FRs from polymer waste at large scale.

2.2 Simulated Moving Bed Design and Optimization

The only large-scale SEC-SMB process is UOP's Molex® process, which separates n-paraffins from branched/cyclic hydrocarbons [27,28]. Lab-scale SEC-SMB studies have been reported for several important compounds. Some of these systems include influenza [53] and adenovirus [54] production for vaccines, recombinant protein purification [55], insulin purification [31,32,56,57], lactose removal from human milk [34], and polyethylene glycol fractionation by MW [35]. Only lab-scale operations have been performed for high MW molecules (MW >5 kDa). No studies on the separation of organophosphorus FRs from large polymers using SEC-SMB have been reported in the literature.

The simplest method for designing the five operating parameters (four zone velocities and one port velocity) is the local equilibrium theory or "triangle" theory. It is widely used and works well for ideal systems (no mass transfer resistance) [58]. However, for non-ideal systems (with mass transfer resistance), this theory only gives the range of possible operating parameters where separation of the components will occur. It does not guarantee purity or yield and it does not give optimum operating parameters for non-ideal systems (most low pressure systems).

The Standing Wave Design (SWD) was first developed by Ma and Wang in 1997 for binary, linear adsorption systems with mass transfer resistances [59]. For fixed material properties, yields, and equipment parameters, the SWD determines the five optimum operating parameters to maximize productivity and minimize solvent consumption. It was extended to multicomponent linear systems [60] and nonlinear systems [61–63]. Pressure limit considerations were incorporated into the SWD [64] by checking that the resulting operating parameters did not violate the pressure constraint.

The SWD method has been incorporated into various optimization routines, based on grid search [32], genetic algorithms [65], simulated annealing [66,67], or combined simulated annealing and genetic algorithm (SAGA) [68]. Optimization variables include particle size (R_p), column length (L_c), column configuration (N^j), and yields (Y_i) [69]. These techniques cannot guarantee global optima and they do not provide an overview of how solvent consumption, sorbent productivity, and separation cost are related to material properties and design parameters.

Another method for SMB design is the Standing Wave Design (SWD), which was first developed by Ma and Wang in 1997 for binary, linear adsorption systems with mass transfer resistances [59]. For fixed yields, material properties (size-exclusion factors, diffusivities, particle porosity, bed void fraction, and particle size), and equipment parameters (column length, dead volume, column configuration, and pressure limit), the SWD determines the five optimum operating parameters to maximize productivity and minimize solvent consumption.

The SWD was extended to multicomponent linear systems [60] and nonlinear systems [61–63]. Pressure limit considerations were incorporated into the SWD [64] by checking that the resulting operating parameters did not violate the pressure constraint.

CHAPTER 3. THEORY

3.1 General Principles of Sequential Extraction with Mixed Solvents

Our goal has been to develop an economical method for physically extracting high-purity polycarbonates with high yield from solid polymer mixtures. The recovered polycarbonates should have the same or similar MW distribution as the virgin polycarbonates. The MW distribution plays an important role in the properties of the polycarbonate. Low MW polymers provide easy processing, whereas high MW polymers are needed for toughness and resistance to environmental stress cracking.

No single solvent was found to selectively dissolve PC or dissolve all the other components in the polymer waste shown in Figure 1.2. For this reason, we developed a new process using two solvents sequentially for extraction. The first extraction step aims to dissolve some impurities but not PC, leaving the PC and other polymer impurities in solid form. In the second step, the PC would dissolve, again leaving behind other components in solid form. This process requires a “weak” solvent that dissolves little PC in the first extraction step and a “strong” solvent which easily dissolves PC in the second extraction step. Since many experiments would be required to discover suitable solvents for each extraction step, we used instead the Hansen Solubility Parameters (HSP) to identify potential strong and weak solvents for polycarbonates and the other major impurities of the polymers from electronic waste [70].

The HSP values account for three types of possible interactions, resulting from dispersion forces (δ_D), permanent dipole-permanent dipole forces (δ_P), and hydrogen bonding (δ_H). Tables of HSP values for different polymers and solvents are available [71]. Each material is represented as a point in the "Hansen solubility parameter space." The interaction radius R_0, which is the radius of the "solubility sphere" of that material, has been experimentally determined [71]. The solubility parameter "distance" *Ra* between a polymer (subscript 1) and a solvent (subscript 2) is defined in Eq. (3.1).

$$(Ra)^2 \equiv 4(\delta_{D2} - \delta_{D1})^2 + (\delta_{P2} - \delta_{P1})^2 + (\delta_{H2} - \delta_{H1})^2 \tag{3.1}$$

The relative energy difference (*RED*) is defined as ratio of *Ra* to R_0, Eq. (3.2).

$$RED \equiv \frac{Ra}{R_0} \tag{3.2}$$

RED indicates the extent to which the polymer is soluble in the solvent; if $RED < 1$, the polymer is soluble in the solvent; if $RED > 1$, the polymer is insoluble; and if $RED = 1$, the polymer is partially soluble. Solvents outside the solubility spheres, $RED \geq 1$, are "weak," and solvents inside the polymer solubility sphere, $RED < 1$, are "strong." Since the HSP theory does not consider electrostatic or induced dipole interactions, some solvents with $RED > 1$ may still be strong, and the Hansen theory may not apply. Furthermore, rates of dissolution are not considered.

The HSP values are temperature dependent [72,73]. To reduce the complexity and cost of the polymer recycle process, this study will focus on room temperature HSP values. The HSP values for polymers can also be affected by molecular size and molecular shape [74]. The HSP values for polycarbonates used in this work for initial solvent screening are for amorphous Lexan® polycarbonate samples [71,75].

3.2 Simulated Moving Bed Design

In this section, the basic concept of the Standing Wave Design (SWD) method reported in the literature is briefly reviewed in Section 3.2.1. The development of new general equations using dimensionless groups is explained in Section 3.2.2. These new equations are called the Speedy Standing Wave Design (SSWD) because they provide an overview of the solvent consumption, sorbent productivity, and cost over a wide range of design parameters. The SSWD equations are simplified for diffusion- and dispersion-controlled systems in Sections 3.2.2.1 and 3.2.2.2, respectively. Optimization of decision variables to achieve minimum solvent consumption, maximum productivity, or minimum cost using the SSWD is discussed in Section 3.2.2.3. Finally, preloading strategies for fast startup of SMB are discussed in Section 3.2.3.

3.2.1 Standing Wave Design (SWD)

The SWD for ideal and non-ideal, linear adsorption isotherm systems was first developed by Ma and Wang in 1997 [59]. For an ideal system, the SWD matches the port velocity to the velocity of the concentration wave of the “standing” component in each zone in a continuous moving bed. For a non-ideal system, a difference in port velocity and wave velocities is used to confine selected waves in their respective zones. This concept is illustrated for a binary, non-ideal system in Figure 3.1.

The fast moving solute (SAN, component 1) is removed in the raffinate, while the slow moving solute (RDP, component 2) is removed in the extract. The arrows point to the wave which is confined in that zone.

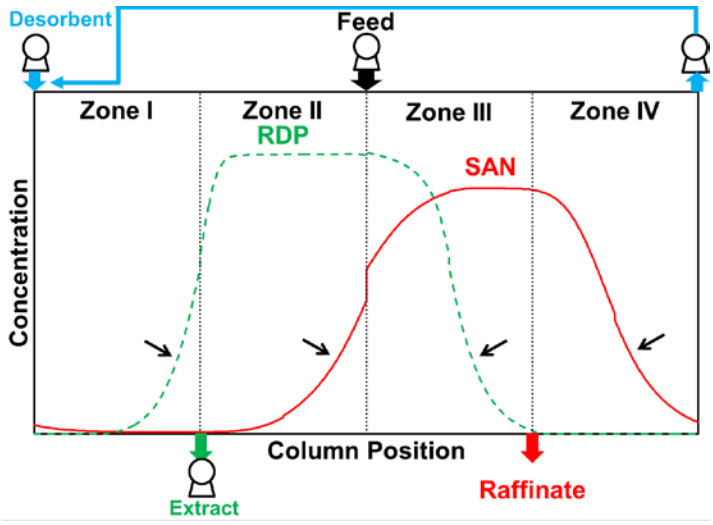

Figure 3.1. Standing Wave Design end-step concentration profiles for a binary, non-ideal separation. The black arrows indicate the standing waves in each of the four zones.

The equations for the design of linear systems with mass transfer effects are presented in Eq. (3.3) [59],

$$u_0^I = (1+\phi\delta_2)\nu + \frac{\beta_2^I}{L^I}\left[E_{b,2}^I + \frac{\phi(\delta_2\nu)^2}{K_2^I}\right] \tag{3.3a}$$

$$u_0^{II} = (1+\phi\delta_1)\nu + \frac{\beta_1^{II}}{L^{II}}\left[E_{b,1}^{II} + \frac{\phi(\delta_1\nu)^2}{K_1^{II}}\right] \tag{3.3b}$$

$$u_0^{III} = (1+\phi\delta_2)\nu - \frac{\beta_2^{III}}{L^{III}}\left[E_{b,2}^{III} + \frac{\phi(\delta_2\nu)^2}{K_2^{III}}\right] \tag{3.3c}$$

$$u_0^{IV} = (1+\phi\delta_1)\nu - \frac{\beta_1^{IV}}{L^{IV}}\left[E_{b,1}^{IV} + \frac{\phi(\delta_1\nu)^2}{K_1^{IV}}\right] \tag{3.3d}$$

$$u_F = u_0^{III} - u_0^{II} \tag{3.3e}$$

where u_0^j is the interstitial velocity of the fluid in zone j (zone velocity); u_F is the feed velocity; ϕ is the phase ratio which is equal to $(1-\varepsilon_b)/\varepsilon_b$; δ_i is the apparent retention factor for component i; ν is the port velocity; β_i^j is the natural logarithm of the ratio of the highest

concentration to the lowest concentration of the standing wave of component i in zone j and it is directly related to the yield, Eq. (A1.1); L^j is the length of zone j and is equal to the product of N^j and L_c; $E_{b,i}^j$ is the axial dispersion coefficient for component i in zone j; and K_i^j is the lumped mass transfer parameter for component i in zone j.

The overall mass transfer resistance, $\frac{1}{K_i^j}$, can be written explicitly as mass transfer resistances in series for linear systems, as shown in Eq. (3.4).

$$\frac{1}{K_i^j} = \frac{R_p^2}{15K_{se,i}\varepsilon_p D_{p,i}} + \frac{R_p}{3k_{f,i}} \tag{3.4}$$

where $K_{se,i}$ is the size-exclusion factor for component i (fraction of the pore volume that can be accessed by the component), $D_{p,i}$ is the pore diffusivity of component i, and $k_{f,i}$ is the film mass transfer coefficient. For most low pressure systems, the film mass transfer resistance is negligible compared to that of intraparticle diffusion or axial dispersion [76].

For linear systems, the apparent retention factor of component i is given by Eq. (3.5) [31],

$$\delta_i = \varepsilon_p K_{se,i} + \left(1 - \varepsilon_p K_{se,i}\right) a_i + \frac{DV}{(1-\varepsilon_b)} \tag{3.5}$$

where a_i in Eq. (3) is the Langmuir "a" value for adsorption and DV is the total dead volume as a fraction of the total sorbent packing volume. For size-exclusion systems, there is no adsorption so the equation for the retention factors is simplified into Eq. (3.6).

$$\delta_i = \varepsilon_p K_{se,i} + \frac{DV}{(1-\varepsilon_b)} \tag{3.6}$$

Table 3.1 contains a summary of the definitions and descriptions of the major dimensionless groups which will be derived in the rest of this section.

Table 3.1. Dimensionless variables and groups for binary, SEC-SMB.

Symbol	Name	Definition	Description
δ_i	Retention factor	$\delta_i = \varepsilon_p K_{se,i} + \frac{DV}{(1-\varepsilon_b)}$	Measure of how much each component is retained by the sorbent
α	Selectivity	$\alpha = \frac{\delta_2}{\delta_1}$	Ratio of retention factors: $\alpha > 1$ for separation
β_i^j	-	$\beta_i^j = \ln\left(\frac{C_{max,i}^j}{C_{min,i}^j}\right)$	Natural log of ratio of max. conc. to min. conc. of standing component i in zone j
γ	Diffusivity ratio	$\gamma = \frac{D_{p,2}}{D_{p,1}}$	Ratio of intraparticle diffusivities
λ	Size-exclusion ratio	$\lambda = \frac{K_{se,2}}{K_{se,1}}$	Ratio of size-exclusion factors; equal to α for no dead volume
ϕ	Phase ratio	$\phi = \frac{1-\varepsilon_b}{\varepsilon_b}$	Particle phase relative to bed void
$N_{D,i}$	-	$N_{D,i} = \frac{\phi\varepsilon_p K_{se,i} D_{p,i}}{{R_p}^2}\frac{L_c}{v} = \frac{t_s}{t_{D,i}}$	Step time relative to diffusion time
N_D^*	-	$N_D^* = \frac{N_{D,1}(\alpha-1)}{\phi\delta_1} = \frac{N_{D,2}(\alpha-1)}{\lambda\gamma\phi\delta_1}$	Component-independent N_D; $N_{D,1}$ as base
$N_{\Delta P}$	-	$N_{\Delta P} = \frac{\Delta P_{max}{R_p}^2}{37.5\phi\mu L_c v} = \frac{t_s}{t_c^I}$	Step time relative to pressure-limited convection time
$N_{\Delta P,diff}$	-	$N_{\Delta P,diff} = \frac{\Delta P_{max}{R_p}^4}{37.5\phi\mu D_{p,1}{L_c}^2} = \frac{t_{D,1}}{t_c^I}$	Diffusion time relative to pressure-limited convection time
P_{eb}^j	Peclet number	$P_{eb}^j = \frac{vL_c}{E_b^j} = \frac{t_{Dax}}{t_s}$	Axial dispersion time relative to step time
Γ^j	Axial dispersion ratio	$\Gamma^j = \frac{E_b^j}{E_b^{IV}}$	Ratio of axial dispersion coefficients Zone IV as base
P_{eb}^*	-	$P_{eb}^* = \phi(\delta_2 - \delta_1)P_{eb}^j\Gamma^j$	Zone-independent Peclet number, Zone IV as base

An often referred to parameter is the selectivity of a system. The definition of selectivity for SEC- SMB is given by Eq. (3.8).

$$\alpha = \frac{\delta_2}{\delta_1} \tag{3.7}$$

Given yields, material properties, and equipment parameters, Eq. (3.3) is solved to obtain the five operating parameters (u_0^j and ν). The maximum feed flow rate can be found by increasing the set feed flow rate until the mass transfer limit does not allow further increase.

3.2.2 Speedy Standing Wave Design (SSWD)

In this study, solvent consumption and sorbent productivity are expressed in terms of dimensionless groups. Such solutions can be used to elucidate the effects of equipment, material, and operating parameters on solvent consumption and sorbent productivity. Furthermore, designs for minimum cost, maximum productivity, or minimum solvent consumption can be found very quickly. This advanced SWD method is called the Speedy Standing Wave Design (SSWD) method.

Eq. (3.3) is simplified using the dimensionless groups defined in Table 3.1. Two key dimensionless groups are used to separate the mass transfer effects due to diffusion from the mass transfer effects due to dispersion. The dimensionless group which is a ratio of diffusion rate to convection rate is $N_{D,i}$ and is defined in Eq. (3.8).

$$N_{D,i} = \frac{\phi \varepsilon_p K_{se,i} D_{p,i}}{{R_p}^2} \frac{L_c}{\nu} = \frac{\text{Diffusion rate}}{\text{Convection rate}} = \frac{t_s}{t_{D,i}} = \frac{\text{Step time}}{\text{Effective diffusion time}} \tag{3.8}$$

The port velocity is chosen as the characteristic velocity. To separate the influence of the column configuration from that of diffusion, column length, instead of zone length,

is chosen as the characteristic length. Particle radius (R_p) is chosen as the characteristic diffusion length. A characteristic diffusion time ($t_{D,i}$) can be defined as R_p^2 divided by the effective diffusivity ($\phi\varepsilon_p K_{se,i} D_{p,i}$), while a characteristic convection time can be defined as L_c divided by ν, or the step time (t_s) in SMB. Thus, $N_{D,i}$ can be thought of as the ratio of the step time to the diffusion time. A large $N_{D,i}$ means that in the time between port switches, there is plenty of time for the solute to diffuse through the sorbent particles, which in turn means that the wave spreading due to diffusion is small. A small $N_{D,i}$ means that there is not enough time for the solute to diffuse through the particle within the step time, which in turn means wave spreading due to diffusion is significant.

For a binary separation, there are two $N_{D,i}$ values, one for each component. These two $N_{D,i}$ are related by the definition of the dimensionless group as shown in Eq. (3.9)

$$\frac{N_{D,2}}{N_{D,1}} = \frac{K_{se,2} D_{p,2}}{K_{se,1} D_{p,1}} = \lambda\gamma \tag{3.9}$$

where λ is the ratio of the size-exclusion factors and γ is the ratio of the intraparticle diffusivities.

The dimensionless group which is a ratio of convection rate to axial dispersion rate is the Peclet number, and is defined in Eq. (3.10).

$$Peb_i^j = \frac{\nu L_c}{E_{b,i}^j} = \frac{\text{Convection rate}}{\text{Dispersion rate}} = \frac{t_{Dax}}{t_s} = \frac{\text{Axial dispersion time}}{\text{Step time}} \tag{3.10}$$

The characteristic dispersion time (t_{Dax}) can be defined as L_c^2 divided by the dispersion coefficient ($E_{b,i}^j$), while a characteristic convection time can be defined as L_c divided by ν, or the step time (t_s). The Peclet number can also be thought of as the ratio of a characteristic time for dispersion (t_{Dax}) to the step time (t_s). If the Peclet number is very large, then the

step time is much smaller than the dispersion time and thus there is a very small effect of dispersion on the wave spreading. If the Peclet number is small, then the dispersion time is closer to the step time and the effects from dispersion are significant.

For a four-zone SMB, there are four Peclet numbers, but they are related by Eq. (3.11),

$$\frac{{P_{eb}}^{IV}}{{P_{eb}}^{j}} = \frac{E_b^j}{E_b^{IV}} = \Gamma^j \tag{3.11}$$

where Γ^j is the ratio of the axial dispersion coefficient of zone j to the axial dispersion coefficient of Zone IV.

Eqs. (3.8-3.11) allow for Eq. (3.3) to be written using the $N_{D,i}$ of one component and the $P_{eb}{}^j$ of one zone and are shown in Eq. (3.12).

$$u_0^I = \nu\left(1 + \phi\delta_2 + \frac{\beta_2^I \Gamma^I}{P_{eb}^{IV} N^I} + \frac{\phi^2 \beta_2^I {\delta_2}^2}{15 N_{D,1} \lambda\gamma N^I}\right) \tag{3.12a}$$

$$u_0^{II} = \nu\left(1 + \phi\delta_1 + \frac{\beta_1^{II} \Gamma^{II}}{P_{eb}^{IV} N^{II}} + \frac{\phi^2 \beta_1^{II} {\delta_1}^2}{15 N_{D,1} N^{II}}\right) \tag{3.12b}$$

$$u_0^{III} = \nu\left(1 + \phi\delta_2 - \frac{\beta_2^{III} \Gamma^{III}}{P_{eb}^{IV} N^{III}} - \frac{\phi^2 \beta_2^{III} {\delta_2}^2}{15 N_{D,1} \lambda\gamma N^{III}}\right) \tag{3.12c}$$

$$u_0^{IV} = \nu\left(1 + \phi\delta_1 - \frac{\beta_1^{IV}}{P_{eb}^{IV} N^{IV}} - \frac{\phi^2 \beta_1^{IV} {\delta_1}^2}{15 N_{D,1} N^{IV}}\right) \tag{3.12d}$$

For large-scale production, the solvent consumption of the SMB is an important factor for the separation cost. Solvent cost is related to a ratio of the desorbent flow rate (*D*) and the feed flow rate (*F*). This ratio (*D/F*) is also related to the dilution of the products. *D* and *F* are determined by Eq. (3.13) and Eq. (3.14), respectively where *S* is the cross-sectional area of a column.

$$D = \varepsilon_b S(u_0^I - u_0^{IV}) \tag{3.13}$$

$$F = \varepsilon_b S(u_0^{III} - u_0^{II}) \tag{3.14}$$

Taking the ratio of Eq. (3.13) to Eq. (3.14) and substituting the zone velocities with Eq. (3.12) results in Eq. (3.15).

$$\frac{D}{F} = \frac{\phi(\delta_2 - \delta_1) + \frac{1}{P_{eb}^{IV}}\left(\frac{\beta_2^I \Gamma^I}{N^I} + \frac{\beta_1^{IV}}{N^{IV}}\right) + \frac{\phi^2 {\delta_1}^2}{15 N_{D,1}}\left(\frac{\beta_2^I \alpha^2}{\lambda\gamma N^I} + \frac{\beta_1^{IV}}{N^{IV}}\right)}{\phi(\delta_2 - \delta_1) - \frac{1}{P_{eb}^{IV}}\left(\frac{\beta_2^{III}\Gamma^{III}}{N^{III}} + \frac{\beta_1^{II}\Gamma^{II}}{N^{II}}\right) - \frac{\phi^2 {\delta_1}^2}{15 N_{D,1}}\left(\frac{\beta_2^{III}\alpha^2}{\lambda\gamma N^{III}} + \frac{\beta_1^{II}}{N^{II}}\right)} \tag{3.15}$$

The ν, ε_b, and S all cancelled out in Eq. (3.15). This solution applies to systems where both diffusion and dispersion are significant. For an ideal SMB with no mass transfer spreading, the terms with $N_{D,1}$ or ${P_{eb}}^{IV}$ are negligible and the value of D/F is 1.

Another useful parameter for evaluating SMB designs is productivity. Productivity (P_R) has dimensions (usually in mass of product per mass of sorbent per time). Eq. (3.16) defines P_R in the way that it will be discussed throughout this work.

$$P_{R,i} = \frac{\varepsilon_b S(u_0^{III} - u_0^{II}) C_{F,i} Y_i}{S L_c N (1 - \varepsilon_b) \rho_p} \tag{3.16}$$

$C_{F,i}$ is the feed concentration of component i (mass solute / volume of feed), N is the total number of columns in the SMB, and ρ_p is the particle density (mass sorbent / particle volume). Substituting the zone velocities in Eq. (3.17) with Eq. (3.13) results in Eq. (3.17).

$$P_{R,i} = \frac{Y_i C_{F,i}}{N t_s \phi \rho_p}\left[\phi(\delta_2 - \delta_1) - \frac{1}{P_{eb}^{IV}}\left(\frac{\beta_2^{III}\Gamma^{III}}{N^{III}} + \frac{\beta_1^{II}\Gamma^{II}}{N^{II}}\right) - \frac{\phi^2 {\delta_1}^2}{15 N_{D,1}}\left(\frac{\beta_2^{III}\alpha^2}{\lambda\gamma N^{III}} + \frac{\beta_1^{II}}{N^{II}}\right)\right] \tag{3.17}$$

For an ideal system, the terms with $N_{D,1}$ and ${P_{eb}}^{IV}$ are negligible and the productivity is the first term on the right-hand side of Eq. (3.17).

Table 3.2. SSWD equations for binary SEC-SMB.

	General		Diffusion controlled		Dispersion controlled	
u_0^I	$\nu\left(1+\phi\delta_2+\frac{\beta_2^I\Gamma^I\phi(\delta_2-\delta_1)}{P_{eb}^*N^I}+\frac{\phi\beta_2^I\alpha^2(\delta_2-\delta_1)}{15N_D^*\lambda\gamma N^I}\right)$	(3.20a)	$\nu\left(1+\phi\delta_2+\frac{\phi\beta_2^I\alpha^2(\delta_2-\delta_1)}{15N_D^*\lambda\gamma N^I}\right)$	(3.26a)	$\nu\left(1+\phi\delta_2+\frac{\beta_2^I\Gamma^I\phi(\delta_2-\delta_1)}{P_{eb}^*N^I}\right)$	(3.33a)
u_0^{II}	$\nu\left(1+\phi\delta_1+\frac{\beta_1^{II}\Gamma^{II}\phi(\delta_2-\delta_1)}{P_{eb}^*N^{II}}+\frac{\phi\beta_1^{II}(\delta_2-\delta_1)}{15N_D^*N^{II}}\right)$	(3.20b)	$\nu\left(1+\phi\delta_1+\frac{\phi\beta_1^{II}(\delta_2-\delta_1)}{15N_D^*N^{II}}\right)$	(3.26b)	$\nu\left(1+\phi\delta_1+\frac{\beta_1^{II}\Gamma^{II}\phi(\delta_2-\delta_1)}{P_{eb}^*N^{II}}\right)$	(3.33b)
u_0^{III}	$\nu\left(1+\phi\delta_2-\frac{\beta_2^{III}\Gamma^{III}\phi(\delta_2-\delta_1)}{P_{eb}^*N^{III}}-\frac{\phi\beta_2^{III}\alpha^2(\delta_2-\delta_1)}{15N_D^*\lambda\gamma N^{III}}\right)$	(3.20c)	$\nu\left(1+\phi\delta_2-\frac{\phi\beta_2^{III}\alpha^2(\delta_2-\delta_1)}{15N_D^*\lambda\gamma N^{III}}\right)$	(3.26c)	$\nu\left(1+\phi\delta_2-\frac{\beta_2^{III}\Gamma^{III}\phi(\delta_2-\delta_1)}{P_{eb}^*N^{III}}\right)$	(3.33c)
u_0^{IV}	$\nu\left(1+\phi\delta_1-\frac{\beta_1^{IV}\phi(\delta_2-\delta_1)}{P_{eb}^*N^{IV}}-\frac{\phi\beta_1^{IV}(\delta_2-\delta_1)}{15N_D^*N^{IV}}\right)$	(3.20d)	$\nu\left(1+\phi\delta_1-\frac{\phi\beta_1^{IV}(\delta_2-\delta_1)}{15N_D^*N^{IV}}\right)$	(3.26d)	$\nu\left(1+\phi\delta_1-\frac{\beta_1^{IV}\phi(\delta_2-\delta_1)}{P_{eb}^*N^{IV}}\right)$	(3.33d)
$\frac{D}{F}$	$\frac{1+\frac{1}{P_{eb}^*}\left(\frac{\beta_2^I\Gamma^I}{N^I}+\frac{\beta_1^{IV}}{N^{IV}}\right)+\frac{1}{15N_D^*}\left(\frac{\beta_2^I\alpha^2}{\lambda\gamma N^I}+\frac{\beta_1^{IV}}{N^{IV}}\right)}{1-\frac{1}{P_{eb}^*}\left(\frac{\beta_2^{III}\Gamma^{III}}{N^{III}}+\frac{\beta_1^{II}\Gamma^{II}}{N^{II}}\right)-\frac{1}{15N_D^*}\left(\frac{\beta_2^{III}\alpha^2}{\lambda\gamma N^{III}}+\frac{\beta_1^{II}}{N^{II}}\right)}$	(3.20)	$\frac{1+\frac{1}{15N_D^*}\left(\frac{\beta_2^I\alpha^2}{\lambda\gamma N^I}+\frac{\beta_1^{IV}}{N^{IV}}\right)}{1-\frac{1}{15N_D^*}\left(\frac{\beta_2^{III}\alpha^2}{\lambda\gamma N^{III}}+\frac{\beta_1^{II}}{N^{II}}\right)}$	(3.27)	$\frac{1+\frac{1}{P_{eb}^*}\left(\frac{\beta_2^I\Gamma^I}{N^I}+\frac{\beta_1^{IV}}{N^{IV}}\right)}{1-\frac{1}{P_{eb}^*}\left(\frac{\beta_2^{III}\Gamma^{III}}{N^{III}}+\frac{\beta_1^{II}\Gamma^{II}}{N^{II}}\right)}$	(3.34)
$P_{R,i}$	$\frac{\nu Y_i C_{F,i}(\delta_2-\delta_1)}{NL_c\rho_p}\left[1-\frac{1}{P_{eb}^*}\left(\frac{\beta_2^{III}\Gamma^{III}}{N^{III}}+\frac{\beta_1^{II}\Gamma^{II}}{N^{II}}\right)-\frac{1}{15N_D^*}\left(\frac{\beta_2^{III}\alpha^2}{\lambda\gamma N^{III}}+\frac{\beta_1^{II}}{N^{II}}\right)\right]$	(3.21)	$\frac{Y_i C_{F,i}(\alpha-1)^2\varepsilon_p K_{se,1}D_{p,1}}{N\rho_p {R_p}^2 N_D^*}\left[1-\frac{1}{15N_D^*}\left(\frac{\beta_2^{III}\alpha^2}{\lambda\gamma N^{III}}+\frac{\beta_1^{II}}{N^{II}}\right)\right]$	(3.29b)	$\frac{\nu Y_i C_{F,i}(\delta_2-\delta_1)}{10N\varepsilon_b R_p\rho_p\left[P_{eb}^*\frac{(1+\phi\delta_1)}{\phi(\delta_2-\delta_1)}-\frac{\beta_1^{IV}}{N^{IV}}\right]}\left[1-\frac{1}{P_{eb}^*}\left(\frac{\beta_2^{III}\Gamma^{III}}{N^{III}}+\frac{\beta_1^{II}\Gamma^{II}}{N^{II}}\right)\right]$	(3.39b)
$N_{\Delta P}$	$\frac{\Delta P_{max}{R_p}^2}{37.5\phi\mu L_c\nu}=\phi\left(1+\phi\delta_2+\frac{\beta_2^I\Gamma^I\phi(\delta_2-\delta_1)}{P_{eb}^*N^I}+\frac{\phi\beta_2^I\alpha^2(\delta_2-\delta_1)}{15N_D^*\lambda\gamma N^I}\right)$	(3.25)	$\frac{\Delta P_{max}{R_p}^4}{37.5\phi\mu D_{p,1}{L_c}^2}=\frac{\phi^2(\alpha-1)^2\varepsilon_p K_{se,1}}{N_D^*}\left(\frac{1+\phi\delta_2}{\phi(\delta_2-\delta_1)}+\frac{\beta_2^I\alpha^2}{15N_D^*\lambda\gamma N^I}\right)$	(3.32a)	$\frac{\Delta P_{max}{R_p}^2}{37.5\phi\mu L_c\nu}=\phi\left[1+\phi\delta_2+\frac{\beta_2^I\Gamma^I\phi(\delta_2-\delta_1)}{P_{eb}^*N^I}\right]$	(3.41)

One can define component-independent N_D and zone-independent P_{eb} by Eqs. (3.18) and (3.19), respectively.

$$N_D^* = \frac{(\delta_2 - \delta_1)N_{D,1}}{\phi {\delta_1}^2} = \frac{N_{D,2}(\delta_2 - \delta_1)}{\lambda\gamma\phi {\delta_1}^2} \tag{3.18}$$

$$P_{eb}^* = \phi(\delta_2 - \delta_1)P_{eb}^{IV} = \phi(\delta_2 - \delta_1)P_{eb}^j \Gamma^j \tag{3.19}$$

Equations (3.18, 3.19) can be substituted into Eq. (3.12). The resulting u_0^j equations are presented in the first column of Table 3.2, Eq. (3.20). The *D/F* and P_R expressions resulting from using Eq. (3.20) for the zone velocities are shown in Table 3.2, Eqs. (3.21) and (3.22), respectively.

The column configuration which achieves the highest P_R can be obtained from Eq. (3.22). For a fixed total number of columns (N), the question is how to distribute the columns between the zones. Since N^I and N^{IV} do not appear in Eq. (3.22), columns placed in these zones do not affect P_R with the same operating conditions. This means Zones I and IV should have the minimum number of columns (i.e. one). Increasing N^{II} or N^{III} will increase P_R. The column configuration that yields the maximum productivity can be obtained by taking the partial derivative of Eq. (3.22) with respect to N^{II}, or N^{III}, and setting the resulting equation equal to zero. The fractional column configuration for maximum P_R is given by Eq. (3.23).

$$\frac{N^I}{N} = \frac{1}{N} \tag{3.23a}$$

$$\frac{N^{II}}{N} = \frac{N^{III}}{N}\sqrt{\frac{\beta_1^{II}\left[\frac{\Gamma^{II}}{P_{eb}^*} + \frac{1}{15N_D^*}\right]}{\beta_2^{III}\left[\frac{\Gamma^{III}}{P_{eb}^*} + \frac{\alpha^2}{15N_D^*\lambda\gamma}\right]}} \tag{3.23b}$$

$$\frac{N^{III}}{N} = \frac{1 - \frac{N^{I}}{N} - \frac{N^{IV}}{N}}{1 + \sqrt{\frac{\beta_1^{II}\left[\frac{\Gamma^{II}}{P_{eb}^*} + \frac{1}{15N_D^*}\right]}{\beta_2^{III}\left[\frac{\Gamma^{III}}{P_{eb}^*} + \frac{\alpha^2}{15N_D^*\lambda\gamma}\right]}}} \tag{3.23c}$$

$$\frac{N^{IV}}{N} = \frac{1}{N} \tag{3.23d}$$

For systems where diffusion and dispersion are significant, the column configuration that results in the highest P_R is dependent on both N_D^* and P_{eb}^*. Once these two dimensionless groups, the material properties, yields, and the total number of columns are fixed, the optimum configuration can easily be calculated.

Previous studies have shown that the true moving bed assumption holds for SMBs with two or more columns per zone [59]. Having only one column in a zone may violate the true moving bed assumption of the SWD. If this assumption is violated, the purities and yields can be lower than those specified by SWD. Column configurations that have a zone with one column should be simulated to ensure that the waves are actually confined [32]. To avoid the need for simulations, the minimum number of columns per zone is set to be two in this work.

A major factor for equipment cost and sorbent cost is a pressure limitation. Systems may be limited by pressure if the sorbent is very soft. In the example system studied in Chapter 7, the pressure drop per packing length is limited [32]. Other systems may be limited by the maximum pressure allowed by pumps, valves, or columns. The pressure drop across a uniformly packed bed of monodisperse, spherical particles can be estimated using the simplified Ergun equation [77].

$$\Delta P = \frac{37.5\mu L_c u_0^I \phi^2}{{R_p}^2} \tag{3.24}$$

ΔP is the pressure drop and μ is the viscosity of the fluid. Because the velocity in Zone I is always the largest in SEC-SMB, it is used to calculate the maximum pressure drop (ΔP_{max}) across a column in the SMB. Substitution of Eq. (3.21a) into Eq. (3.25) and rearranging results in Eq. (3.26).

$$\frac{\Delta P\ {R_p}^2}{37.5\phi\mu L_c \nu} = \phi\left(1 + \phi\delta_2 + \frac{\beta_2^I \Gamma^I \phi(\delta_2 - \delta_1)}{P_{eb}^* N^I} + \frac{\phi\beta_2^I \alpha^2(\delta_2 - \delta_1)}{15 N_D^* \lambda\gamma N^I}\right) = N_{\Delta P} = \frac{t_s}{t_c^I} \tag{3.25}$$

This dimensionless group, $N_{\Delta P}$, can be considered as a dimensionless pressure drop, which is equal to the ratio of step time to the pressure-limited convection time through a column in Zone I (t_c^I). It is analogous to the Bejan number, which was developed for the pressure drop across a channel [78].

3.2.2.1 Diffusion Controlled

Equations (3.20-3.23) and (3.25) can be simplified for diffusion controlled systems. The results are summarized in the middle column of Table 3.2. If the Peclet number is very large, dispersion effects are negligible. The zone velocities are controlled by Eq. (3.26). The resulting equation for *D/F* is presented in Eq. (3.27).

Equation (3.27) indicates that increasing the zone length ($N^j L_c$) in any zone will decrease *D/F* by decreasing the effects from diffusion. The optimum column configuration is controlled by the selectivity (α), diffusivity ratio (γ), and size-exclusion factor ratio (λ). For SEC-SMBs with small dead volumes (*DV*), λ is approximately equal to α. If γ is much larger than α, Zone IV should have more columns than Zone I, and Zone II should have more columns than Zone III. A large value of γ indicates that the fast solute has a lower

diffusivity than the slow solute, resulting in broader waves of the fast solute. This column configuration uses the extra columns in Zones II and IV to better confine the trailing wave and advancing wave of the fast solute, respectively. However, when γ is large, the column configuration does not have a large impact on *D/F* because the terms inside the parentheses in Eq. (3.27) are already relatively small. The column configuration will have a larger impact on systems where α is larger than γ.

The denominator of Eq. (3.27) must be positive for SEC-SMB. Therefore there is a minimum value of N_D^* for the operation to be feasible, which is shown in Eq. (3.28).

$$N_{D,min}^{*} = \frac{1}{15}\left(\frac{\beta_{2,\min N_D^*}^{III}\alpha^2}{\lambda\gamma N^{III}} + \frac{\beta_{1,\min N_D^*}^{II}}{N^{II}}\right) \tag{3.28}$$

For Eq. (3.22), the terms with Peclet numbers are negligible and the step time can be replaced by the definition of N_D^*, resulting in Eq. (3.29)

$$P_{R,i} = \frac{\phi\delta_1 Y_i C_{F,i}\varepsilon_p K_{se,1} D_{p,1}}{N\rho_p {R_p}^2 N_{D,1}}\left[(\alpha-1) - \frac{\phi\delta_1}{15N_{D,1}}\left(\frac{\beta_2^{III}\alpha^2}{\lambda\gamma N^{III}} + \frac{\beta_1^{II}}{N^{II}}\right)\right] \tag{3.29a}$$

The second term in the brackets of Eq. (3.29b), Table 3.2, represents the loss of productivity due to diffusion effects compared to the productivity of an ideal system. For the productivity to be positive, the value of the second term in the in the bracket, $\frac{1}{15N_D^*}\left(\frac{\beta_2^{III}\alpha^2}{\lambda\gamma N^{III}} + \frac{\beta_1^{II}}{N^{II}}\right)$, must be less than one. When the other parameters are fixed, there is a minimum γ, for the productivity to be positive.

For diffusion controlled systems, the step time is proportional to N_D^*. As N_D^* increases, the loss of productivity due to diffusion effects decrease, but the step time increases. These competing effects result in a maximum in the productivity. Taking the

partial derivative of Eq. (3.29b) with respect to N_D^* and setting the resulting equation equal to zero can solve for the N_D^* which achieves the maximum P_R. The result is shown in Eq. (3.30).

$$N_{D,\max P_R}^{*} = \frac{2}{15}\left(\frac{\beta_{2,\max P_R}^{III}\alpha^2}{\lambda\gamma N^{III}} + \frac{\beta_{1,\max P_R}^{II}}{N^{II}}\right) \tag{3.30a}$$

$$P_{R,i,max} = \frac{15\varepsilon_b Y_i C_{F,i}(\alpha-1)^2\varepsilon_p K_{se,1} D_{p,1}}{4N\rho_p {R_p}^2\left(\frac{\beta_{2,\max P_R}^{III}\alpha^2}{\lambda\gamma N^{III}} + \frac{\beta_{1,\max P_R}^{II}}{N^{II}}\right)} \tag{3.30b}$$

Eq. (3.25) and Eq. (3.27) indicate that the N_D^* to achieve maximum productivity ($N_{D,\max P_R}^{*}$) is about twice the value of the minimum N_D^* for the SEC-SMB to be feasible ($N_{D,min}^{*}$). The maximum productivity, given by Eq. (3.30b), is inversely proportional to R_p^2. Larger productivity can be achieved with smaller particles, longer fractional zone length (N^j/N) for Zones II and III, or larger feed concentration, selectivity, size-exclusion factor, and diffusivity.

The optimum column configuration for maximum P_R for diffusion controlled systems is shown in Eq. (3.31).

$$\frac{N^I}{N} = \frac{1}{N} \tag{3.31a}$$

$$\frac{N^{II}}{N} = \frac{N^{III}}{N}\sqrt{\frac{\beta_1^{II}\lambda\gamma}{\beta_2^{III}\alpha^2}} \tag{3.31b}$$

$$\frac{N^{III}}{N} = \frac{1-\frac{N^I}{N}-\frac{N^{IV}}{N}}{1+\sqrt{\frac{\beta_1^{II}\lambda\gamma}{\beta_2^{III}\alpha^2}}} \tag{3.31c}$$

$$\frac{N^{IV}}{N} = \frac{1}{N} \tag{3.31d}$$

The maximum productivity configuration for diffusion controlled systems is not a function of N_D^*. As such, there is one column configuration which will have a larger productivity than other configurations at every N_D^*. Once α, λ, γ, Y_i, and N are specified, the maximum productivity configuration can be determined from Eq. (3.31).

The values of β's for Zones II and III are often similar, so the maximum productivity column configuration mainly depends on γ/α, for small DV (< 0.02). A large γ/α indicates that more columns should be placed in Zone II than Zone III to contain the wave of the fast solute. The sharp wave of the slow solute in Zone III does not need as many columns when the diffusivity of the slow solute is very large. A small γ/α means the reverse. More columns are needed in Zone III to confine the spreading wave of the slow solute and Zone II does not need as many columns because there is enough difference in the wave velocities to keep the trailing wave of the fast solute confined in Zone II.

Equation (3.25) can be simplified since the term with the Peclet number is negligible. Additionally, the port velocity can be replaced with a function of N_D^*. Rearrangement results in Eq. (3.32a), Table 3.2.

This group can be considered as a ratio of the diffusion time ($t_{D,1}$) to pressure-limited convection time through a column in Zone I (t_c^I). Eq. (3.29a) indicates that $N_{\Delta P,\text{diff}}$ decreases with increasing N_D^*. For fixed material properties, yields, and equipment parameters, Eq. (3.29a) can be used to find the minimum N_D^* to satisfy the pressure limit. For a fixed diffusion time, a large value of $N_{\Delta P,\text{diff}}$ corresponds to a small pressure-limited convection time, or higher zone velocities.

The N_D^* for maximum sorbent productivity can be found from Eq. (3.27). This value can be used in Eq. (3.29a) to determine $N_{\Delta P,\mathrm{diff},\max P_R}$, which is the combination of $\Delta P_{max} R_p^4/L_c^2$ necessary to achieve the maximum sorbent productivity, Eq. (3.32b).

$$N_{\Delta P,\mathrm{diff},\max P_R} = \frac{\Delta P_{max} {R_p}^4}{37.5\phi\mu {D_{p,1}} {L_c}^2} = \frac{15\phi^2(\alpha-1)^2\varepsilon_p K_{se,1}}{2\left(\frac{\beta_{2,\max P_r}^{III}\alpha^2}{\lambda\gamma N^{III}}+\frac{\beta_{1,\max P_r}^{II}}{N^{II}}\right)}\left(\frac{1+\phi\delta_2}{\phi(\delta_2-\delta_1)}+\frac{\beta_2^I\alpha^2}{2\lambda\gamma N^I\left(\frac{\beta_{2,\max P_r}^{III}\alpha^2}{\lambda\gamma N^{III}}+\frac{\beta_{1,\max P_r}^{II}}{N^{II}}\right)}\right) \tag{3.32b}$$

For fixed material properties, yields, and column configuration, the right hand side of Eq. (3.32b) is fixed. Thus, the value of $\Delta P_{max} R_p^4/L_c^2$ for maximum productivity is fixed. For fixed particle size and operating pressure (limited by equipment or resin material), there is only one column length that can achieve the maximum productivity.

3.2.2.2 Dispersion Controlled

For axial dispersion controlled systems, N_D^* is very large and diffusion effects become negligible. The dispersion controlled versions of Eqs. (3.20-3.23) and (3.25) are shown in the last column of Table 3.2. The zone velocities for dispersion controlled systems are shown in Eq. (3.33). The resulting equation for *D/F* is presented in Eq. (3.34). For low Reynolds numbers, P_{eb}^* is independent of port velocity. When P_{eb}^* is 50 or larger, the effects of dispersion on *D/F* and P_R become negligible.

Similar to the diffusion controlled case, there is a minimum Peclet number for the SEC-SMB operation to be feasible and it is given by Eq. (3.35).

$$P_{eb,min}^* = \left(\frac{\beta_{2,\min P_{eb}}^{III}\Gamma_{min\,P_{eb}}^{III}}{N^{III}}+\frac{\beta_{1,\min P_{eb}}^{II}\Gamma_{min\,P_{eb}}^{II}}{N^{II}}\right) \tag{3.35}$$

Equation (3.22) shows that P_R depends on L_c and P_{eb}^*. However, L_c can be expressed as a function P_{eb}^* using the Chung and Wen correlation for low Reynolds numbers ($Re < 10$), for which E_b^j is related to ε_b, R_p, and u_0^j as follows. [79].

$$E_b^j = 10\varepsilon_b R_p u_0^j \tag{3.36}$$

Since $P_{eb}^{IV} = L_c v/E_b^j$, Table 3.1, one can obtain Eq. (3.37).

$$P_{eb}^{IV} = \frac{L_c v}{10\varepsilon_b R_p u_0^{IV}} \tag{3.37a}$$

$$P_{eb}^{*} = \frac{\phi(\delta_2-\delta_1)L_c v}{10\varepsilon_b R_p u_0^{IV}} \tag{3.37b}$$

The u_0^{IV} in Eq. (3.37) can be replaced by Eq. (3.33d) to obtain Eq. (3.38a) and rearranged to solve for column length, Eq. (3.38b).

$$P_{eb}^{*} = \frac{\phi(\delta_2-\delta_1)}{(1+\phi\delta_1)}\left[\frac{L_c}{10\varepsilon_b R_p} + \frac{\beta_1^{IV}}{N^{IV}}\right] \tag{3.38a}$$

$$L_c = 10\varepsilon_b R_p \left[\frac{P_{eb}^*(1+\phi\delta_1)}{\phi(\delta_2-\delta_1)} - \frac{\beta_1^{IV}}{N^{IV}}\right] \tag{3.38b}$$

Equation (3.38b) can be substituted for the column length in Eq. (3.22), where the terms with N_D^* are negligible, to obtain Eq. (3.39).

$$P_{R,i} = \frac{\nu Y_i C_{F,i}}{10N\varepsilon_b R_p\left[P_{eb}^{IV}(1+\phi\delta_1) - \frac{\beta_1^{IV}}{N^{IV}}\right]\phi\rho_p}\left[\phi\delta_1(\alpha-1) - \frac{1}{P_{eb}^{IV}}\left(\frac{\beta_2^{III}\Gamma^{III}}{N^{III}} + \frac{\beta_1^{II}\Gamma^{II}}{N^{II}}\right)\right] \tag{3.39a}$$

The P_{eb}^* for maximum P_R ($P_{eb,\max P_R}^*$) can be found by taking the partial derivative of Eq. (36b) with respect to P_{eb}^* and setting the resulting equation to zero. The value of $P_{eb,\max P_R}^*$ can be determined from yields, material properties, and column configuration, see Appendix A3. The optimum column configuration for maximum P_R for dispersion controlled systems is shown in Eq. (3.40).

$$\frac{N^I}{N} = \frac{1}{N} \tag{3.40a}$$

$$\frac{N^{II}}{N} = \frac{N^{III}}{N}\sqrt{\frac{\beta_1^{II}\Gamma^{II}}{\beta_2^{III}\Gamma^{III}}} \tag{3.40b}$$

$$\frac{N^{III}}{N} = \frac{1 - \frac{N^I}{N} - \frac{N^{IV}}{N}}{1 + \sqrt{\frac{\beta_1^{II}\Gamma^{II}}{\beta_2^{III}\Gamma^{III}}}} \tag{3.40c}$$

$$\frac{N^{IV}}{N} = \frac{1}{N} \tag{3.40d}$$

Equation (3.25) can be simplified into Eq. (3.41) because the term with N_D^* is negligible, Table 3.2. This group can be considered as a ratio of step time to pressure-limited convection time through a column in Zone I. The column length in Eq. (3.41) can be replaced by Eq. (3.38b). Thus, for fixed material properties and maximum pressure, the maximum port velocity at every P_{eb}^* can be found. The value of $P^*_{eb,\max P_R}$ (Appendix A3) can be substituted into Eq. (3.41) and rearranged to find the port velocity for maximum P_R, Eq. (3.42).

$$\nu_{\max P_R} = \frac{\Delta P_{max} R_p}{375\phi^2\mu\varepsilon_b\left[\frac{P^*_{eb}(1+\phi\delta_1)}{\phi(\delta_2-\delta_1)} - \frac{\beta_1^{IV}}{N^{IV}}\right]\left[1 + \phi\delta_2 + \frac{\beta_2^I\Gamma^I\phi(\delta_2-\delta_1)}{P^*_{eb,\max P_R}N^I}\right]} \tag{3.42}$$

The port velocity in Eq. (3.42) will achieve the maximum productivity when yields, material properties, column configuration, viscosity, and maximum operating pressure are specified. If R_p is fixed, there is only one L_c that can satisfy $P^*_{eb,\max P_R}$, as expected from Eq. (3.38b). Using this port velocity to achieve maximum P_R, ensures that the minimum cost design will not be pressure limited.

3.2.2.3 Optimization Using SSWD

The values of the 15 decision variables (Y_i, R_p, L_c, DV, N^j, ΔP_{max}, u_0^j, and ν), which will achieve minimum solvent, maximum productivity, or minimum cost can be found using the SSWD. Overviews of D/F and P_R as functions of N_D^* and P_{eb}^* can be generated using Eq. (3.21) and Eq. (3.22), respectively, for given input parameters (material properties, yields, column configuration, dead volume, and maximum operating pressure). Minimum solvent consumption and maximum productivity can easily be identified from these overviews. With given cost functions, the total cost surface can also be generated as a function of N_D^* and P_{eb}^*. By varying the input parameters of interest, the surfaces can be used to determine optimum input parameters for minimum solvent consumption, maximum productivity, or minimum cost.

Optimization of the decision variables for maximum productivity becomes simpler for the limiting cases already discussed in Sections 3.2.2.1 and 3.2.2.2. For diffusion controlled systems, the value of N_D^* and the column configuration can be analytically determined using Eq. (3.30a) and Eq. (3.31), respectively. For dispersion controlled systems, the value of P_{eb}^* and the column configuration can be analytically determined using Eq. (A3.1a) and Eq. (3.41), respectively. However, the values of N_D^* and P_{eb}^* for maximum productivity may not be achievable because not all combinations of port velocity and column length can satisfy a given pressure limit, Eq. (3.25).

For cost optimizations in this work, the costs are based on $/kg of product. Detailed cost functions are given in Appendix A4. The overall separation cost (total cost) consists of equipment cost, sorbent (or resin) cost, and solvent cost. Equipment cost is mainly controlled by the maximum allowable pressure and total number of columns, Eq. (A4.2).

Resin cost can be calculated from the sorbent productivity, Eq. (A4.3). Solvent cost can be calculated from solvent consumption, Eq. (A4.4).

Optimization of decision variables for minimum cost can be achieved by evaluating the total cost using the zone velocities and port velocity determined from the SSWD equations. For the insulin example discussed in Chapter 7, four of the decision variables (Y_i, R_p, and DV) are fixed and the remaining 11 are optimized. The algorithm used to optimize the 11 decision variables (column configuration, column length, operating pressure, zone velocities, and port velocity) to achieve minimum cost is shown in Appendix A5, Figure A5.A.1. The example algorithm can easily be extended to optimize the remaining decision variables.

3.2.3 Preloading Strategies for Fast Startup of SMB

The SWD method gives the operating parameters to achieve desired product purity or yield at steady state. However, it does not give the time for an SMB system to reach cyclic steady state (startup time), which can be determined using experiments or a simulation program, such as VERSE (description in Section 4.4). Generally, for an SMB starting from clean columns to reach cyclic steady state, the ports must move around the loop three or more times (cycles) [62]. Fast startup methods are needed to significantly reduce the time and materials required for startup.

A number of strategies for startup of SMB systems have been reported in the literature. One proposed method is for the operating parameters to be different from their cyclic steady-state values [80,81]. Xie et al. [57] proposed the following preloading strategy to reduce SMB startup time. Several columns were preloaded with feed solution.

The columns were then connected and elution was used to obtain approximately the steady-state concentration profiles predicted by VERSE.

In this work, two strategies were developed and compared to the literature method of Xie et al. and startup from clean columns. To better approximate the steady-state column profiles, the first strategy involves preloading different columns with solutions of different concentrations, which were determined by VERSE simulations. The columns in Zone I were preloaded with a solution of the slow-moving solute at the steady-state concentration of the extract obtained from VERSE. Similarly, the columns in Zone III were preloaded with a solution of the fast-moving solute at the steady-state concentration of the raffinate obtained from VERSE. The columns in Zone II were preloaded with a solution of both solutes at the same concentrations as the other two preloading solutions. The columns were then connected and elution was used to shift the solute bands into their stead-state positions. The second strategy uses the same method as the first, except the preloading concentrations were set to be the same as the product concentrations determined by mass balance using the zone velocities determined from SSWD.

CHAPTER 4. METHODS AND MATERIALS

4.1 Materials

Pure standards of polycarbonate (PC), brominated polycarbonate (BrPC), styrene acrylonitrile (SAN), polystyrene (PS), resorcinol bis-diphenylphosphate (RDP), and bisphenol A bis-(diphenyl phosphate) (BPADP) were obtained from SABIC Innovative Plastics (SABIC-IP) in Mt. Vernon, IN. RDP and BPADP are blended with polymers for their flame retardant properties. A computer housings waste with a high PC content, simply referred to as "crude waste," was also obtained from SABIC-IP. A second type of crude polymer waste from recyclers was provided by SABIC-IP and was given the designation "Trommel" based on the type of separation used at the recycling facility. Tetrahydrofuran (THF) was obtained from Aldrich chemical company, Milwaukee, WI, USA. Acetonitrile (ACN) and isopropanol (IPA) were obtained from Mallinckrodt Baker, Inc. from Phillipsburg, NJ, USA. Dichloromethane (DCM) and acetone (ACE) were obtained from Macron Fine Chemicals, US. All solvents were > 99.5% pure. Blue dextran (average molecular weight = 2,000,000 Da) was obtained from Sigma-Aldrich. The packing material used for SMB experiments was Amberlite XAD 1180N, which was purchased from DOW Water and Process Solutions. The average particle size was 450 μm with an average pore size of 450 Å.

4.2 Equipment

An Agilent 1100 HPLC with micro vacuum degasser, two binary pumps, autosampler, and variable wavelength detector was used for all HPLC analyses. The column was an Inertsil ODS-2 HPLC column, which was 150 mm in length, had an inner diameter of 4.6 mm, and particle size of 5 microns. Centrifugation was done with a Beckman Coulter Allegra 21 series centrifuge. Mass measurements less than 200 g were done on a Mettler Toledo NewClassic MF. Mass measurements greater than 200 g were done using a Denver Instrument XL-3100. Chopping of the crude waste particles was accomplished using a Cuisinart model BFP-10CH blender.

Batch SEC chromatography experiments were accomplished using a diode array detector (Agilent 1260 DAD VL), two Agilent PrepStar SD-1 pumps, a manual injection system, and an Agilent 440-LC fraction collector.

The SMB experiments were performed using a SEMBA Biosciences Octave 100 SMB unit with four pumps, all of which were compatible with dichloromethane. The pump configuration is shown in Figure 3.1. The 8 columns for the SMB experiments were obtained from ACE Glass, Inc. and were 65 cm in length with an inner diameter of 2.54 cm. SMB column packing that required recirculating solvent used an IsmaTec IP 65 pump.

4.3 Procedures

4.3.1 HPLC Analysis

A method to analyze SAN and the flame retardants (RDP, BPADP) was developed based on the principle of gradient polymer elution (GPEC) chromatography [24]. In GPEC, the sample was injected into a poor solvent for the components so that the components

precipitated on the solid phase [82]. The mobile phase was then gradually changed to become a stronger solvent for the components, such that the components would redissolve at different mobile phase compositions. The different solubilities of the components in different mobile phase compositions provided the necessary separation for the components to be detected by a UV detector.

The poor solvent used was ACN and the strong solvent was THF. The main UV signal used for detection was 260 nm. The column was heated to 32°C and the injection volume was set to 10 μL. Pure component standards were used to develop calibration curves. The flowrate and solvent gradient are shown in Table 4.1.

Table 4.1. ACN/THF gradient for analytical HPLC method.

Time (min)	Flowrate (mL/min)	%ACN	%THF
0.0	0.1	99	1
12.0	0.1	99	1
12.1	1	99	1
12.5	1	72	28
12.7	1	73	27
15.2	1	70	30
15.5	1	64	36
15.7	1	65	35
16.7	1	65	35
17.0	1	50	50
17.2	1	51	49
18.2	1	51	49
18.4	1	1	99
20.0	2	1	99
20.1	2	99	1
22.5	2	99	1

4.3.2 GPEC Screening

GPEC was used to quickly evaluate the effective polymer separation of all the possible compositions between a strong solvent and a weak solvent. The GPEC solvent pairs were tested by equilibrating the HPLC column with 100% weak solvent and then injecting samples of polymer standards dissolved in DCM. The mobile phase was kept as pure weak solvent for at least two minutes in order to allow sufficient time for the polymers to precipitate on the solid phase in the column. After the initial wait time, the mobile phase composition (vol.%) was changed linearly from 0% to 100% strong solvent over at least 8 minutes. The mobile phase was kept at 100% strong solvent for at least 2 minutes in order to ensure complete dissolution of all the polymers from the column. The mobile phase was then changed back to pure weak solvent over a time period of six seconds. The mobile phase composition was kept at pure weak solvent for at least two minutes in order to re-equilibrate the column to be ready for the next injection. Flowrate, injection volume, and detection wavelength for each pair are summarized in Table 4.2.

Table 4.2. Flowrates, solvent gradients, detection wavelengths, and injection volumes for GPEC experiments with four solvent pairs.

Parameter	**MeOH/ DCM**	**HEX/ THF**	**IPA/ THF**	**ACN/ THF**
Flowrate (mL/min)	1.0	1.0	0.5	1.0
Injection volume (μL)	20	10	10	20
Detection wavelength (nm)	254	260	260	260
Time from injection to start of gradient (min)	2	4	4	2
Linear gradient time (min)	8	28	10	10
Time composition held at pure strong solvent (min)	3	5	2	2
Re-equilibration time (min)	2	3	3	1

4.3.3 Visual Dissolution Tests

A 0.5 g sample of a polymer standard was added to a 10 mL mixture of ACE and DCM at room temperature and continuously stirred at 100 rpm. The polymer was considered to have sufficient solubility in the mixed solvent if the solid polymer pellets were no longer visible within 12 hours. If the polymer pellet was still visible after 12 hours, the polymer was considered to be insufficiently soluble in the mixed solvent. ACE/DCM compositions were tested until compositions with sufficient solubility were found for each polymer standard. Compositions were chosen by interval halving from ACE to DCM. Thus, pure acetone was tested first, followed by 50/50 (vol.%) ACE/DCM, then 25/75 ACE/DCM, etc.

4.3.4 Extraction

The solid crude was ground using a Cuisinart blender and blending on low for 10 minutes. The ground particles were sieved to collect the particle between 250 and 850 microns in diameter. Particles larger than 850 microns were sent back to the blender for further size reduction.

Extraction steps were performed in canning jars (approximately 400 mL). The tight seals of the canning jars were ideal when dealing with solvents with high vapor pressures (ACE and DCM). Between 0.25 and 30 grams of the solid particles were added to a canning jar along with a magnetic stir bar. The extraction solvent was pre-mixed, and then added to the same jar to reach between 5 and 25 wt.% solids. The solution was continuously stirred at 50-150 rpm at 20°C in the fume hood. Unless noted otherwise, extractions were left overnight and sampling occurred the next day.

Filtration of the solids from the liquid after an extraction step was performed by pouring the solution into a ceramic Büchner funnel lined with filter paper with 40 µm pores. The liquid was allowed to pass through the filter paper and drip through the funnel into a beaker. The solids remaining in the funnel were rinsed with clean solvent (same solvent as was used for that extraction) in order to remove any inter-particle solution contaminated with dissolved polymers.

When centrifugation was used to separate the liquid phase(s) from the solid phase(s), it was done by collecting samples (~ 10 mL) into glass vials with screw caps. These vials were placed in the centrifuge and spun at 8,000 rpm for 30 minutes. The liquid phase(s) could then be poured into another container without disrupting the solids. If the solids were needed for another extraction, then the solids were rinsed with solvent of the same composition as the previous extraction, centrifuged one more time, the solvent was then poured into waste and the solids were dried and then poured into the next extraction vessel.

4.3.5 Column Packing

The XAD 1180N resin was packed with sodium chloride and sodium carbonate salts in the pores to prevent bacterial growth. These salts must be removed to access all the pore space in the particles so the resin was washed with reverse-osmosis (RO) water using a resin to water ratio of 1:1.5 under stirring conditions for over 3 hours to remove the salts from the particles. The liquid was decanted, and the resin was washed two more times in the same manner to ensure that the salts were removed. After washing, the resin was dried overnight at room temperature in a fume hood and then weighed. Isopropanol (IPA) was added to the resin particles in a 1:1 volume mixture and sonicated for 30 minutes to

removed bubbles from the porous particles. The low density of IPA ensured that all the resin particles were completely submerged and IPA can be easily displaced by the acetone/dichloromethane mixture which was used in later experiments. The mixture was allowed to settle overnight.

The dead volume for each column was determined by weighing the column caps dry and then reweighing the caps after pumping RO water through the caps until air bubbles were no longer produced.

Once the dry weights of all the parts of the column were obtained, a slurry, which consists of equal volumes of resin and IPA, was poured into the column with one end fitting attached at the column outlet without a plug, so the IPA was allowed to flow out of the column. When the top of the resin packing reached the top of the column, the bottom fitting was plugged and the other end fitting of the column was attached and plugged. IPA was recycled using downward flow at more than 30 mL/min. If the resin packing height was reduced, then more resin/IPA slurry was added to the top of the column and the IPA recycle was repeated. If the packing height did not change after more than 2 hours, the column was considered packed.

4.3.6 Column Characterization

To determine the interparticle bed void fraction (ε_b), 10 mL pulses of 0.5 g/L blue dextran in 50/50 IPA/water were detected at a wavelength of 500 nm. The flowrate was 5 mL/min with a downward flow direction. After the bed void fraction was determined, the solvent in the columns was exchanged for 50/50 (vol.%) DCM/ACE.

The total void fraction (ε_t) was determined from long pulses of RDP since it was small enough to completely penetrate all the pores of the particles. Long pulses were

performed by feeding 1-1.3 column volumes (CV) of the polymer or flame retardant solution to the column, and then changing the feed to clean eluent to wash the column. The resulting breakthrough and wash curves were used to determine size exclusion factors of the different components. VERSE simulations of the experiments were used to determine apparent pore diffusivities for each component by fitting the simulations to the experimental data. Initial estimates for the pore diffusivities were obtained from the Brownian diffusivities, D_∞ (calculated using the Stokes-Einstein equation [83]), and the Mackie-Meares correlation [84]. The hydrodynamic radius for polymers was approximated by using a correlation by Fetters et al. for the size of polystyrene in cyclohexane at different molecular weights [85]. The flowrate was 5 mL/min in downward flow.

Since the mobile phase was 50% ACE by volume, SAN, RDP, and BPADP could not be monitored by the UV detector because of the large absorbance of ACE at all detectable wavelengths. To obtain breakthrough curves, effluent samples were collected periodically and analyzed by HPLC.

4.3.7 SMB Fast Startup

The SEMBA system allowed for a feed solution to be pumped through specific columns and then sent to waste. For each preloading, a solution was pumped at 15 mL/min through a single column for 20 minutes. During this period, effluent samples were taken at 11, 13, 15, 17, and 19 minutes after the start of the loading. If the solution contained SAN, sampling times were added at 7 and 9 minutes. The samples were analyzed using HPLC to obtain breakthrough curves, which can be compared with VERSE simulations to verify the parameters.

After the 20 minutes had elapsed, the SEMBA unit added the next column in series to the original column. The same solution was again pumped at 15 mL/min for 20 minutes with the same sampling schedule. After two columns had been loaded, the solution was changed and the process was repeated for the next set of columns.

This procedure was performed for Runs 1, 4, and 6. For Runs 4 and 6, an elution step was added after the three sets of columns were loaded. Clean eluent was pumped through all 8 columns connected in series at 5 mL/min for 20 minutes. This elution step shifted the concentration profiles into the same positions as the steady-state concentration profiles, which reduced the amount of time for the SMB experiments to reach cyclic steady state.

4.3.8 SMB Operation

The feed solutions were made by dissolving SAN, RDP, or BPADP in 50/50 DCM/ACE by volume. The eluent was clean 50/50 ACE/DCM by volume. The pump flowrates and switching time were determined from the Speedy Standing Wave Design (SSWD) method and set in the SEMBA program. Glass bottles (~100 mL) were used to collect the extract and raffinate product streams for HPLC analysis. Immediately after a switch, a set of bottles (Set 1) was substituted with a new set of bottles (Set 2) while the currently full set was weighed. Samples of roughly 20 mL were taken from the bottles for archival purposes. Small (~1 mL) samples were taken and analyzed by HPLC to determine the polymer concentrations in each product stream. Extract samples were diluted to 50% of the original concentration to keep RDP concentrations within the linear region of the established calibration curve. The bottles of Set 1 were then emptied, rinsed with DCM, and dried before replacing the bottles of Set 2 after the next switch.

4.4 Simulation

A detailed rate-model simulation package, VErsatile Reaction and SEparation (VERSE) [86], was used to verify the material properties and SMB operating parameters. Given the material properties, equipment parameters, and operating parameters, VERSE can generate transient column profiles, effluent histories, and product concentrations.

The VERSE simulation program was developed in Wang's group and is an expanded version of an earlier rate model for batch chromatography, which was based on axial dispersion, film mass transfer, intraparticle pore diffusion, and equilibrium competitive adsorption and ion exchange [87]. The original VERSE program was expanded to include nonequilibrium (or slow) adsorption and desorption [88], aggregation reactions in the mobile phase [89–91], denaturation reactions in the stationary phase [92], surface diffusion, and parallel pore and surface diffusion [93]. VERSE was further expanded from batch systems to carousel [94] and SMB [60,95] systems, in addition to expanded and fluidized beds [96,97].

VERSE has been validated with experimental data from many different batch chromatography and SMB processes [98–100]. Purities and yields from VERSE can be compared to those specified in SWD. Verification of the SWD using VERSE reduced the number of SMB experiments for process development. VERSE simulations also were used to develop strategies to reduce startup time. Lab-scale SMB experiments were performed to verify the component splitting, purity, and yield predicted by VERSE as well as to validate the SSWD equations for ternary mixtures and the fast startup methods.

CHAPTER 5. RESULTS – MIXED-SOLVENT EXTRACTION FOR POLYCARBONATE

5.1 Hansen Solubility Parameters for Polymers in Common Solvents

An initial screen based on HSP values yielded 11 strong solvents and 11 weak solvents for polycarbonates, Figure 5.1. No HSP values for RDP and BPADP were found. Nonetheless, both compounds were soluble in the solvents tested. ABS, by contrast, was found to have a negligible solubility in DCM in a 24 hour test. For these reasons, the solubility spheres of RDP, BPADP, and ABS are not shown in Figure 5.1.

The solubility spheres of PC, PS, and SAN have large overlapping regions because they have similar properties. Strong solvents for PC, such as DCM and THF, which are within the solubility sphere of PC, are also strong solvents for SAN and PS. Similarly, weak solvents for PC, such as methanol and ACN, are also weak solvents for the other two polymers. To recover PC from SAN and PS in a single extraction step, a solvent must be located within the PC solubility sphere and outside the solubility spheres of SAN and PS. As shown in Figure 5.1, none of the 11 strong solvents for PC exist in this region.

According to the HSP values, three pure solvents may be used sequentially to separate PC from RDP, BPADP, PS, SAN, and ABS. Acetone can be used first to dissolve SAN, RDP, and BPADP. Benzene is then used to dissolve PS, leaving behind PC and ABS.

Lastly, DCM can be used to extract PC from ABS. However, this method requires three extraction steps and uses benzene, which is an expensive solvent with a relatively high boiling point, or a high solvent recycle cost.

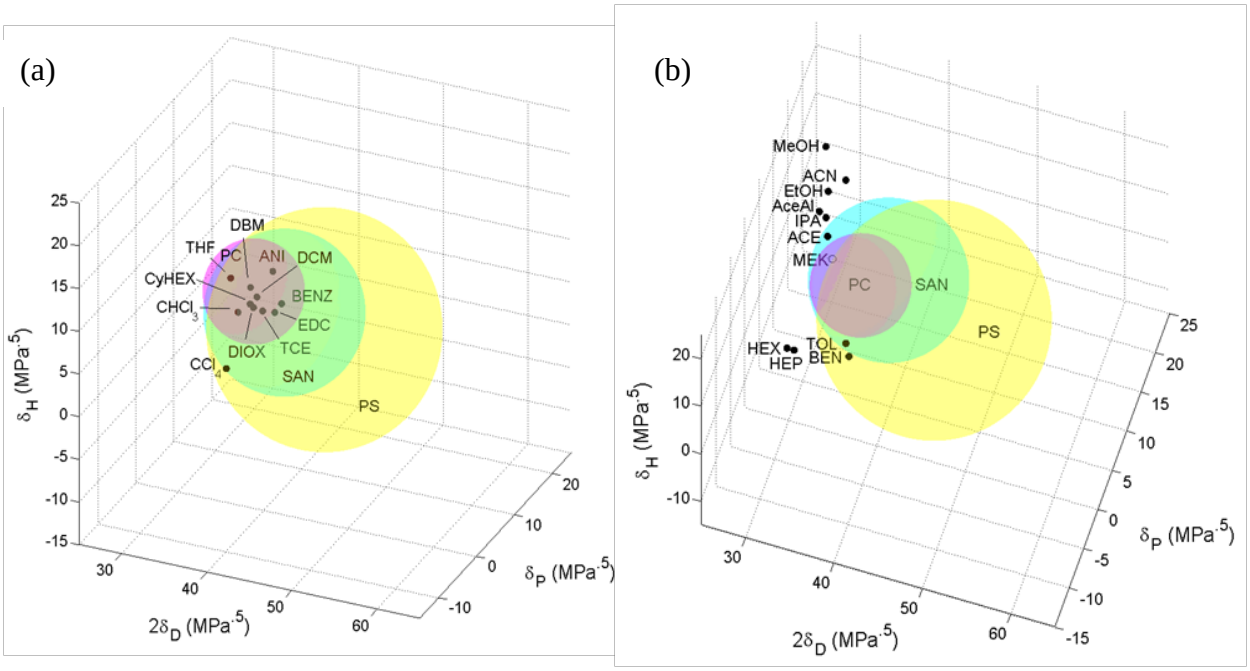

(c) Strong Solvents

Chemical	Cost ($/kg)[c]	B.P. (°C)
Dichloromethane (DCM)	0.50	40
1,2-Ethylene dichloride (EDC)	0.56	84
Chloroform ($CHCl_3$)	0.70	61
1,4-Dioxane (DIOX)	1.00	101
1,1,2,2-Tetrachloroethane (TCE)	1.00	147
Aniline (ANI)	1.60	184
Cyclohexanone (CyHEX)	1.90	156
Carbon tetrachloride (CCl_4)[d]	2.00	77
Tetrahydrofuran (THF)	2.50	66
Benzaldehyde (BENZ)	2.50	178
Dibromomethane (DBM)	5.00	97

(d) Weak Solvents

Chemical	Cost ($/kg)[c]	B.P. (°C)
Methanol (MeOH)	0.35	65
Ethanol (EtOH)	0.60	78
Isopropyl alcohol (IPA)	0.66	83
Acetone (ACE)	0.70	56
Methyl ethyl ketone (MEK)	0.70	80
Acetonitrile (ACN)	0.71	82
Toluene (TOL)	0.85	111
Acetaldehyde (AceAl)	0.90	20
Benzene (BEN)	1.03	80
n-hexane (HEX)	1.28	68
n-heptane (HEP)	1.40	99

[c] Costs retrieved from alibaba.com or ICIS.com
[d] Experimental data indicates carbon tetrachloride can dissolve PC

Figure 5.1. Hansen solubility spheres for PC, PS, and SAN plotted with strong solvents (a) and weak solvents (b). Solvent costs and boiling points are listed in (c) for strong solvents and (d) for weak solvents.

A reduction in the number of extraction steps from three to two can reduce significantly the cost and the environmental impact of the process. A weak solvent for PC, which is located within the solubility spheres of PS and SAN, can dissolve PS, SAN, RDP, and BPADP, leaving behind PC and ABS. A strong solvent (DCM) can then be used to recover PC from ABS. However, none of the 11 weak solvents for PC fall in this region.

While none of the pure solvents can dissolve both SAN and PS with RDP and BPADP, a mixture of two miscible solvents may have an intermediate HSP property to meet this requirement. If there are no significant non-ideal molecular interactions between the two solvents, their HSP's are expected to be additive. Then the resulting HSP of a mixed solvent should form a straight line between the values of the two single solvents [102,103]. As shown in Figure 5.2a, a DCM/ACE mixture should have properties along the dashed line, which passes through the overlapping region of the PS and SAN solubility spheres. A portion of the dashed line is outside the PC solubility sphere. Therefore, a DCM/ACE mixture should be able to dissolve RDP, BPADP, SAN, and PS in one extraction step, leaving PC and ABS behind. DCM can be used next to extract PC, leaving ABS behind.

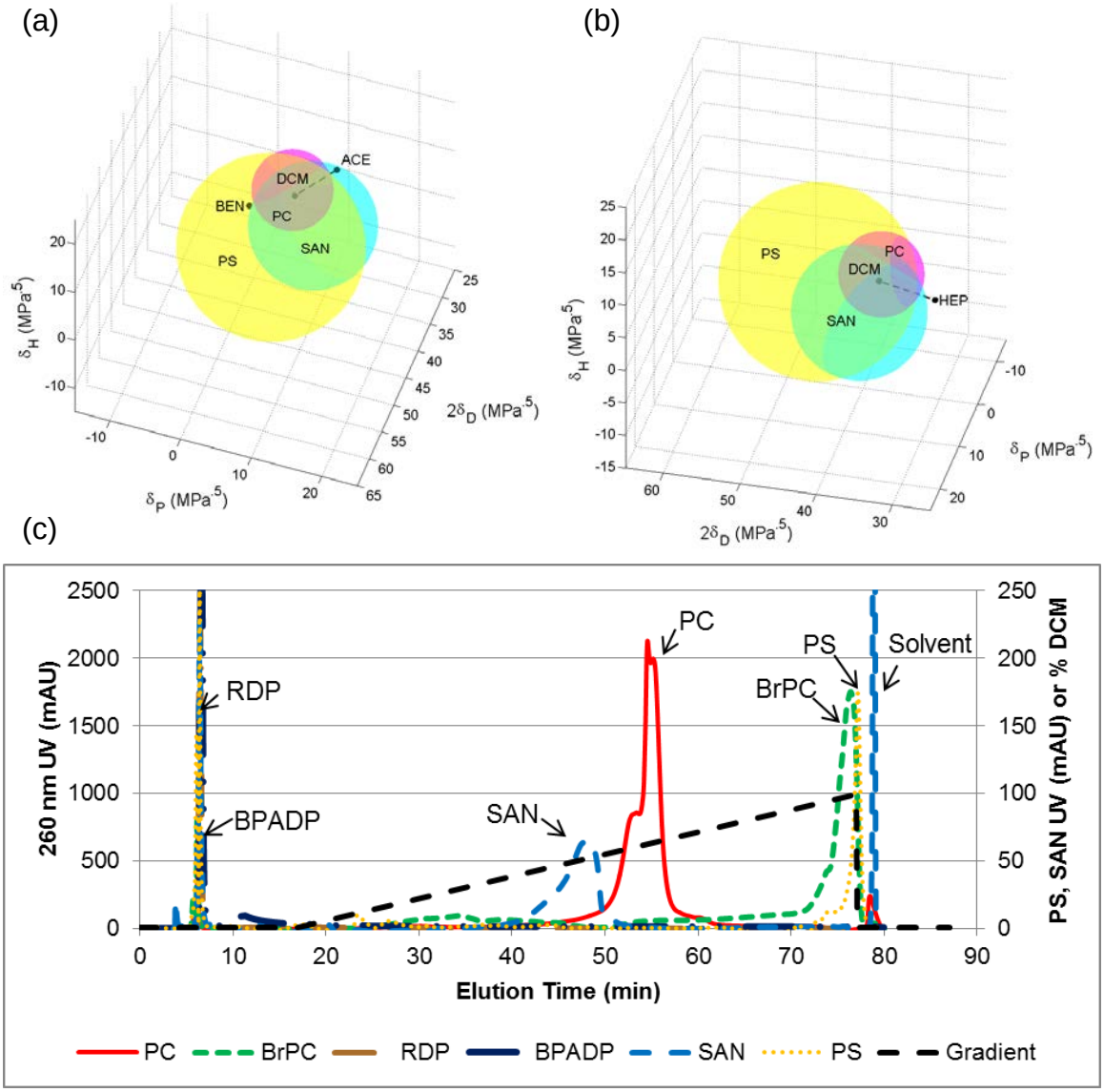

Figure 5.2. Hansen solubility parameter plots showing the solubility spheres of PC (red), PS (gold), and SAN (blue) along with pairs of strong and weak solvents: (a) ACE and DCM, (b) HEP and DCM. The dashed lines represent the linear combinations of solubility parameters for the two pairs of solvents. (c) Chromatogram of GPEC of polymer standards using a linear heptane/DCM gradient (black dashed line). Column outlet gradient is shown in order to easily determine solvent compositions for extractions.

5.2 HPLC Analysis of Polymer Mixtures

The overlaid chromatograms of the pure component standards are shown in Figure 5.3. Since low MW polymers dissolve in weaker solvents than high MW polymers, it can be inferred that this first PC peak was composed of low MW PC. The higher MW PC dissolved when the THF composition increased to 99%. The total PC concentration was determined by summing the areas of these two peaks. The next major set of peaks was from BrPC. BrPC dissolved at multiple THF compositions, which was indicative of the MW distribution of the polymer. The majority of the BrPC dissolved at 51/49 ACN/THF. This is a unique peak for BrPC, so it was used for calibration. The major component of the dissolvable polymers is PC. The SAN and low MW PC peaks overlapped at this concentration. Estimation of the SAN peak area by peak deconvolution allows for the composition of the crude to be determined.

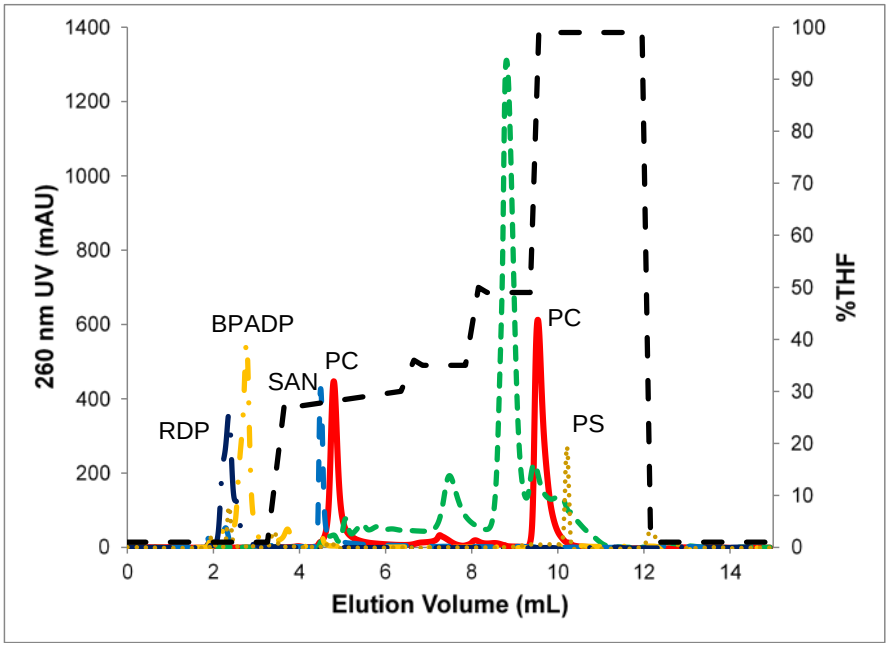

Figure 5.3. Superimposed chromatograpms of pure polymer standards dissolved in DCM (1.0 wt.%) using an ACN/THF solvent gradient to anlyze polymer mixtures.

The calibration curve created from polymer standards for the ACN/THF GPEC analysis is shown in Figure S2. The linear regressions for each polymer fit very well. R^2 values are > 0.98 for all polymers except PS. Since PS has a comparatively low absorbance at 260 nm, the regression does not fit as well, even though it is still has an R^2 of about 0.95.

(a)

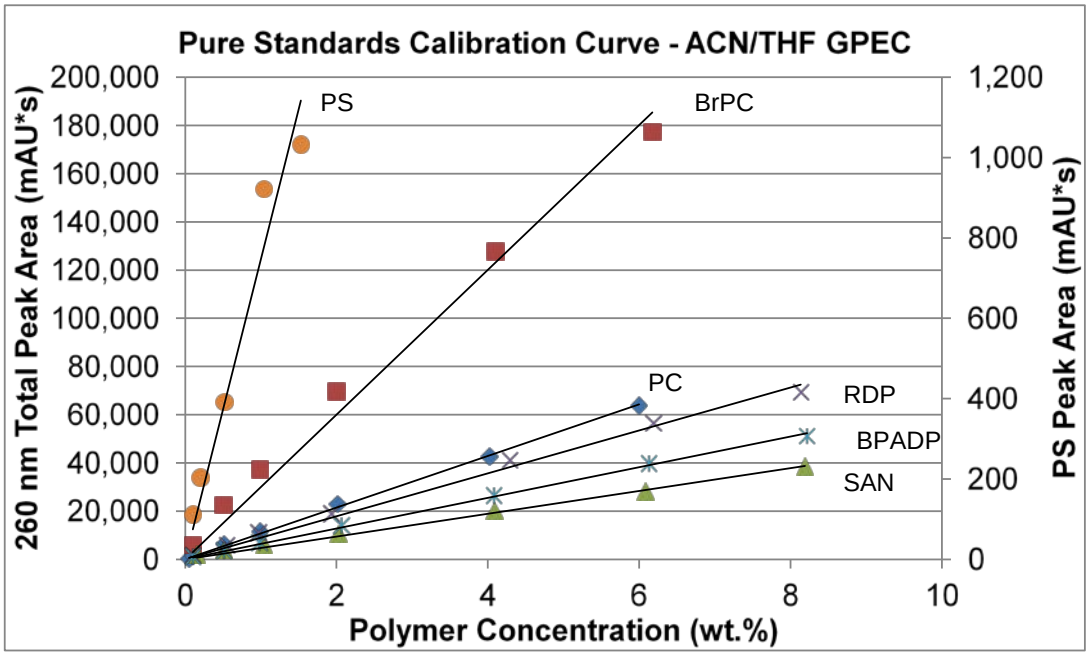

(b)

Component	Slope (mAU*s/wt.%)	R^2
PC	10,713	0.9987
BrPC	30,021	0.9867
PS	746	0.9465
SAN	4,727	0.9941
RDP	8,917	0.9928
BPADP	6,366	0.9984

Figure 5.4. (a) Calibrations of pure polymer standards dissolved in DCM using ACN/THF solvent gradient. (b) Table of linear regressions passing through (0,0) and curve R^2 values.

5.3 Gradient Polymer Elution Chromatography to Screen Potential Solvent Pairs

A challenge of designing a mixed solvent, however, is that there are a large number of binary pairs, up to 121 for the solvents in Figure 5.1. Among the miscible pairs, there are at least 10 potential compositions for each pair, leading to many experiments. Gradient polymer elution chromatography (GPEC) was used as a second screening tool to greatly reduce the number of experiments needed to find the solvent mixture compositions which can achieve selective PC separation from the other components. In addition, GPEC can also test the predictions of the HSP theory and the key assumptions made in choosing the solvent pair, namely that there are no kinetic limitations and no non-ideal interactions in the solvent pair.

GPEC has been used for the analysis of many different polymer mixtures [25,104,105]. It is based on polymer precipitation and redissolution mechanisms [24,82,106]. The column is pre-equilibrated with a weak solvent for the polymers. As the polymer sample is injected into the column, the polymers precipitate near the column inlet. The solvent strength is then gradually increased by increasing the concentration of the strong solvent in the mobile phase. As the solvent strength of the mobile phase increases, different polymers are re-dissolved and eluted at different times according to their solubilities [24]. The composition of the mobile phase, which can dissolve each individual polymer, can be readily identified from the GPEC chromatogram, Figure 5.2c. The elution order of the polymers can be determined by using pure standards of the polymers present in the waste. This information can help find the compositions of the mixed solvents needed in single extraction or sequential extraction processes. A specific example for PC separation is discussed below.

One promising solvent pair found from the HSP screening is heptane as the weak solvent and DCM as the strong solvent, Figure 5.2b. A mixture rich in heptane is expected to extract RDP and BPADP. As the DCM fraction increases, SAN is expected to dissolve first, followed by PC. PS is expected to dissolve last in a mixture rich in DCM. This qualitative prediction from HSP theory was tested using GPEC. The elution sequence in Figure 5.2c is consistent with the HSP predictions.

The solvent compositions corresponding to the polymer elution peaks in Figure 5.2c can be used for developing a sequential extraction scheme using two mixed solvents to recover PC. The first extraction uses 45/55 (vol.%) heptane/DCM to dissolve RDP, BPADP, and SAN, while leaving PC, BrPC, PS, and ABS in the solid polymer. PC can then be extracted using a mixture of 20/80 (vol.%) heptane/DCM, leaving BrPC, PS, and ABS behind as solids.

The extraction order can be reversed if needed. A mixture of 20/80 (vol.%) heptane/DCM (a strong solvent for PC) can be used in the first extraction step, while in the second extraction step, a mixture of 45/55 (vol.%) heptane/DCM (a weak solvent) is used. In this scheme, the first extraction step dissolves RDP, BPADP, SAN, and PC, leaving BrPC, PS, and ABS behind. Heptane would then be added to the liquid fraction to bring the solvent composition up to 45/55 (vol.%) heptane/DCM. PC would precipitate, while RDP, BPADP, and SAN would remain in solution.

Both options would lose a small amount of low molecular weight PC, which has a similar solubility as SAN. In the second scheme, some entrainment may occur during the PC precipitation, which can result in a lower PC purity.

Four other potential solvent pairs identified from HSP were tested using GPEC and the results are shown in Figures D.1-D.4 in Appendix D. Overall, the use of GPEC confirmed the predictions from HSP, except for one pair (IPA and THF), in which hydrogen bonding interactions between IPA and THF can occur [107]. More importantly, GPEC helped determine the two potential mixed-solvent compositions, which can be used in two sequential extraction steps to selectively separate a specific polymer from other polymer impurities. If the polymer of interest is found to elute first or last in GPEC, only one mixed solvent is needed to isolate it.

While GPEC can help screen all the solvent compositions, it does not provide adequate information on the maximum concentrations of the dissolved polymers. GPEC also requires that the redissolution kinetics of the polymers be fast (< 1 minute) in order to determine the optimal solvent compositions. The polymers should have high solubility in the solvent for the extraction process to be economical. Solubility tests are needed once the mixed-solvent compositions have been determined from GPEC.

5.4 Sequential Extraction for Polymer Recovery

To develop a sequential mixed-solvent extraction process to recover PC from a specific electronic waste stream (Figure 1.2), strong and weak solvents were screened using HSP and GPEC. The numbers of solvent pairs were reduced further by considerations of miscibility, purchase price, boiling point, which affects the solvent recycle cost, safety, and environmental impact. DCM was chosen as the best strong solvent because of its low recycle cost, low price, high polymer solubility, and its extensive use in industry for polymer processing. ACE and methanol were considered the best weak solvent candidates

for the same criteria. Heptane was not deemed to be a suitable weak solvent, because of its high price and recycle cost. The GPEC results for methanol/DCM, however, showed that methanol has no selectivity for PS vs. PC (Appendix D). Since PS is a major component in some wastes (Appendix E), the methanol/DCM pair was not used. Finally, ACE was chosen as the best weak solvent. Because of the large UV absorbance of ACE, the concentrations of the dissolved polymers could not be detected using the GPEC equipment so visual solubility tests were done for the ACE/DCM pair, Table 5.1.

Table 5.1. DCM volume percent for polymer standards to visibly dissolve in ACE/DCM mixtures – determined by visual inspection.

Solute	**Solvent Composition (ACE/DCM)**
PC	15/85
BrPC	50/50
PS	50/50
SAN	100/0
RDP	100/0
BPADP	100/0

All the polymers that are present in the tested crude wastes, other than PC and ABS, were shown to dissolve in 50/50 (vol.%) ACE/DCM. PC did not dissolve completely in mixtures with less than 85 vol.% DCM; and ABS is insoluble in DCM. Therefore, ACE/DCM solvent pairs with a composition from 16 to 50 vol.% ACE can be used to extract the other polymers from the crude waste, leaving behind a solid containing PC and ABS. In a second step, ACE/DCM mixtures with 0 to 15 vol.% ACE can be used to extract pure PC from the residual solid from the first extraction step. The liquid solution resulting from the second extraction step can be evaporated to recover solid PC, and the solvents can be recycled. The proposed process was tested at a lab scale. The results are summarized below and an overview of the PC recovery process is shown in Figure 5.5.

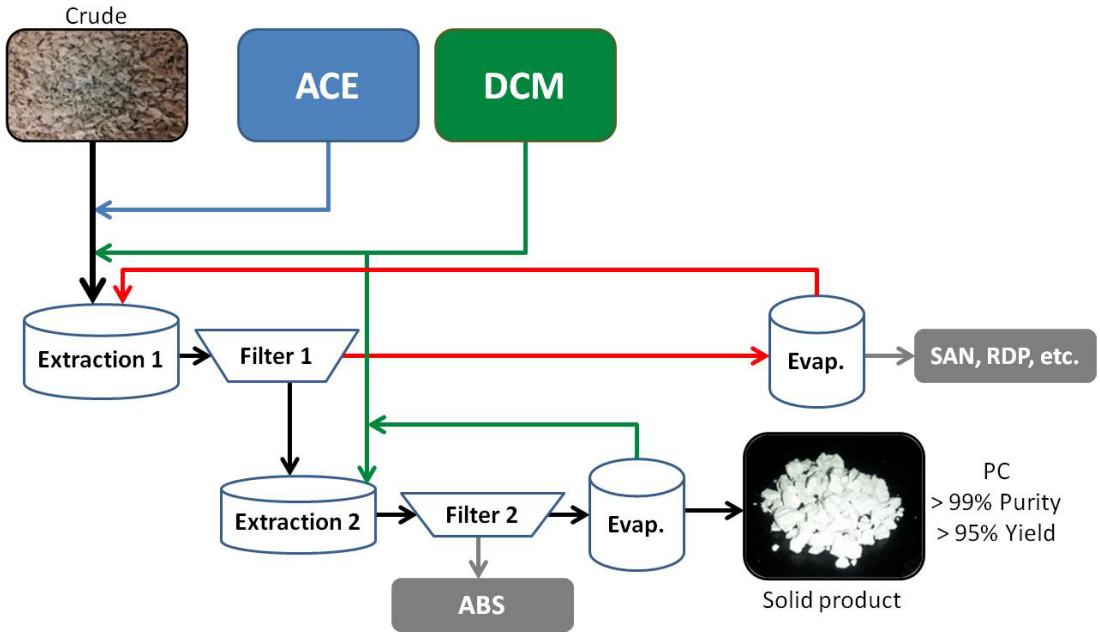

Figure 5.5. Purdue SEPoR process for PC recovery.

The crude waste was ground, dissolved in DCM, and analyzed. The results are shown in Figure 5.6a and Table 5.2. This particular crude did not contain PS.

In the first extraction step (Extraction 1, Figure 5.5), the polymer crude was ground, sieved to 250-850 μm diameter, and extracted using 50/50 ACE/DCM. As expected, most of the PC was not extracted. RDP, BPADP, SAN, and a small amount of an unknown impurity were extracted, Figure 5.6b. Component mass balances (Table 5.2) showed that in this step all these components were removed from the waste. PC balance and GPC analysis of the final PC product showed that a small amount of low MW PC (< 5 wt.%) was removed in the first extraction step. The crude has a small amount of BrPC (~2 wt.%), Figure 5.6a. Although BrPC was expected to be extracted by this mixed solvent, but it was not detected in the extract, Figure 5.6b. Since BrPC was found in the solution of the second extraction step discussed below, it was inferred that a small amount of BrPC might have

formed aggregates with PC and could not be extracted until the PC dissolved.

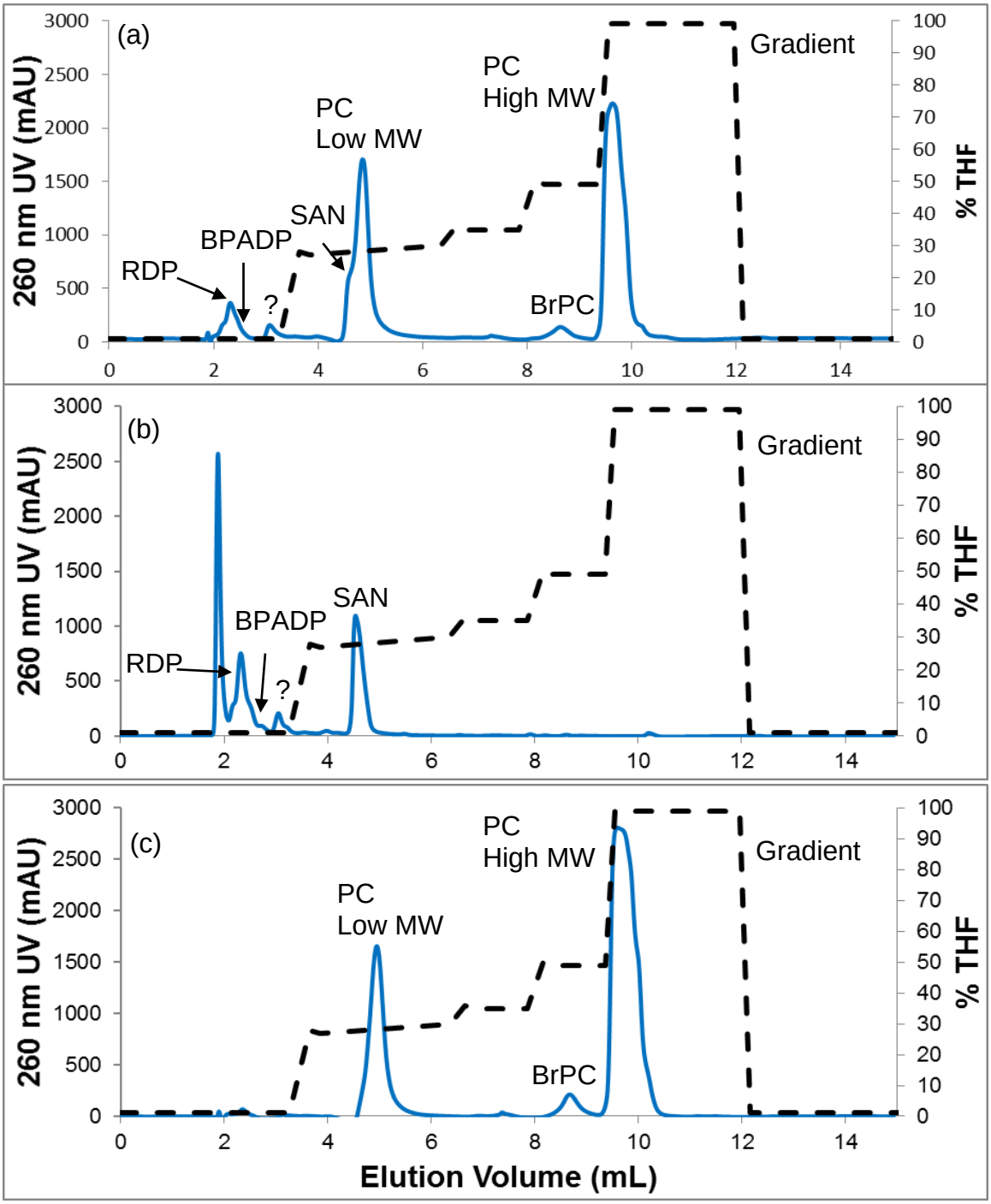

Figure 5.6. Chromatograms of: (a) crude waste dissolved in DCM; (b) sample from the first extraction (50/50 vol.% ACE/DCM); (c) sample from second (DCM) extraction.

Table 5.2. Overall mass balances for PC extraction process from crude waste.

Stream	Phase	Amount of Polymers Relative to Feed (g)	Solvent (ACE/ DCM) (vol.%)	Composition (Mass Fraction of Polymers)				
				PC	BrPC	SAN	RDP, BPADP	ABS + others
Crude	Solid	1.00	-	0.57	0.02	0.10	0.06	0.25
E1	Liquid	0.17	50/50	0.05	0	0.60	0.35	0
F1	Solid	0.83	-	-	-	-	-	-
E2	Liquid	0.58	0/100	0.98	0.02	0	0	0
F2	Solid	0.25	-	0	0	0	0	1

After the first extraction step, the solid particles were washed with 50/50 ACE/DCM for removing the liquid between the particles. After the particles were dried, DCM was added to extract the PC. HPLC analysis of the second extract is shown in Figure 5.6c. The amounts of RDP or BPADP were below the HPLC detection limits. Table 5.2 showed that the extracted polymers were mostly PC (98 wt.%) and a small amount of BrPC (2 wt.%), and the yield of PC was higher than 95%. The purity and yield were reproduced multiple times. The mass balance results indicate that a small amount of BrPC was entrained with the PC and was not extracted until the PC was dissolved in the second extraction step.

The PC product was also analyzed by Fourier Transform Infrared Spectroscopy (FTIR) and Gel Permeation Chromatography (GPC) at SABIC by Dr. David Zoller. The product was precipitated by adding acetone to the second extract. Then the particles were filtered. The purity of the particles determined by FTIR was higher than 99%. The small amount of BrPC, ca. 2 wt.%, determined from HPLC was not detectable by FTIR (Appendix E1). GPC results (Appendix E1) showed that the PC product had the nearly the same MW distribution as virgin PC, except in the low MW region. The results were

consistent with the HPLC and PC mass balance results, which indicated that a small amount of low MW PC (< 5 wt.% of PC) was lost in the first extraction step.

One important consideration for the PC product is how much solvent remains in the product. Chlorinated solvents, such as DCM, can be very difficult to completely remove from PC and other polymers [108,109]. Many methods have been used for recovering the solvent from polymer solutions (flash vaporization, vented extrusion, devolatilizing extrusion, etc.). These processes can produce polymers with < 1,000 ppm solvent [110]. If very low solvent content is required, then the polymer can be precipitated, as was done for the PC product in this work, and the solvent can be baked off, leaving about 2 ppm solvent in the solid polymer [110].

The mass balances were checked for each component after each extraction step. Input mass and output mass for each component agreed to within HPLC experimental error. The overall component mass balances for the process are shown in Table E.1, Appendix E. RDP, BPADP, SAN, and a small amount of low MW PC were removed in the first extraction step. A small amount of BrPC and the majority of the PC were removed during the second extraction step. The purity, yield, and solvent usage were reproduced in multiple experiments. The PC purity based on FTIR was higher than 99%. The average PC yield was higher than 95%. The ABS recovered as a byproduct can be used for other applications.

A second polymer waste (“Trommel”), which had a significant amount of PS (41 wt.%) and a lower concentration of PC (19 wt.%), was also tested. The solvent compositions for the extraction steps remained the same. The Trommel was treated with the same process as the waste from computer housings, but the presence of large amounts

of PS caused gel formation during the first extraction step. The gel made solid/liquid separations very difficult. In this case, reversing the extraction steps is beneficial. The Trommel waste was first dissolved in pure DCM and filtered to remove solid ABS. The solvent composition of the polymer solution was then adjusted to 50/50 (vol.%) ACE/DCM, by slowly adding acetone, to precipitate PC, leaving RDP, BPADP, SAN, and PS in solution. This SEPoR process produced 99% pure PC with BrPC (1% PS) with 93% yield. The composition of the second polymer waste and the extraction results are shown in Appendix E2. The results of the Trommel experiments demonstrate that the SEPoR process can be developed for polymer wastes with different compositions. However, modification of the method may be needed if gel formation or polymer aggregation occurs. Ideally the same or similar polymer blends should be used in electronics so that one standard separation process can be used for recycling the polymers. For polymer wastes in general, the methodology developed in this study using a combination of screening with HSP, GPEC, and solubility tests can reduce the time and effort in identifying effective solvent mixtures and developing an efficient sequential extraction process.

The amount of solvent required was about 23 kg solvent per kg PC for the entire process. Most (99%) of the solvent in SEPoR can be recycled using conventional solvent recovery methods. Steam has been used to precipitate the polymers and evaporate the solvent, which can then be recovered by distillation. Solvent recovery rates as high as 99.9% have been reported [111]. The recovered solvents can be directly reused in the extractions, with only a small addition of makeup solvent. Solvent recycle costs are expected to be a major cost at an industrial scale. At a scale of one ton of PC per day with 99% solvent recycle, the estimated cost of production was found to be less than $1.5 per kg PC, Table

5.3. This is about $1.00 below the current bulk sales price for polycarbonates. The energy cost for solvent recycle, using evaporation and condensation, was about 18 MJ/kg PC (Table 5.4), which is 16% of the energy used to produce virgin PC (113 MJ/kg) [17]. Hence, this method is economical and promising.

Table 5.3. Cost estimate of PC recovery from crude waste.

Equipment	**Size**	**Unit Cost ($)**	**# of Units**
Extraction tank	2,000 gal	33,000	2
Mixer for extraction	-	1,500	2
Centrifuge decanter (LW-250)	17 – 84 L/min (270 – 1330 gal/h)	50,000	1
Evaporator	10,000 gal/day	35,000	1
DCM storage tank	10,000 gal	165,000	1
ACE storage tank	3,000 gal	55,000	1
Equipment Costs			
Equipment purchase cost ($)			374,000
Installation cost (assumed) ($)			575,000
Total equipment cost ($)			949,000
Equipment cost ($/kg PC)[h]			**0.52**
Solvent Costs			**$/kg solvent**
Purchase DCM			0.803
Purchase Acetone			1.200
Recycle[i]			0.002
Overall Costs			**$/kg PC**
Feed[i]			**0.64**
Solvent[j]			**0.25**
Equipment			**0.52**
Total			**1.41**

[h]Assume 5 year depreciation and 1,000 kg PC produced per day
[i]Obtained from private communication with SABIC
[j]Assume 99% solvent recycle and 22.7 kg solvent/kg PC

Table 5.4. Energy consumption estimate for PC recovery from crude waste.

Property	**Acetone (ACE)**	**Dichloromethane (DCM)**
MW (g/mol)	58.1	84.9
Boiling point (BP) (°C)	56.0	40.0
Heat capacity (J mol^{-1} K^{-1})	125.5	102.3
Heat of vaporization (kJ mol^{-1})	31.3	28.6
Mass used (kg)[k]	3.2	19.5
Energy[l]	(MJ/kg PC)	(MJ/kg PC)
Energy to raise and lower temp. [20°C to BP to 20°C][m]	0.5	0.9
Energy to evaporate and then condense	3.4	13.2
Total energy consumed (MJ/kg PC)	18.0	

[k]Assume 22.7 kg solvent / kg PC
[l]Assume all energy consumption due to solvent recycle
[m]Assume room temperature is 20°C

In summary, the method of using HSP, GPEC, and solubility tests has the potential for developing mixed-solvent, sequential extraction processes to recycle polymers from various wastes. More than 280 million tons of polymers are produced globally each year and less than 10% of the polymers are recycled. Effective polymer recycling would reduce raw materials from petroleum or other sources, energy required for polymer synthesis, and CO_2 emissions. It would also reduce the environmental hazards associated with the polymer wastes accumulating in landfills and in the ocean.

However, there are two side streams to the SEPoR process for PC recovery. The solid streams (mostly ABS and other insoluble) can be used in low quality applications, such as filler in asphalt. The other side stream is a mixture mostly comprised of SAN and flame retardants in 50/50 vol.% ACE/DCM. The flame retardants are valuable compounds which should be recovered. Because of the large MW difference, size-exclusion chromatography can be used to separate the flame retardants from the polymer.

CHAPTER 6. RESULTS – SEC-SMB FOR FLAME RETARDANT RECOVERY

Results in this chapter are reprinted from J. of Chromatogr. A, 1422, Weeden et al., Size-Exclusion simulated moving bed for separating organophosphorus flame retardants from a polymer, 99-116, Copyright (2015) [112], with permission from Elsevier.

6.1 Intrinsic Parameters for SSWD and VERSE Simulations

HPLC calibration results are shown in Figure 6.1. This calibration is different from that shown in Figure 5.4a because the HPLC analysis used for the SEC-SMB experiments was performed at SABIC instead of at Purdue.

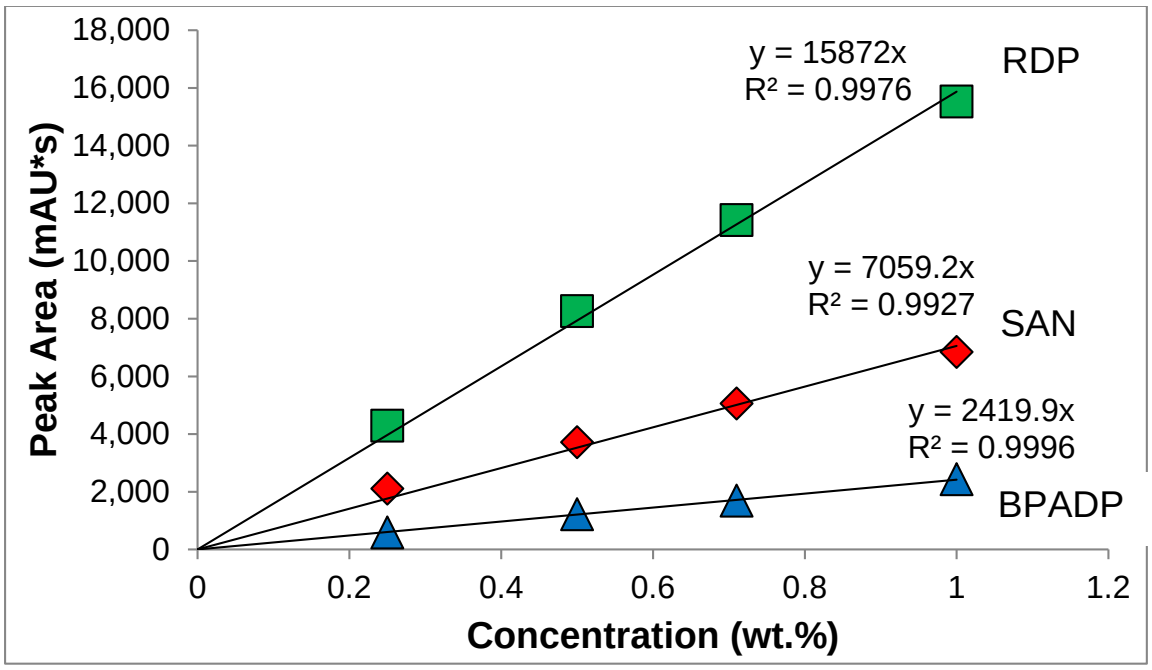

Figure 6.1. HPLC calibration results for RDP, BPADP, and SAN for SMB experiments at SABIC.

Column packing and characterization results are presented in Table 6.1, along with numerical parameters used in VERSE simulations. Average particle size was provided by the manufacturer.

Bed void (ε_b) and total void (ε_t) fractions were determined using blue dextran pulses and RDP frontals, respectively. Particle porosity (ε_p) was determined from the other two void fractions. The dead volume (*DV*), in terms of percent of one column volume (CV), includes the system dead volume per CV and the dead volume in the caps of a column.

Table 6.1. Summary of material, system, and numerical properties for FR SMB.

Column Packing Parameters

R_p (μm) XAD-1180N	L_c (cm)		*ID* (cm)	ε_b	ε_p	ϕ	*DV* (% CV)
	Batch	SMB					
225	65	63	2.54	0.37	0.69	1.70	1.9

Mass Transfer Parameters

Solute	D_∞ [e] (cm^2/min)	D_p (cm^2/min)	K_{se}		δ		E_b (cm^2/min)	k_f (cm/min)
			Batch	SMB	Batch	SMB		
SAN	1.0×10^{-4}	0.7×10^{-5}	0.63	0.61	0.43	0.42	Chung and Wen correlation	Wilson and Geankoplis correlation
BPADP	1.0×10^{-2}	40.0×10^{-5}	1.00	0.96	0.69	0.66		
RDP	1.0×10^{-3}	10.0×10^{-5}	1.00	1.00	0.69	0.69		

Numerical Parameters

No. of axial elements	Collocation Points		Tolerance	
	Axial	Particle	Absolute	Relative
100	4	1	0.001	0.001

[e] Brownian diffusivities.

Apparent pore diffusivities (D_p) and size-exclusion factors (K_{se}) listed under the Batch column were estimated from column frontal data. The K_{se} values of SAN and BPADP were fine-tuned using SMB data and are listed under the SMB column.

6.2 Column Characterization

Chromatograms of the component frontals and blue dextran pulses are shown in Figure 6.2. The mass center of the blue dextran pulse gives the bed void fraction (0.37). The component frontals were fit with VERSE simulations to determine their size-exclusion factors and diffusivities, which are reported in Table 6.1. The estimated intraparticle diffusivities are less than 10% of the Brownian diffusivities. These ratios are similar to those of other polymeric resins reported in the literature [62].

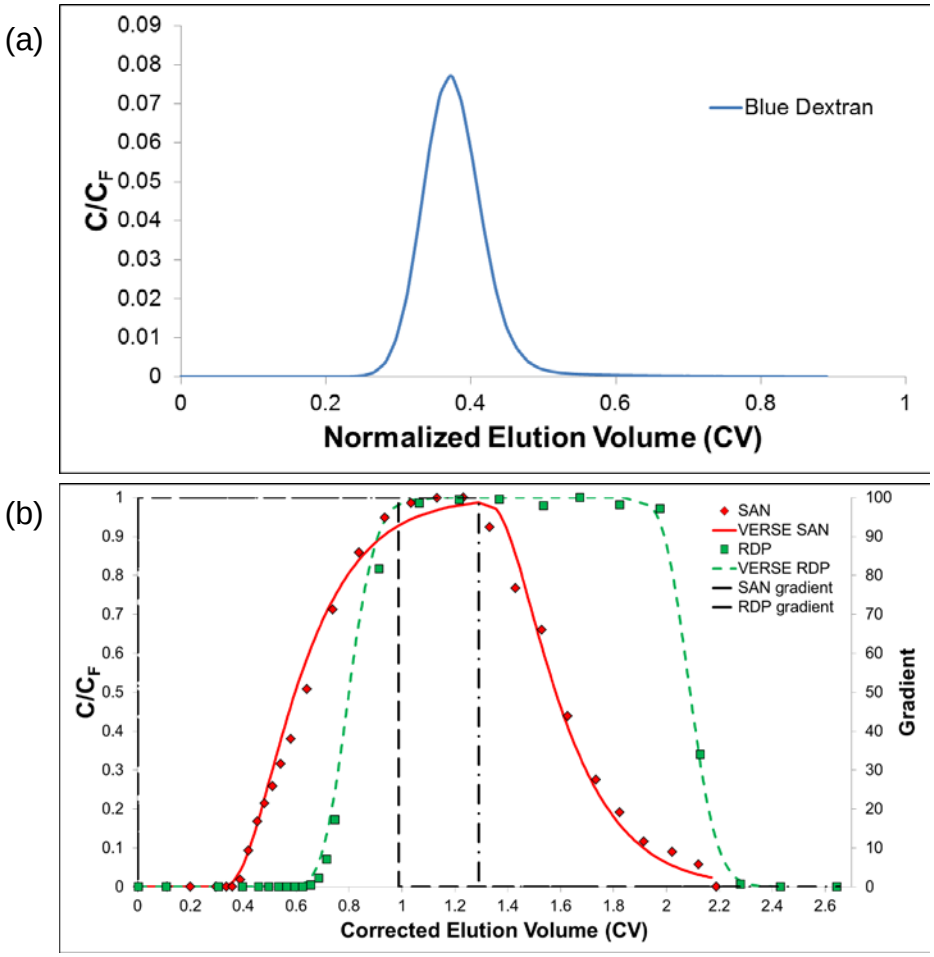

Figure 6.2. (a) Blue dextran pulse to determine bed void fraction, and (b) component frontals to determine size-exclusion factors and diffusivities of each component. BPADP frontal not shown as it overlaps with the RDP data.

6.3 Experimental Testing of SSWD and Fast Startup Methods

The intrinsic parameters obtained from batch chromatography in Table 6.1 were used to design the SMB flowrates and switching times for Runs 1-3. After these runs, the parameters were fine-tuned by comparing the VERSE column profiles with experimental profiles near cyclic steady-state to fit the experimental data. The SMB design for Run 4 was obtained using the new parameters. Fast startup methods based on the design of Run 4 were compared to the literature fast startup method and to startup from clean columns. Run 5 was designed to separate a ternary mixture. The results were used to fine-tune the size-exclusion factor for BPADP, which was overestimated from batch SEC experiments. The fine-tuned size-exclusion factor was used to design Run 6. Summaries of the SMB designs (operating parameters) and experimental results are presented in Table 6.2 and Table 6.3, respectively.

Table 6.2. Summary of designs for SMB runs.

Design		**Flowrates (mL/min)**								**Step time (min)**
Run	L_c[f] **(cm)**	**Feed**	**Desorbent**	**Extract**	**Raffinate**	**Zone I**	**Zone II**	**Zone III**	**Zone IV**	
1	65	0.59	1.97	0.79	1.77	7.45	6.66	7.25	5.48	36.9
2	65	0.4	1.18	0.49	1.09	4.59	4.1	4.5	3.41	59.7
3	65	0.59	1.97	0.79	1.77	7.45	6.66	7.25	5.48	36.9
4	63	0.36	0.54	0.39	0.51	2.21	1.82	2.18	1.67	119.6
5	65	0.4	1.18	0.49	1.09	4.59	4.1	4.5	3.41	59.7
6	63	0.36	0.65	0.45	0.56	2.59	2.14	2.5	1.94	102.5

[f] L_c is the packing length used in the SSWD

Table 6.3. Summary of results for SMB experiments.

Run	Feed Conc. (wt.%)			SWD Purity		Exp. Purity		End step	Comments
	SAN	RDP	BPADP	Extract (FR)	Raffinate (SAN)	Extract (FR)	Raffinate (SAN)		
1	5	5	0	95	95	100	98[g]	33	Verify fast startup, quickly verify intrinsic parameters
2	5	5	0	97	97	100	92[h]	51	Longer run time, fast start from end of Run 1, packing length inaccurate
3	5	5	0	95	95	100	87[h]	56	Repeat of Run 1 design, fast start from end of Run 2, new simulated length
4	7	7	0	99	99	100	99.8	27	Cleaned, then fast start, designed for 63 cm length
5	5	5	5	99.5	98.0	100	65[i]	50	3-component, clean start, verify BPADP parameters – inaccurate
6	5	5	5	99.5	98.0	100	97.6	40	Tuned BPADP parameters, fast start

[g] The high raffinate purity of Run 1 was a result of the recycle flowrate being 0 every 8 steps. The run had not yet reached steady state.

[h] The raffinate purity of Runs 1-3 should be 88-93% because the SMB designs were based on a packing length of 65 cm, when the effective packing length was 63 cm.

[i] The low raffinate purity was due to the overestimated size-exclusion factor of BPADP.

6.3.1 SMBs for Separating SAN from RDP (Runs 1–4)

6.3.1.1 SMB Run 1

The first SMB run was designed for 95% yield of each component and to verify the estimated intrinsic parameters. To quickly reach cyclic-steady-state, the feed flowrate was set at 0.6 mL/min so that the switching time would be relatively short (~37 min).

To quickly reach steady-state, the columns were preloaded with SAN/RDP solutions to approximate the final steady state column profile predicted from the VERSE chromatography simulation software. The feed solutions were 3 wt.% RDP for columns 1 and 2, 3 wt.% RDP with 2 wt.% SAN for columns 3 and 4, and 2 wt.% SAN for columns 5 and 6. The preloaded column profiles obtained from a rate-model based simulation program (VERSE) are shown in Figure 6.3a.

The column profiles and effluent histories for Run 1 at the end of step 33 are shown in Figure 6.3. The simulated SAN profile lagged behind the experimentally obtained profile, Figure 6.3b. The $K_{se,SAN}$ was reduced from 0.63 to 0.61 to better fit the simulated SAN profile to the experimental results, Figure 6.3c. The raffinate history of Run 1 shows periodic fluctuations, which resulted from the recycle flowrate being set to zero on the fifth step of every cycle. The error was corrected after the 24^{th} step (886 minutes) and the raffinate concentration stabilized very quickly to the value predicted by VERSE simulation.

The experimental RDP concentrations on the plateau are lower than the simulation results, which is most likely due to some dilution of the profile samples because of the dead volume in the sampling tubing. There also may have been some errors in diluting the profile samples for HPLC measurement.

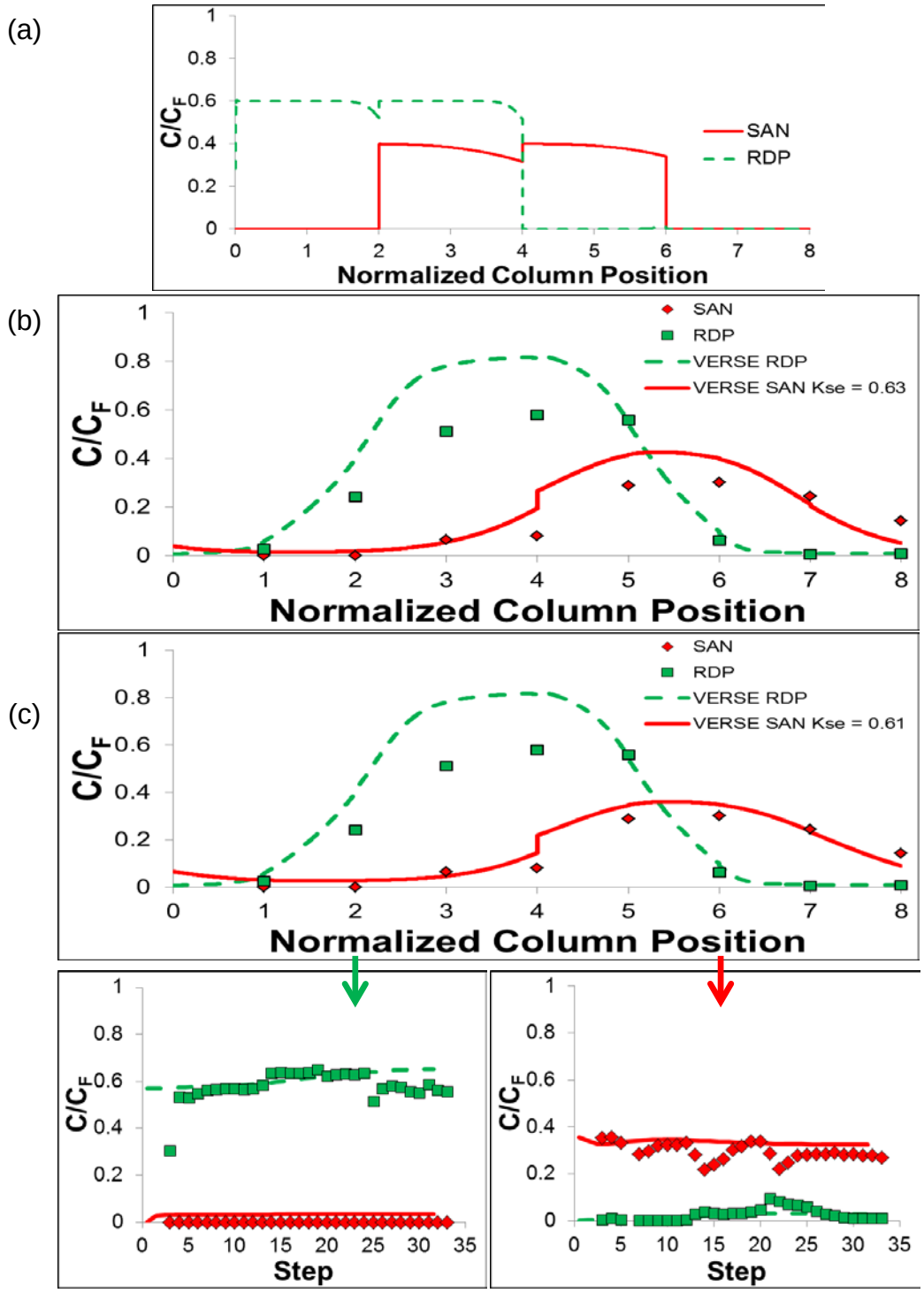

Figure 6.3. (a) SMB Run 1 preloaded column profiles predicted by VERSE, (b) column profiles for Kse,SAN = 0.63 (c) column profiles for Kse,SAN = 0.61 (top), extract history (bottom left), and raffinate history (bottom right) for SMB Run 1, end of step 33. Lines are from VERSE simulations while squares and diamonds are HPLC data points.

6.3.1.2 SMB Run 2

The second SMB experiment did not have a cleaning step between experiments, so the column profile in Figure 6.3b was used as the initial column profile for Run 2 in simulations. The feed for Run 2 was also 5 wt.% of each component, but the desired yield was increased to 97%. The effluent histories and column profiles at the end of 51 steps are shown in Figure 6.4.

The simulated column profiles values lagged behind the experimental profiles when the column length was assumed to be 65 cm, Figure 6.4a. When the packing length was changed to 63 cm, the simulation results fit the experimental data much better, Figure 6.4b. The error in packing length appears more prominently in Run 2 because it was run for a larger number of steps (~84, in total) compared to Run 1 (33 steps). The small error (~3%) in packing length could be from a small error in estimating the bed void fraction or column dead volume, such that the effective packing length was 2 cm shorter than the nominal length. It could also be due to small errors in the length or inner diameter of the glass columns. The rest of the simulations were based on a packing length of 63 cm. The RDP wave was more affected by the column length change than the SAN wave because the size-exclusion factor of RDP is larger than that of SAN. Reducing the column length from 65 cm to 63 cm (3% difference) advances the edge of the RDP trailing wave in Zone I by the difference in retention (i.e. 0.03 * L_c * retention factor (0.69) * 51 steps ≈ 1 L_c). The same reasoning predicts that the SAN waves should differ by ~ 0.6 L_c (retention factor = 0.42). However, the differences for edges of the advancing waves in Zone IV are reduced because the SWD focuses them toward the raffinate port.

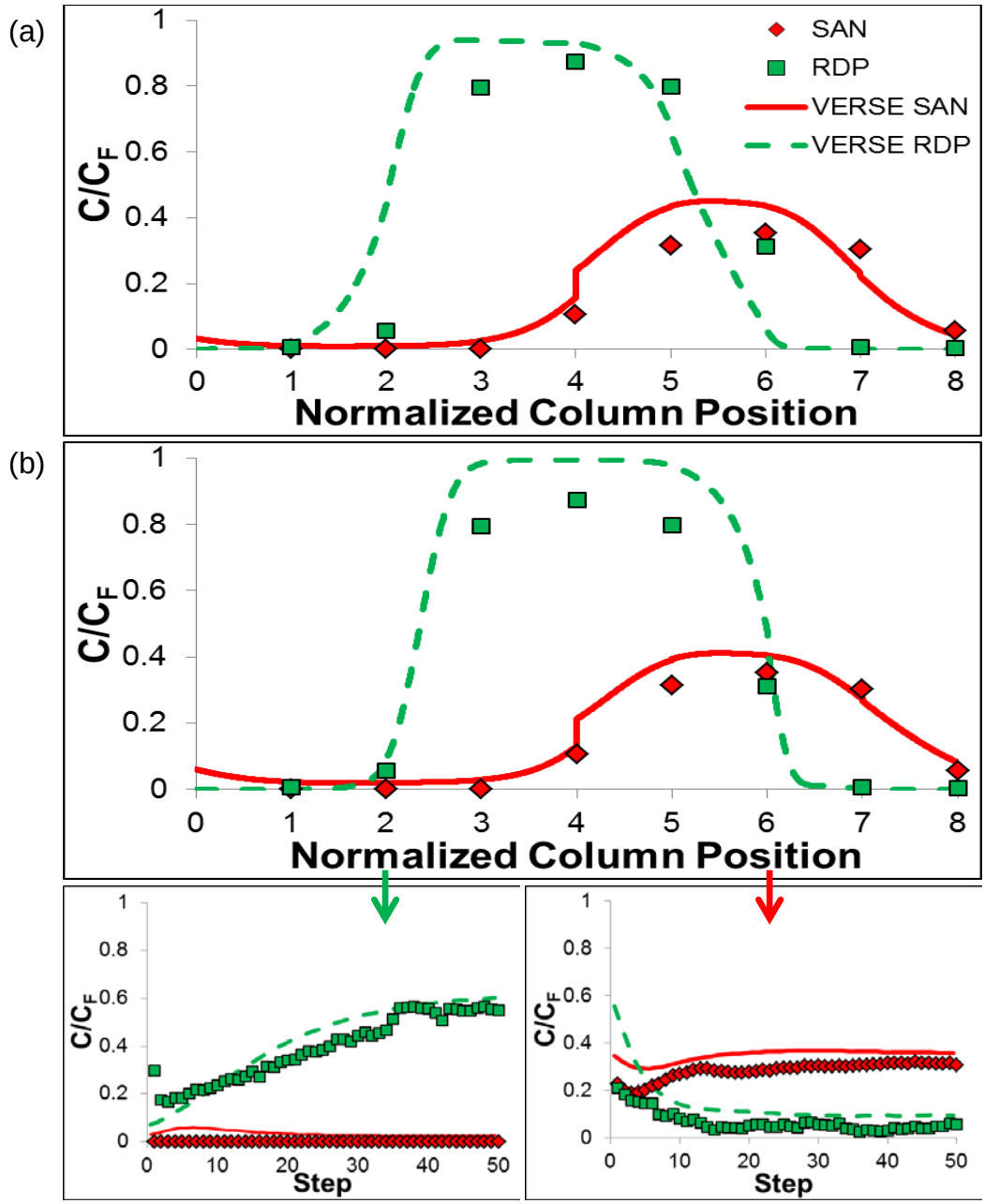

Figure 6.4. (a) Column profiles for Run 2 at the end of the 51st step. VERSE simulations used a column length of 65 cm. (b) column profiles (top), extract history (bottom left), and raffinate history (bottom right) for SMB Run 2 using a column length of 63 cm, end of step 51. Lines are from VERSE simulations while squares and diamonds are HPLC data points.

The initial column profile of Run 2 was the final profile of Run 1 and the desorbent port was located at the inlet of Column 1 (in SEMBA notation). As the operating conditions changed to Run 2, the default location of the desorbent port in SEMBA was the inlet of Column 1. Instead of entering Column 2 as intended, the desorbent again entered Column 1 at the beginning of Run 2. This resulted in low RDP concentration in the extract at the start of the experiment. As SMB operation continued, the concentration waves recovered to their cyclic-steady-state positions. The column profiles at the end of Run 2 agreed with the predicted values from simulation. The effluent histories were well predicted by VERSE, which took into account the port location at the beginning of Run 2.

6.3.1.3 SMB Run 3

Run 3 also did not have a cleaning step, so the initial column profile for Run 3 was the final profile of Run 2 in the simulation. Run 3 was a repeat of the designed operating conditions for Run 1, which were determined from SSWD based on the nominal column length of 65 cm.

The effluent histories and column profiles at the end of step 56 are shown in Figure 6.5. The sharp rise in the RDP concentration around step 17 was most likely due to a flowrate problem caused by the desorbent pump, which produced a lower flowrate than desired. This problem persisted for 3 steps before it could be corrected. After correction, RDP concentrations slowly approached the steady-state value.

From the data obtained from Runs 1-3, the average column length was determined to be 63 cm instead of 65 cm and the size exclusion factor for SAN was reduced to 0.61 from 0.63. The designs of Runs 4 and 6 were based on these new parameters.

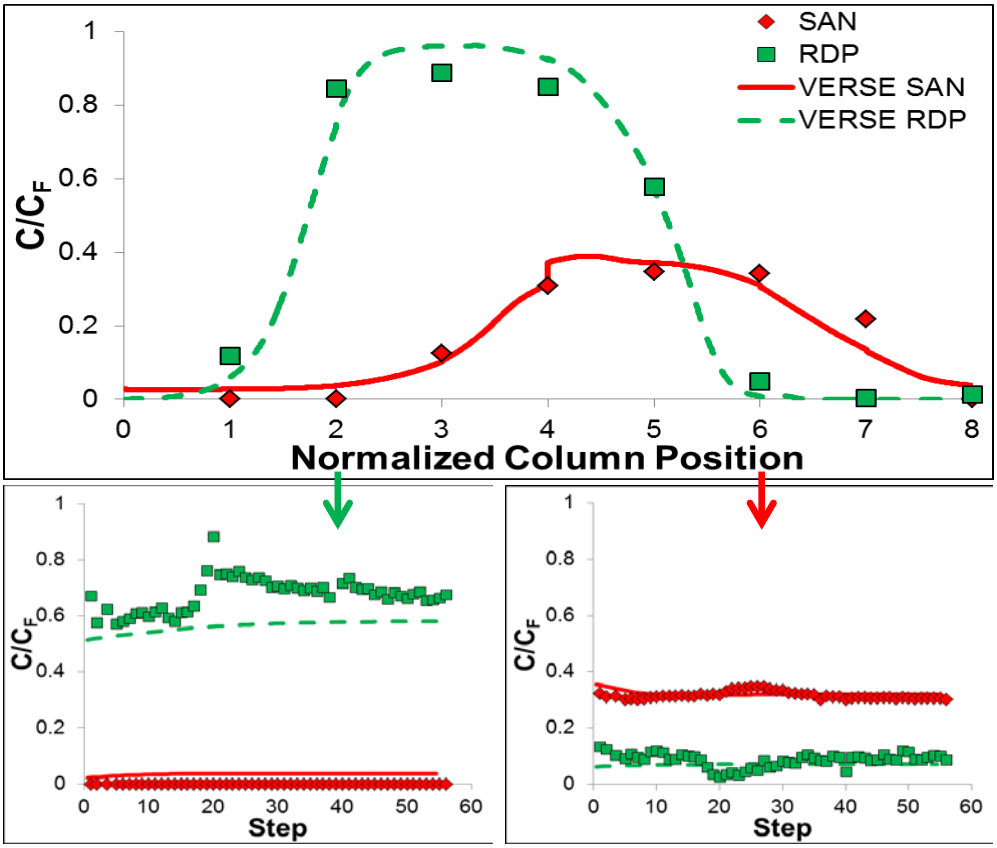

Figure 6.5. Column profiles (top), extract history (bottom left), and raffinate history (bottom right) for SMB Run 3, end of step 56. Lines are from VERSE simulations while squares and diamonds are HPLC data points.

6.3.1.4 SMB Run 4

Run 4 was designed to separate RDP from SAN with higher feed concentrations (7 wt.% each) and a higher yield requirement (99%) compared to the previous runs. The columns were washed with pure solvent after Run 3. The first preloading strategy (VERSE) was used to approximate the steady-state column profile. The preloading solutions were 6.5 wt.% RDP for columns 1 and 2 (Zone I), 6.5 wt.% RDP with 5.7 wt.% SAN for columns 3 and 4 (Zone II), and 5.7 wt.% SAN for columns 5 and 6 (Zone III). All eight columns were then connected in series and eluent was pumped at 5 mL/min for 20 minutes. This

elution step shifted the concentration waves into their steady-state positions. The preloaded column profiles obtained from VERSE are shown in Figure 6.6a. Dips in concentrations on the plateaus are due to incomplete saturation of the columns before elution.

The column profiles and effluent histories of Run 4 at the end of step 27 are shown in Figure 6.6b. The extract flowrate in the first two steps was lower than the set flowrate. After the flowrate was corrected, the effluent data agreed with simulation results. The purities for both streams were greater than 99%. The experimental product concentrations, purities (>99%), and yields (>99%) agreed closely with those of SWD. This preloading strategy effectively shortened the time required for the product concentrations to reach 95% of their cyclic steady-state values to 3 steps.

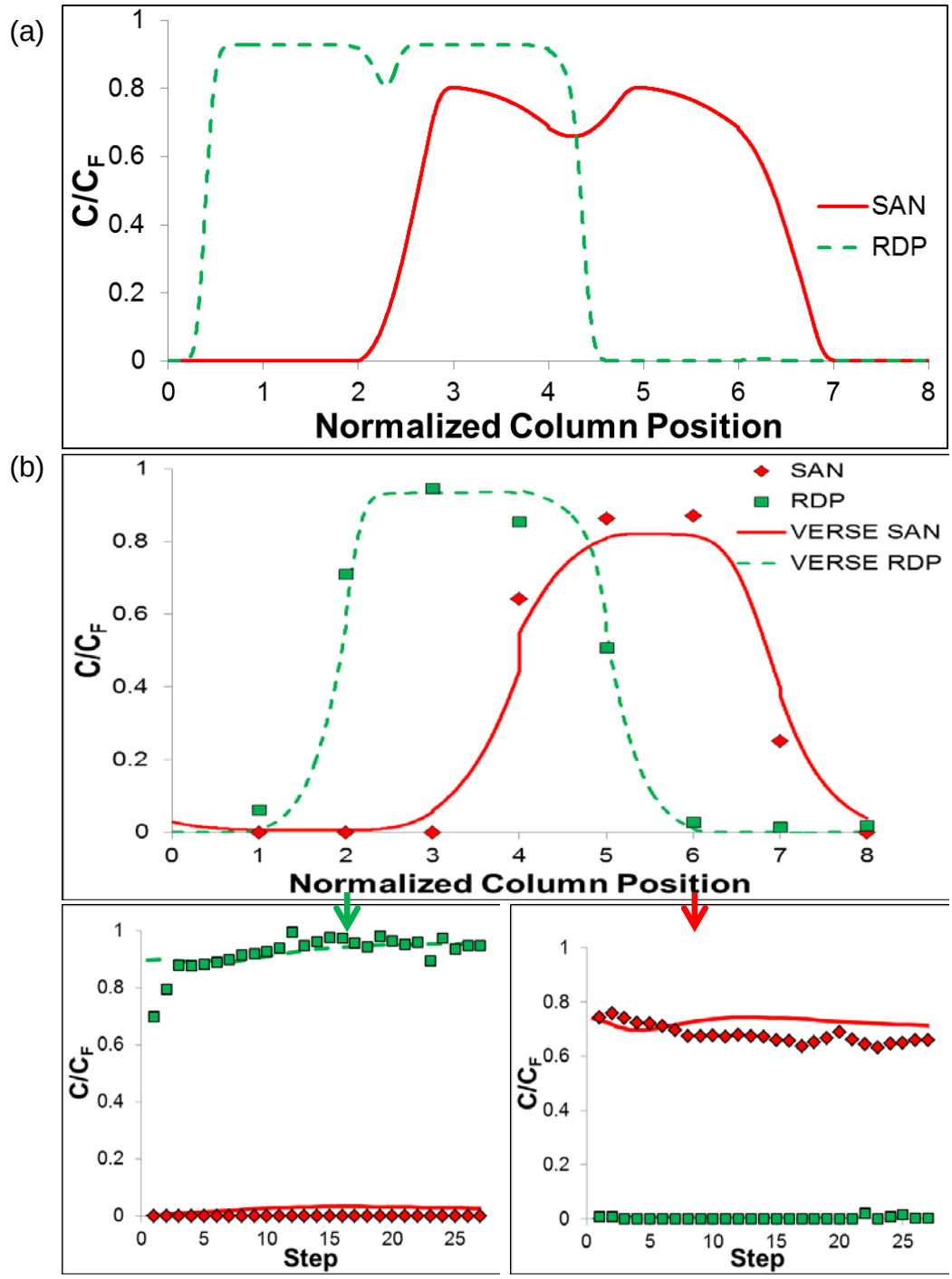

Figure 6.6. (a) Preloaded column profiles obtained from VERSE simulations, (b) column profiles (top), extract history (bottom left), and raffinate history (bottom right) for SMB Run 4, end of step 27. Lines are from VERSE simulations while squares and diamonds are HPLC data points.

6.3.2 Comparison of Fast Startup Methods

Once the first fast startup method was verified with experiments, it was compared to other fast startup methods and startup from clean columns. Run 4 was used as the base case and VERSE simulations were used to determine the startup time for each method. The results of the VERSE simulations of SMB Run 4 are shown in Figure 6.7. A clean startup of Run 4 was simulated for 80 steps. The product concentrations after 80 steps were determined to be the cyclic steady-state values. All the preloading strategies achieved cyclic steady state in fewer steps than the regular startup from clean columns, which took over 36 steps (>4 cycles).

The literature method of preloading four columns with the feed solution was the easiest to implement, but has a longer startup time than the two proposed methods. The extract product had very low purity until after 15 steps and the raffinate product did not reach 95% of the cyclic steady-state value until after 29 steps. However, this strategy does not require already pure solutions for preloading and can be beneficial when first starting up a process.

Within one step, the product concentrations of the first (VERSE) preloading strategy reached 95% of their cyclic steady-state values and the product purities were greater than 99%. This preloading strategy allows for continuous product withdrawal from the first step, unlike the literature method.

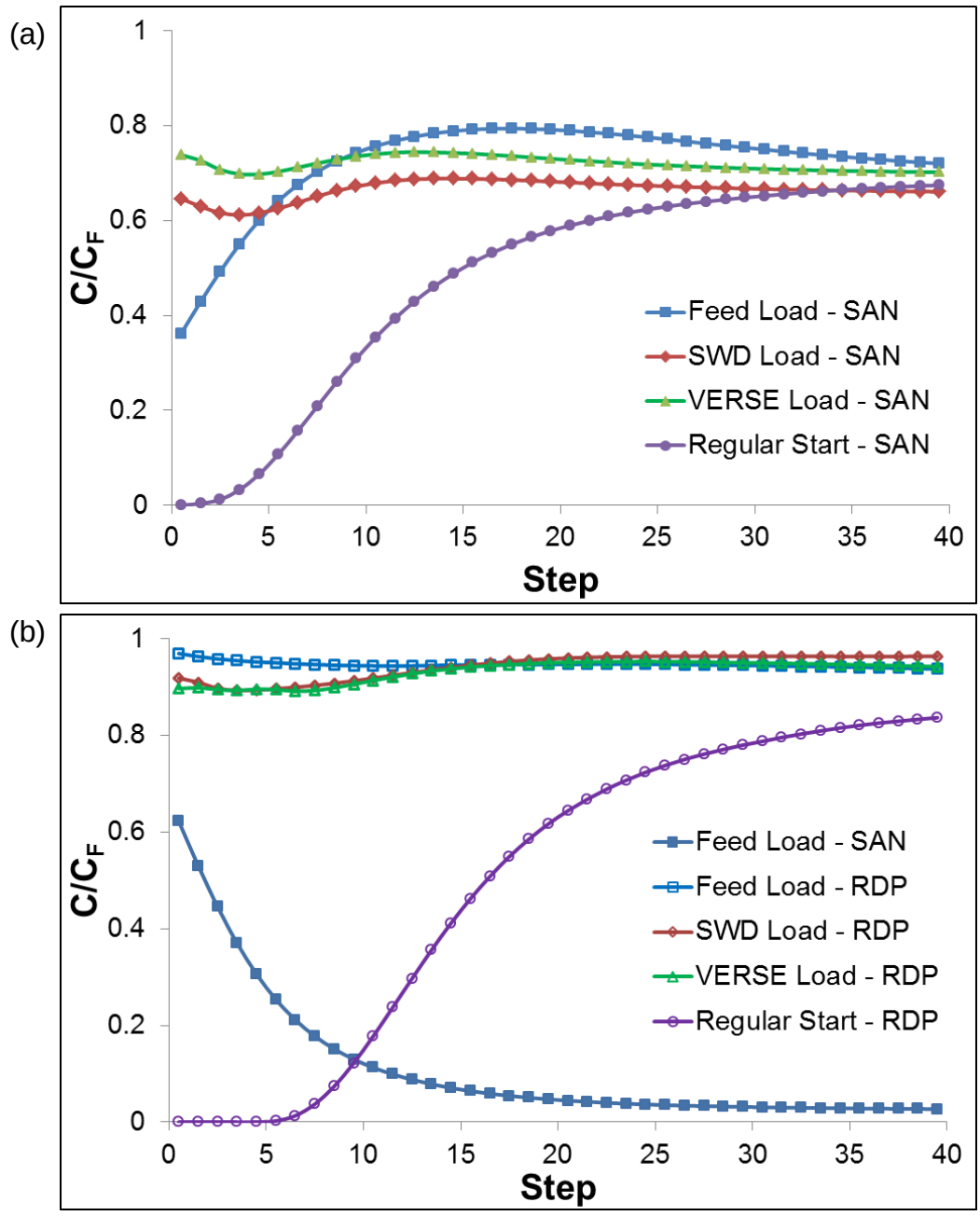

Figure 6.7. Comparison of pre-loading strategies and regular startup for binary SEC-SMB. SMB design is the same as Run 4. Effluent histories: (a) raffinate and (b) extract. RDP concentrations not shown in (a) since all strategies resulted in very low concentrations of RDP throughout the simulations. Likewise the SAN concentrations are not shown in (b) except for the feed loading strategy which has significant SAN contamination.

The second (SWD) strategy can be used when simulation software, such as VERSE, is unavailable. This strategy uses the SWD to determine the four zone flowrates for a given feed flowrate and specified yield. Once the zone flowrates are specified, the product flowrates can be calculated and an overall mass balance can be performed to determine the product concentrations. These concentrations are used for the preloading solutions. However, the first strategy is more general and can take into account components which are allowed to distribute between the product ports. The two preloading strategies give similar effluent histories and reduce the startup time by more than 31 fold.

6.3.3 SMBs for Separating SAN from RDP/BPADP (Runs 5–6)

6.3.3.1 SMB Run 5

A second flame retardant (BPADP) was added to the feed mixture for Run 5. Because the two flame retardants (FRs) can be recovered together, the separation is pseudo-binary. The two flame retardants were expected to migrate at the same speed in SMB, based on the batch experiments. Thus the operating parameters for Run 5 were the same as Run 2. The effluent histories are presented in Figure 6.8.

Some BPADP was found in the raffinate and its concentration in the Extract was lower than that of RDP, most likely due to the overestimation of the size-exclusion factor of BPADP. Column profiles were not taken because raffinate flowrate was found to be lower than the set value and leaks were also observed near the end of the experiment. The results indicated that BPADP migrated faster than predicted and the $K_{se,BPADP}$ was overestimated from batch tests. By reducing $K_{se,BPADP}$ from 1.0 to 0.96, the simulated

raffinate and extract histories of all components agreed closely with the experimental histories over 50 steps, Figure 6.8.

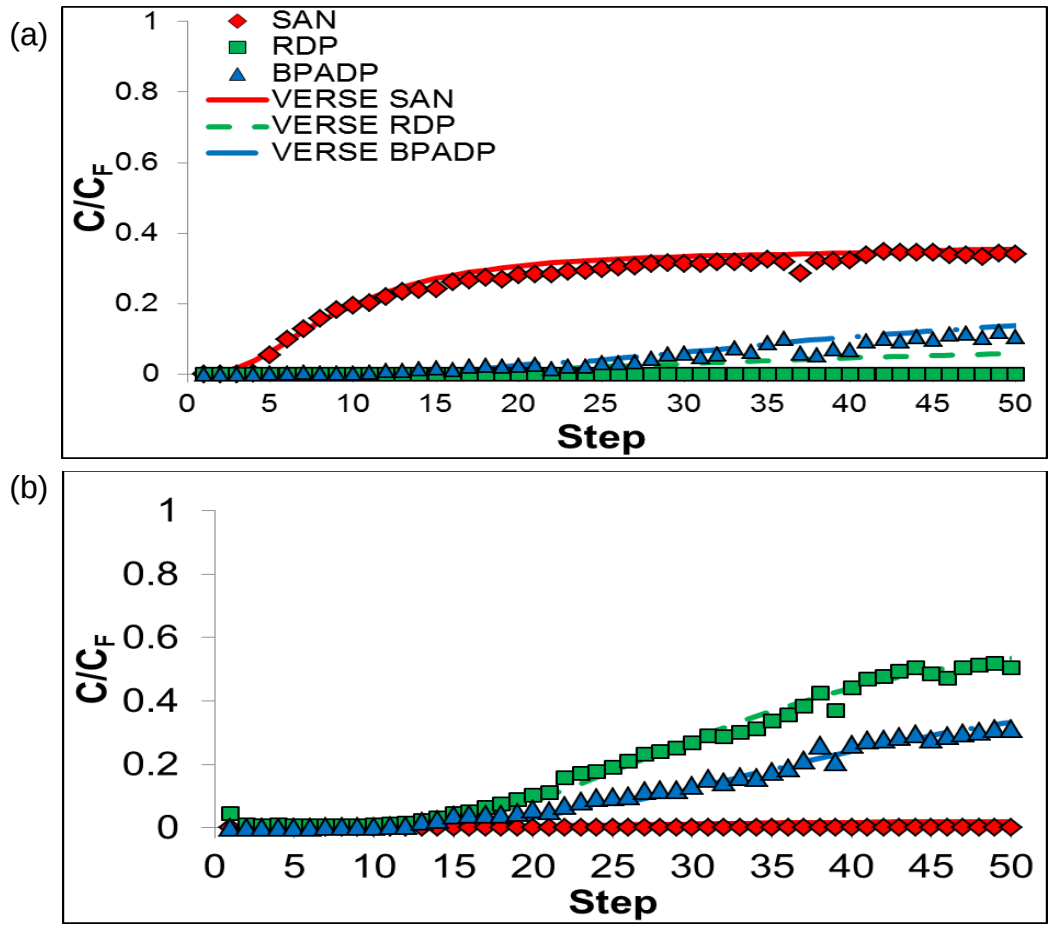

Figure 6.8. (a) Extract and (b) raffinate histories from SMB Run 5. No column profiles were taken for Run 5.

6.3.3.2 SMB Run 6

The revised parameters for BPADP were used in the SSWD to obtain the operating conditions of Run 6. The columns were washed with pure solvent, then preloaded using the first preloading method to approximate the steady-state column profiles.

The preloading solutions were 4.5 wt.% RDP and 4 wt.% BPADP for Zone I, 4.5 wt.% RDP and 4 wt.% BPADP with 4 wt.% SAN for Zone II, and 4 wt.% SAN for Zone

III. All eight columns were then connected in series and eluent was pumped through at 5 mL/min for 20 minutes. This elution step shifted the solute bands into their steady-state positions, Figure 6.9a. The transient column profiles from the preloaded columns to the start of step 40 are shown in Figure 6.9a-f. The simulated effluent histories and column profiles at the end of step 40 are compared with experimental data in Figure 6.9g.

The extract and raffinate histories agree with simulations and reach 95% of their steady-state values within 2 steps (37 steps if starting from clean columns). The preloading strategy reduced the startup time by more than 18 fold. The purities of both streams are also very high (~100% for the extract, 98% for the raffinate) and agree closely with those from SSWD.

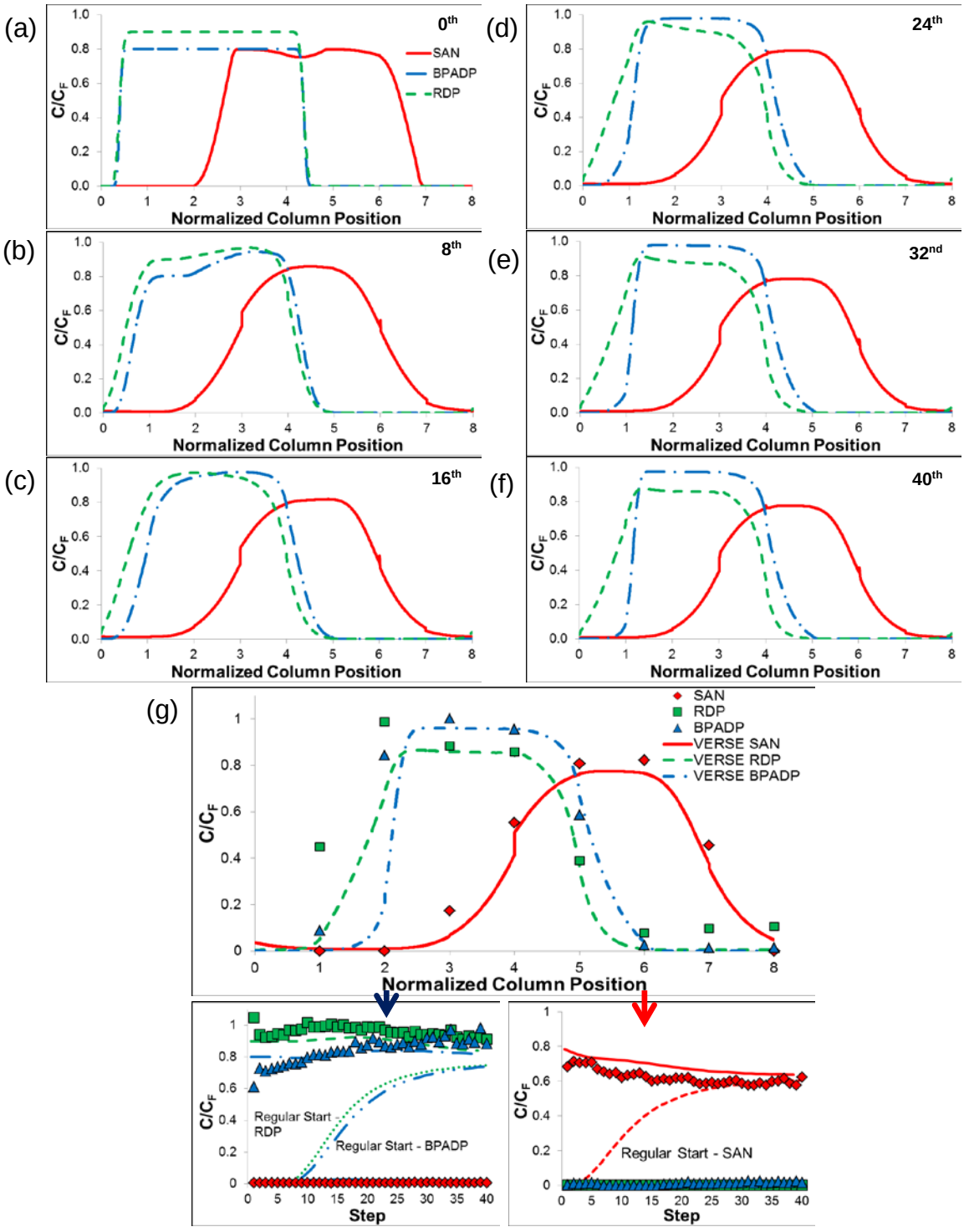

Figure 6.9. (a) SMB Run 6 preloaded column profiles predicted by VERSE, prior to start of SMB operation; (b) SMB column profile at start of step 8; (c) start of step 16; (d) start of step 24; (e) start of step 32; (f) start of step 40; (g) column profiles (top), extract history (bottom left), and raffinate history (bottom right) for SMB Run 6, end of step 40.

6.4 SSWD Optimization of a Large-Scale SEC-SMB

After the intrinsic parameters were fine-tuned and verified with pilot SMB experiments, SSWD was used to optimize a large scale SEC-SMB for the lowest unit separation cost while satisfying an imposed pressure limitation. The production was scaled to 10,000 tonnes of FR/year and the maximum pressure drop was set at 100 psi per zone. The feed concentration was fixed at 10 wt.% FR and 10 wt.% SAN and the viscosity was estimated to be 100 cP [113]. The 15 decision variables that can be optimized are column configuration (4), column length (1), dead volume (1), yields (3), particle size (1), and operating parameters (5). *DV* was fixed at 1.9% of the total column volume. The total number of columns was varied from eight to twelve. In order for the true moving bed assumption to apply to SMBs, a constraint of two or more columns per zone was placed on the column configuration [59]. Because of the high feed viscosity, the column length allowed by the pressure limit is relatively short. In order to obtain a practical column length, the minimum column length was set to be 0.5 m. Because the FRs must be recovered with high purity, the yields were set to be 99% or higher for each component. The particle size was allowed to vary from 0.5–2.0 times the experimental particle radius.

The SSWD equations for the ternary separation of FRs from SAN were used to determine solvent consumption and sorbent productivity for a given SEC-SMB design. These performance criteria combined with cost functions (Appendix C) can generate total separation costs for a large number of SEC-SMB designs by systematically varying the decision variables. The values of the decision variables which result in the lowest total separation cost were found by the algorithm shown in Figure C.1.

The optimal particle size was found to be 112 μm, which was the smallest particle size examined. Assuming the resin cost is independent of particle size, smaller particles result in higher productivity and lower cost. Because of the high feed viscosity, the column length is already relatively short (0.56 m). Decreasing the particle size further would shorten the column length to below 0.5 m.

The column configuration did not have a large effect on the overall separation cost. Adding more columns further reduces the column length. In order to obtain a column length larger than 0.5 m, the optimum column configuration was found to be 2-2-2-2.

The optimal yields were found to be 99% for each component. Increasing the yields of the components increases the total cost of the separation, with a very sharp increase in cost when yields approach 99.9%.

When particle size, column configuration, and yields are fixed at the optimal values, the total cost can be plotted against two key dimensionless groups, P_{eb}^{*} and N_D^{*}. This surface gives an overview of how total cost varies with column length (P_{eb}^{*}) and step time (N_D^{*}) and how a pressure limit constrains column length and step time. Because the total cost surface is concave up, the inverse of total cost is plotted for convenience in Figure 6.10a. The highest point in Figure 6.10a corresponds to the design with the lowest separation cost.

The dark grey surface represents the system's pressure limit. This surface was produced using Eq. (3.25). Particle size, pressure limit, phase ratio, and viscosity are fixed. The column length in the denominator of the left hand side of Eq. (3.25) can be replaced with the Peclet number, Eq. (A.13b), and the port velocity can be replaced by N_D^{*}, Table 3.1. Since the material properties are fixed, Eq. (3.25) is only a function of P_{eb}^{*} and N_D^{*}.

Equation (3.25) can be rearranged to have the left hand side be a constant and the right hand side be a function of P_{eb}^* and N_D^*, which results in a pressure limit line, Figure 6.10b. To visualize the designs which will satisfy the pressure limit, this pressure limit line is extended in the cost dimension as a surface, Figure 6.10a. The intersection of the pressure surface and the cost surface represents the combinations of L_c (P_{eb}^*) and zone velocities (N_D^*) that give the pressure drop in Zone I equal to ΔP_{max}. Designs to the left of the surface, smaller P_{eb}^* (shorter L_c) or larger N_D^* (slower zone velocities), will satisfy the pressure requirement. Lines of constant total cost are plotted in Figure 6.10b along with the pressure limit curve. The minimum cost design which satisfies the pressure limitation is marked with an "x."

Figure 6.11 shows the equipment, solvent, sorbent, and total costs plotted against N_D^* at the optimum P_{eb}^* (~353). The vertical black line represents the pressure limit and designs to the left of the line do not satisfy the pressure requirement. Because the material properties are fixed, the column length can be calculated from P_{eb}^* and the port velocity can be calculated from N_D^*.

Estimated costs for separating FRs from SAN at a scale of 10,000 tonnes of FRs/year for the optimized SEC-SMB and batch SEC elution are shown in Table 6.4. Given the same feed and product requirements, the unit separation cost of SEC-SMB is only 2.6% of that of conventional batch elution SEC. Since the separation cost is less than 10% of the purchase cost of these FRs, this technology is economically attractive at this scale.

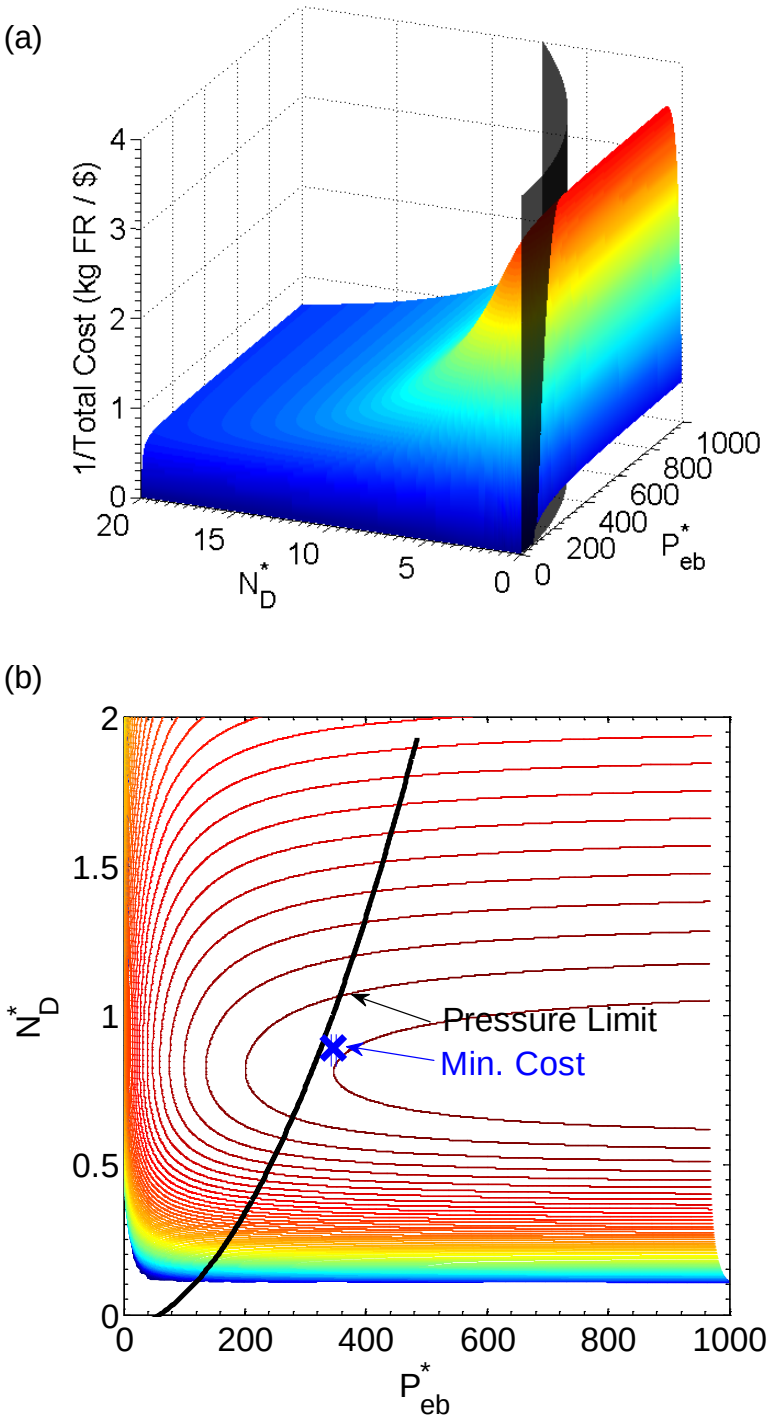

Figure 6.10. (a) Inverse of total cost surface for ternary separation with pressure limit surface and (b) contour plot of (a) with pressure limit (black line) and minimum cost point (x). N^j = 2-2-2-2, DV = 1.9%, ΔP_{max} = 100 psi per zone, Y_i = 99%, R_p = 112 μm.

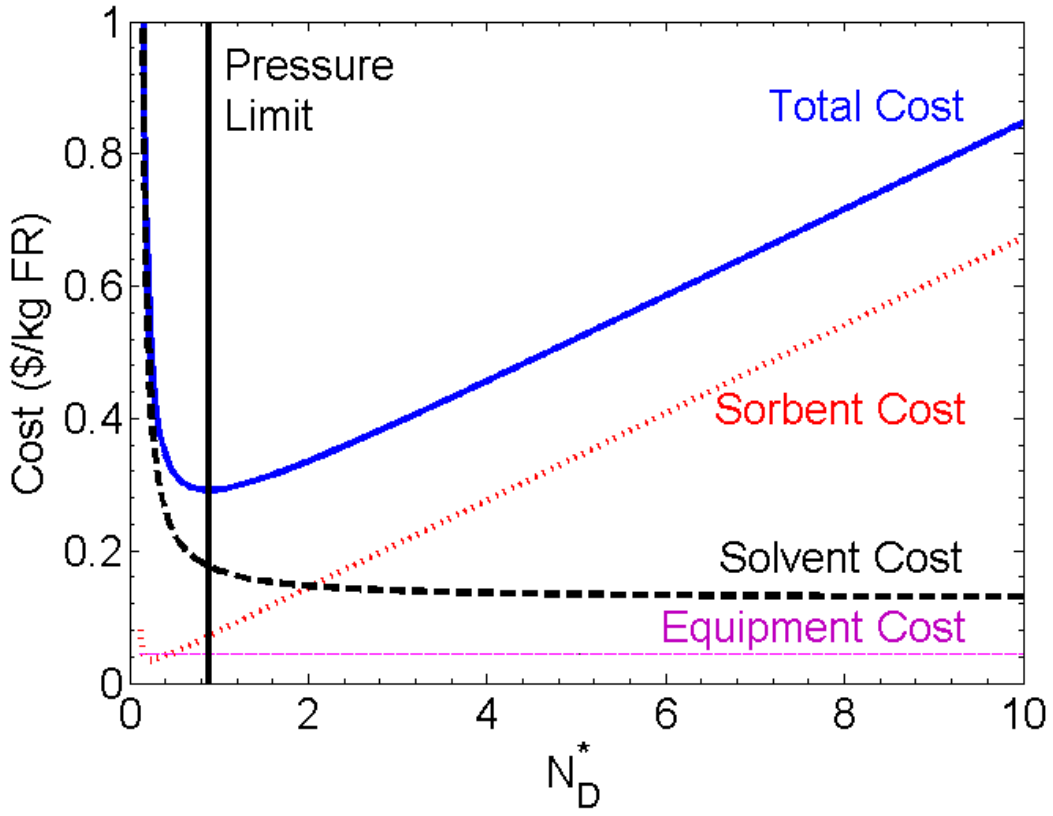

Figure 6.11. Total, sorbent, solvent, and equipment costs versus N_D^* at P_{eb}^* for minimum cost. Vertical black line represents the pressure limit – operating at N_D^* values to the right of the line will satisfy the pressure requirement.

Table 6.4. Comparison of estimated costs[j] of SEC SMB and batch SEC for separating FRs from SAN.

Parameter (10,000 tonnes FR/year)	**Optimized SEC-SMB**	**Batch SEC[k]**
Feed Concentration (wt.%)		
RDP	5	5
BPADP	5	5
SAN	10	10
Product conc./Feed conc.	0.83	0.10
Yield of each component	99	99
Column configuration	2-2-2-2	100 units
Column length (cm)	55.2	126
Inner diameter (m)	9.65	8.19
Feed flowrate (L/min)	175	210 (per unit)
Equipment cost ($/kg FR)	0.04	0.82
Solvent cost ($/kg FR)	0.18	6.05
Sorbent cost ($/kg FR)	0.07	4.40
Total cost ($/kg FR)	0.29	11.27

[j] Cost calculated for product coming from PC extraction technology. Thus, the feed cost and cost of solvent for the feed are considered part of the PC extraction cost and not part of the SMB separation cost. The particle radius used for cost calculations was 112 microns. The estimates do not include cost of concentrating feed.

CHAPTER 7. RESULTS – SPEEDY STANDING WAVE DESIGN OF SEC-SMB

Results in this chapter are reprinted from J. of Chromatogr. A, 1422, Weeden and Wang, Speedy Standing Wave Design of Size-Exclusion Simulated Moving Bed: Solvent Consumption and Sorbent Productivity Related to Material Properties and Design Parameters, 54-76, Copyright (2015) [114], with permission from Elsevier.

7.1 Section Overview

The experimental *D/F* and P_R from three literature cases are compared to those of the SSWD. Additionally, *D/F* and P_R are examined when one dimensionless group is varied at a time. All other variables are held constant. The SEC-SMB for separating insulin from zinc chloride was chosen as the example because the intrinsic parameters for the specific sorbent / buffer system were verified experimentally [31]. The tandem SEC-SMB for insulin purification is then optimized for minimum cost while satisfying an imposed maximum pressure drop per column.

7.2 Comparisons of *D/F* and P_R of Literature Designs with Those of SSWD

The three literature SEC-SMB separations analyzed in this study are polyethylene glycol fractionation by molecular weight (Case 1, Figure 7.1) [35], myoglobin separated from bovine serum albumin (BSA) (Case 2, Fig. 5) [115], and insulin separated from zinc chloride (Case 3, Fig. 6) [31].

A brief summary of the three cases is presented in **Error! Not a valid bookmark self-reference.** with the complete set of material properties and design parameters in Appendix B. The operating parameters of Cases 1 and 2 reported in the literature were obtained using the Triangle theory. The operating parameters of Case 3 were designed using the SWD method at the specific N_D^* of 8.9 (**Error! Not a valid bookmark self-reference.**).

Table 7.1. Table of parameters for three literature cases.

	Case 1	**Case 2**	**Case 3***
Authors	Liang and Liang	Houwing et al.	Xie et al.
Year	2012	2003	2002
Component 1	20,000 MW PEG	BSA	Insulin
Component 2	1,500 MW PEG	Myoglobin	$ZnCl_2$
Design	Triangle	Triangle	SWD
Yield (%) (Comp. 1, Comp. 2)	1A: 65.5, 99.9 1B: 99.9, 99.9 1C: 99.9, 70.7	2A: 46.2, 90.0 2B: 60.5, 90.0 2C: 71.3, 82.5 2D: 86.7, 60.0 2E: 99.8, 40.5	99.0, 99.0
Configuration	2-2-2	2-2-2-2	2-3-3-2
L_c (cm)	30	8.9	13.7
ID (cm)	0.75	1.0	5.1
R_p (μm)	8.5	100	54
N_D^*	~ 4,600	0.36	8.9
P_{eb}^* ($L_c/10\varepsilon_b R_p$)	1,751 (9,688)	35.8 (228)	145 (725)

* Ring B of two ring tandem SMB

The material properties, equipment parameters, and yields for each case reported in the literature were used in the SSWD equations to generate *D/F* and P_R for a wide range of

operating parameters. For Case 1, both N_D^* and P_{eb}^* are very large, making it a nearly ideal system. For Case 2, both N_D^* and P_{eb}^* are relatively small, so both diffusion and dispersion effects are important. For Case 3, N_D^* is relatively small while P_{eb}^* is relatively large, making it a diffusion controlled system.

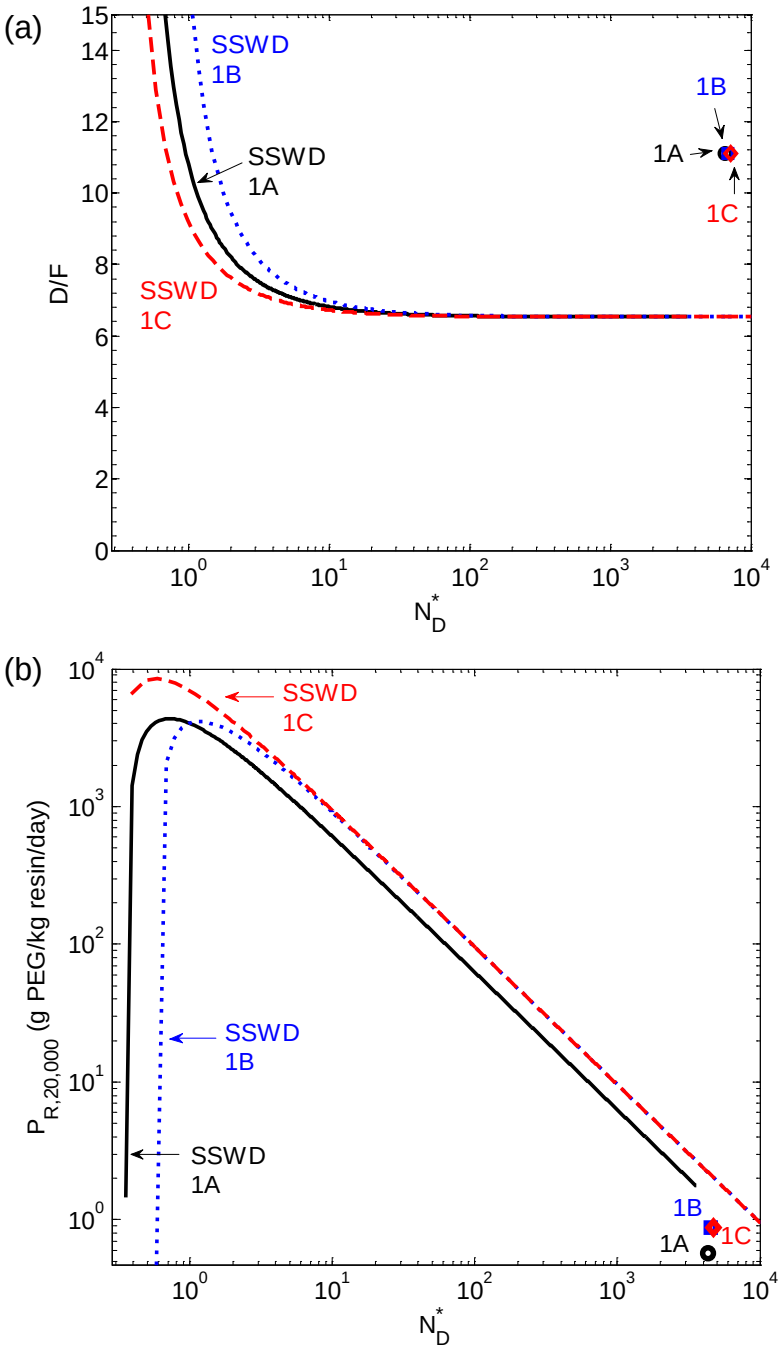

Figure 7.1. Comparison of (a) *D/F* and (b) productivity for Case 1.

Figure 7.1a shows the *D/F* results from SSWD for Case 1, which is a three-zone open-loop SMB. The minimum *D/F* from SSWD is about 6.5 because there is no recirculation of the solvent. The difference between the three curves is due to the yield

requirements, A brief summary of the three cases is presented in **Error! Not a valid bookmark self-reference.** with the complete set of material properties and design parameters in Appendix B. The operating parameters of Cases 1 and 2 reported in the literature were obtained using the Triangle theory. The operating parameters of Case 3 were designed using the SWD method at the specific N_D^* of 8.9 (**Error! Not a valid bookmark self-reference.**).

Table 7.1. Because the N_D^* value for each of the three runs (1A-1C) is over 4,000, diffusion effects in Case 1 are negligible. The solvent consumption for the Case 1 experiments could have been reduced by about 50% if the operating parameters had been obtained from the SSWD method, Figure 7.1, Figure 7.4.

Figure 7.1b shows the P_R results from SSWD for Case 1. Because the N_D^* values are so large, the P_R^* is very low. The results from SSWD show that P_R could increase over 100 fold if the operating parameters were designed based on $N_D^* \sim 4{,}600$.

Figure 7.2 compares the SSWD results with the literature results for Case 2. The experiments in the literature were operated at a relatively low N_D^* (~0.4). The curves generated by the SSWD do not extend to lower N_D^* values because assumptions used to obtain Eq. (3.3) do not hold in the low yield and low N_D^* regime [59]. In Figure 7.2a, the *D/F* curve for 2E is significantly higher than the other curves because the yield for component 1 (BSA) is very large (99.8%) and the yield for component 2 (Myoglobin) is very low (40.5%) compared to the other experiments. The solvent consumption for these experiments could have been reduced 2-9 fold if the operating parameters were designed using SSWD at the same N_D^*, Figure 7.2a, Figure 7.4a.

Figure 7.2b shows the P_R results from SSWD for Case 2. The P_R curves generated by the SSWD do not extend to low N_D^* (< 0.3) because of the low yield specifications. Because the N_D^* values for the literature are lower than those of Case 1, the productivities are much larger. The productivity values for Case 2A-2E are in the same order of magnitude as that of the SSWD at the same N_D^*. However, the P_R for Case 2A-2E could have been increased 4-6 fold if the operating parameters were designed using SSWD at the same N_D^*, Figure 7.2b, Figure 7.4b.

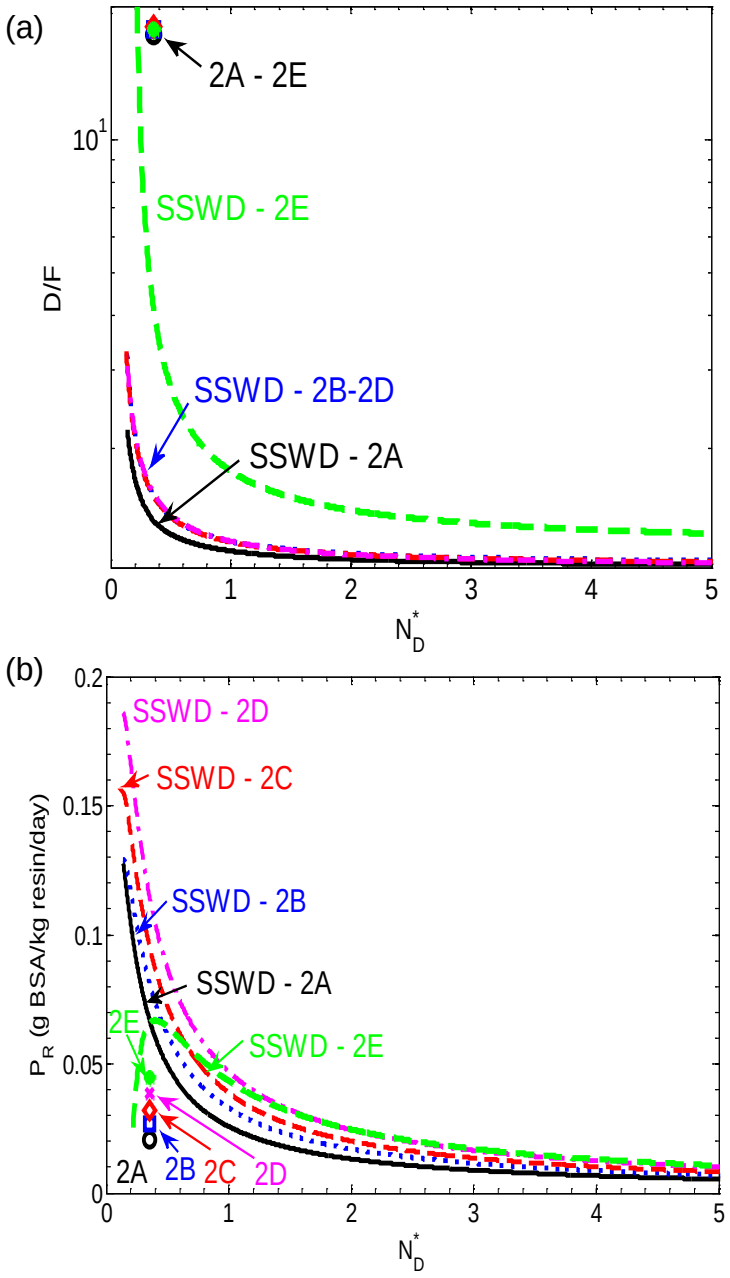

Figure 7.2. Comparison of (a) *D/F* and (b) productivity for Case 2.

Since the operating parameters for Case 3 were designed using SWD, *D/F* and P_R of are the same as those from SSWD at the same N_D^*, column configuration (2-3-3-2), and yields (99.7%), Figure 7.3, Figure 7.4.

The SSWD works for ideal systems, diffusion controlled systems, or systems where both diffusion and dispersion are significant. For given material properties, yields, and equipment parameters, SSWD can quickly generate an overview of D/F and P_R over a wide range of operating parameters. The conditions for maximum P_R or small D/F can be easily identified from such figures. The comparisons with literature results show that all three cases could have been improved by orders of magnitude using the SSWD method to reduce D/F and/or increase P_R. Without the overview provided by the SSWD, it would be challenging to explore the multi-dimensional SEC-SMB design space with simulations or experiments.

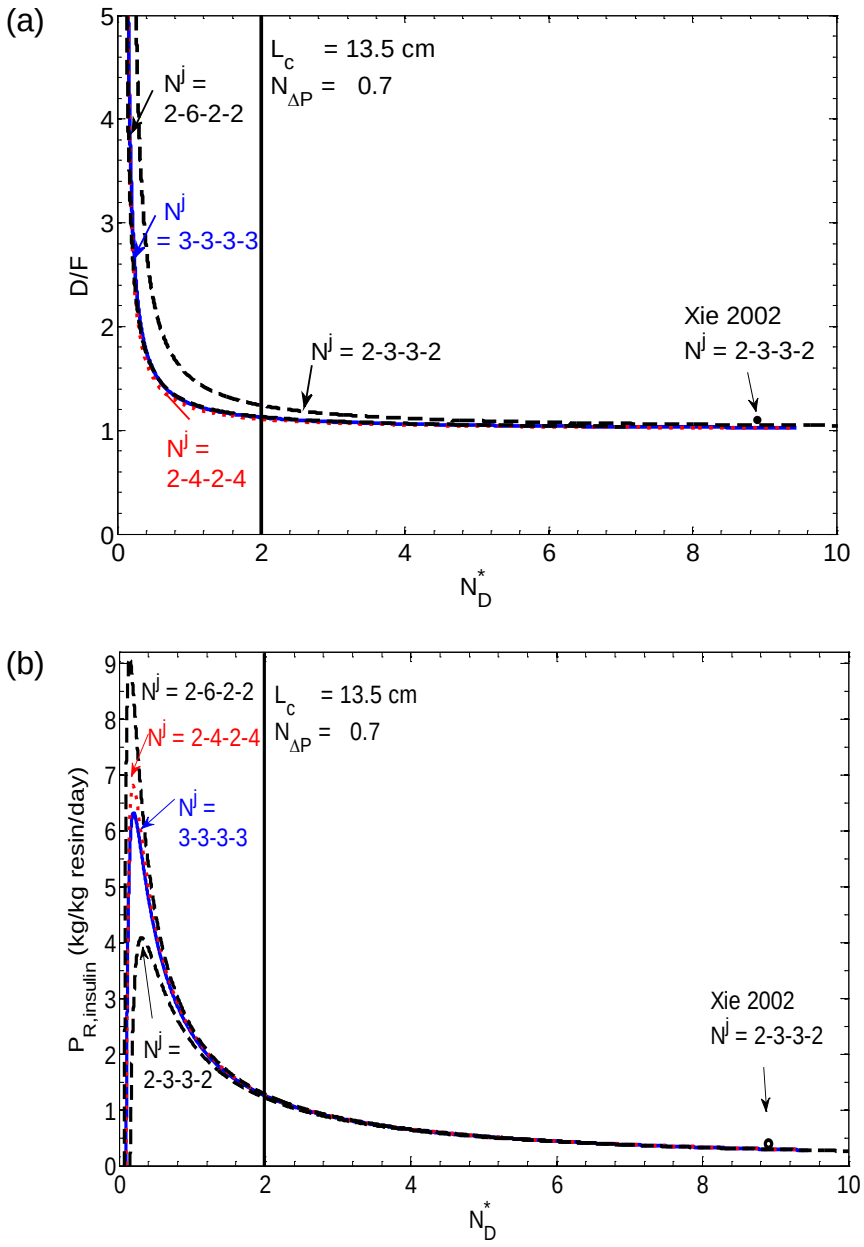

Figure 7.3. (a) *D/F* and (b) P_R for three column configurations with varying N_D^* - diffusion controlled. Vertical line represents the minimum N_D^* allowed by the pressure limitation (designs to the left of the line are not feasible). *D/F* and P_R curves for N^j = 2-3-3-2 are at 99.9% yield to compare to data point from Xie et al.

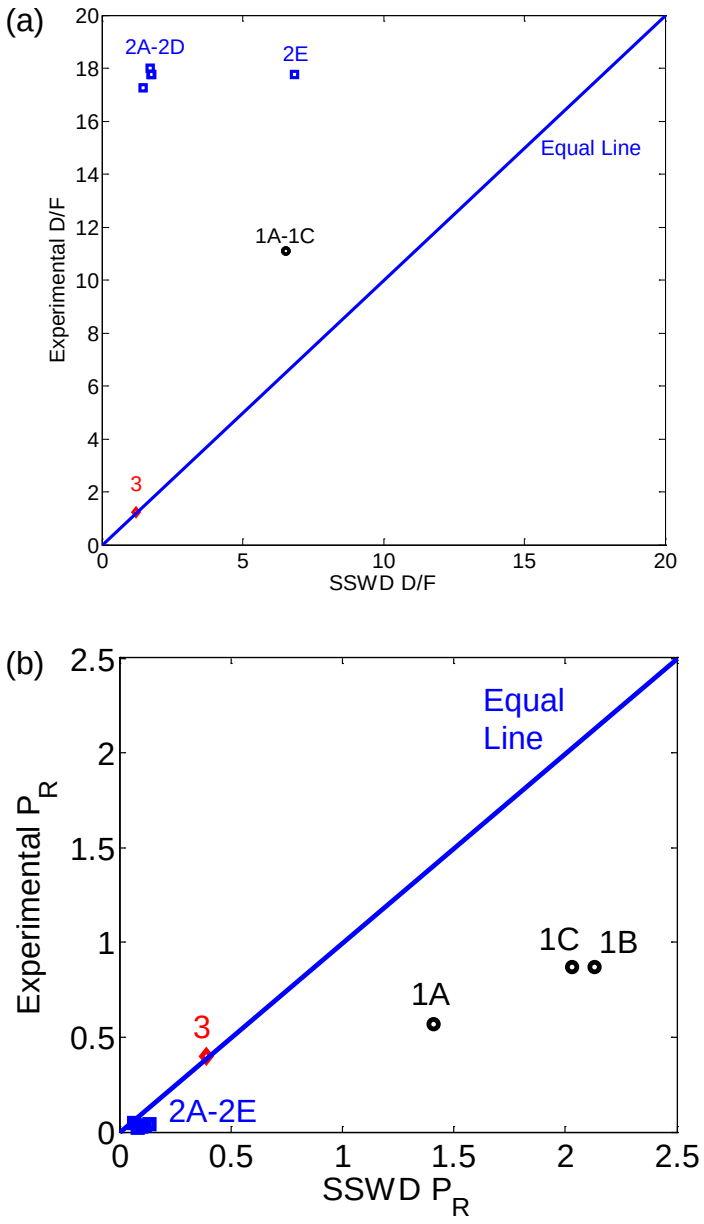

Figure 7.4. Comparison of (a) *D/F* and (b) productivity for literature designs and SSWD of SEC-SMB at the same N_D^*.

7.3 Example System Based on Insulin Purification for Parametric Studies

In the production of insulin, many purification steps are needed [26]. Before crystallization, SEC is used to separate high molecular weight proteins (HMWP) and zinc chloride ($ZnCl_2$) from insulin [31]. This batch chromatography produces 99% pure insulin with 89% yield. In 2002, Xie et al. designed and experimentally verified a tandem SEC-SMB system (two SMBs in series) to obtain 99% pure insulin with 99% yield.

The first ring of the tandem SMB (Ring A) separates the HMWP (fast solute) from insulin (slow solute). No constraints are placed on the zinc chloride, which means that zinc chloride is distributed throughout the entire SMB to reduce the impurity to be removed in Ring B. There is significant insulin fronting due to dimerization reactions that occur in Zone III of Ring A. This fronting can be accounted for by assuming that the axial dispersion coefficient in Zone III is 40 times the value predicted by the Chung and Wen correlation [31]. Because of this large axial dispersion, both diffusion and dispersion effects are important for Ring A. The extract from Ring A is then sent to the second SMB (Ring B) to remove the zinc chloride.

Ring B separates zinc chloride (slow solute) from insulin (fast solute). Because of dilution from Ring A, the insulin fronting is insignificant in Ring B. Thus, Ring B is a diffusion controlled system. The solutions for D/F and P_R are calculated according to Table 3.2. The intrinsic material properties and yields were obtained from Xie et al., 2002, Table 7.2. The dimensionless parameters in Table 7.2 are fixed for all figures unless specified otherwise. Ring A will later be used as a cost optimization example, where both diffusion and dispersion are significant. Ring B is used for the parametric studies in the following

sections. The tandem SMB requires significantly less solvent and less sorbent than the batch SEC, Table 7.3.

Table 7.2. Fixed parameters for insulin parametric study unless otherwise specified.

R_p^* (μm)	ε_b	ε_p	ϕ	DV (%)	Y (%)	$E_{b,i}^j$
54	0.35	0.89	1.86	1.9	99	Chung and Wen Correlation

Component	D_p (cm^2/min)	K_{se}	δ
High Molecular Weight Proteins (HMWP)	2.00×10^{-5}	0.19	0.198
Insulin	2.29×10^{-5}	0.74	0.688
Zinc Chloride	1.65×10^{-4}	0.99	0.910

SMB Ring	α	γ	γ/α
A (Insulin / HMWP)	3.47	1.15	0.33
B ($ZnCl_2$ / Insulin)	1.32	7.21	5.46

$C_{F,i}$ (g/L)	ρ_p (kg sorbent/L particle volume)	μ (cP)	ΔP_{max}^* (psi)
54	0.12	2.5	1.5

*Sephadex G50

Table 7.3. Comparison of batch, SMB, and cost optimized SMB.

Parameter (5,000 kg insulin / year)	**Batch[b]**	**Xie (2002)[b]**	**Optimized SMB[a]**		
			Ring A[b]	**Ring B[c]**	**Overall[b]**
Overall Yield (%)	89	99	99	99	98
Product Concentration (g/L)	45.0	59.0	61.9	47.8	47.8
Column Configuration	12 in series	A: 2-2-4-2 B: 2-3-3-2	2-2-2-2	2-2-2-2	A: 2-2-2-2 B: 2-2-2-2
Feed Flowrate (mL/min)	119 (each)	109	109	-	109
Column Length (cm)	15	A: 13.7 B: 13.7	15.9	11.2	A: 15.9 B: 11.2
Diameter (cm)	45 (12 units)	A: 47.9 B: 58.6	20.4	29.8	A: 20.4 B: 29.8
N_D^*	-	A: 6.0 B: 8.9	14.9	1.48	A: 14.9 B: 1.48
P_{eb}^*	-	A: 145 B: 145	560	108	A: 560 B: 108
Solvent consumption (L/kg insulin)	150.0	42.0	28.0	22.8	50.8
Productivity (kg /kg sorbent /day)	0.05	0.14	4.47	2.80	1.69
Equip. Cost ($/kg insulin)	35.71 (39%)	29.76 (72%)	14.29	14.29	28.58 (81%)
Solv. Cost ($/kg insulin)	15.00 (17%)	3.96 (10%)	2.80	2.28[d]	5.08 (15%)
Resin Cost ($/kg insulin)	40.07 (44%)	7.41 (18%)	0.43	0.79	1.22 (4%)
Total Cost ($/kg insulin)	**90.78**	**41.43**	**17.58**	**17.36**	**34.94**

[a]Under constraint that there is a minimum of two columns per zone.
[b]Feed concentration of insulin is 88.5 g/L.
[c]Feed concentration of insulin for Ring B is product concentration from Ring A.
[d]Ring B solvent cost only includes desorbent cost because feed solvent was already accounted for in Ring A.

7.4 Parametric Studies – Diffusion Controlled

For *D/F*, P_R, and pressure limit curves in this section, the values for α, λ, γ, δ, ϕ, and yields are reported in Table 7.2 and are fixed unless noted otherwise. For *D/F* curves, t_s, R_p, and $D_{p,i}$, are allowed to vary with changing N_D^*. For P_R and pressure limit curves, ε_p, ε_b, $K_{se,i}$, $D_{p,i}$, N, feed concentration ($C_{F,i}$), packing density (ρ_b), and R_p, are fixed at the values reported in Table 7.2, unless noted otherwise. For P_R curves, t_s is allowed to vary

with changing N_D^*. For the pressure limit curves, viscosity (μ) and maximum pressure (ΔP_{max}) are fixed at the values reported in Table 7.2 and L_c is fixed at 13.5 cm.

7.4.1 N_D^* and Column Configuration

Figure 7.3 also shows how column configuration affects solvent consumption and sorbent productivity for diffusion controlled systems. Since most industrial applications have a fixed number of columns or valves, it is more useful to determine the optimum distribution of columns, or column configuration, for a given total number of columns. Three column configurations with 12 columns total are plotted for comparison purposes: minimum *D/F* (2-4-2-4), maximum productivity (2-6-2-2), and an equal distribution (3-3-3-3).

Figure 7.3a illustrates the relation between N_D^* and *D/F* for the three column configurations. As N_D^* increases, the step time increases relative to the diffusion time, which means that diffusion becomes less controlling and the system approaches an ideal system with *D/F* equal to one. Solvent consumption decreases slowly after N_D^* increases beyond 2 for this system. As N_D^* decreases, the denominator of Eq. (3.27) approaches zero, resulting in a sharp rise in *D/F* near $N_{D,min}^*$, which corresponds to the minimum relative diffusion time required for any separation to occur. The vertical line is based on the pressure limits of the system (1.5 psi) [32], and the column length of 13.5 cm, which is the optimal column length to achieve the lowest total cost Ring B (Section 7.7). This line can be found by solving Eq. (32) for N_D^* because $N_{\Delta P,diff}$ is fixed for fixed material properties, yields, and equipment parameters. N_D^* values to the right of this will give port velocities, or interstitial velocities, which do not exceed the pressure limit.

In this example, diffusivity ratio (γ = 7.21) is much larger than the selectivity (α = 1.34). Because the terms inside the parentheses in Eq. (3.27) are already relatively small, the column configuration does not have a large impact on *D/F*.

The effect of N_D^* on P_R is presented in Figure 7.3b. There is a minimum N_D^* for P_R to be positive, $N_{D,min}^*$ (~0.1), which is the same $N_{D,min}^*$ for *D/F*. Increasing N_D^* from $N_{D,min}^*$ to $N_{D,\max P_R}^*$ will increase P_R, as expected from Eq. (3.29b). Increasing N_D^* means sharper concentration waves, which mean more effective utilization of the sorbent, or higher sorbent productivity. The P_R curve peaks near N_D^* = 0.2, Eq. (30). This N_D^* corresponds to $N_{D,1}$ ~ 1, Eq. (3.18), where the step time is approximately equal to the diffusion time. Increasing N_D^* after this point reduces P_R because the increase in step time is more significant than the reduced wave spreading. In general, the maximum P_R for SEC-SMBs occurs at $N_{D,1}$ ~ 1, as evidenced by all three literature cases.

Figure 7.3b also shows how column configuration significantly affects the maximum P_R. Because γ/α is about 5.4, Eq. (31) gives 2-6-2-2 as the column configuration for maximum productivity. For N_D^* larger than 2, the column configuration does not significantly affect the productivity.

The pressure limit for a column length of 13.5 cm is again shown by the vertical line, indicating that the theoretical maximum productivity is not achieved since the pressure limit, column length, particle size, and column configuration are fixed. The productivity for the lowest cost system is less than 15% of the theoretical maximum productivity for the 2-6-2-2 column configuration.

7.4.2 Particle Size and Pressure Limit

P_R is strongly affected by particle size, as seen in Figure 7.5a. From Eq. (3.29b), it is obvious that P_R is inversely proportional to R_p^2 for a fixed N_D^*. However, reducing R_p also increases the pressure drop across a column (ΔP). As discussed previously, Eq. (30) and Eq. (32) can be used to determine the combination of pressure limit, column length, and particle size ($\Delta P_{max} R_p^4 / L_c^2$), which is needed to achieve the maximum productivity.

In Figure 7.5b, $\Delta P / L_c^2$ is plotted for a wide range of R_p (5-500 μm) for fixed column configuration (3-3-3-3) and other material properties (Table 7.2). The yield for each solute is varied from 90% to 99.9%. This result shows that the pressure drop rapidly increases when R_p is below 50 μm. For a 10 cm column packed with R_p = 50 μm, the pressure drop required to realize the maximum productivity is 10 psi. For R_p = 25 μm, the productivity can be four times higher (Figure 7.5a), but the pressure drop will be about 1,000 psi, which requires high pressure equipment. Conversely, for high pressure SMB equipment with a maximum operating pressure of 1,500 psi, one can find the combination of particle size and column length to maximize productivity. The trade-off between pressure and productivity can be optimized if appropriate cost functions are known.

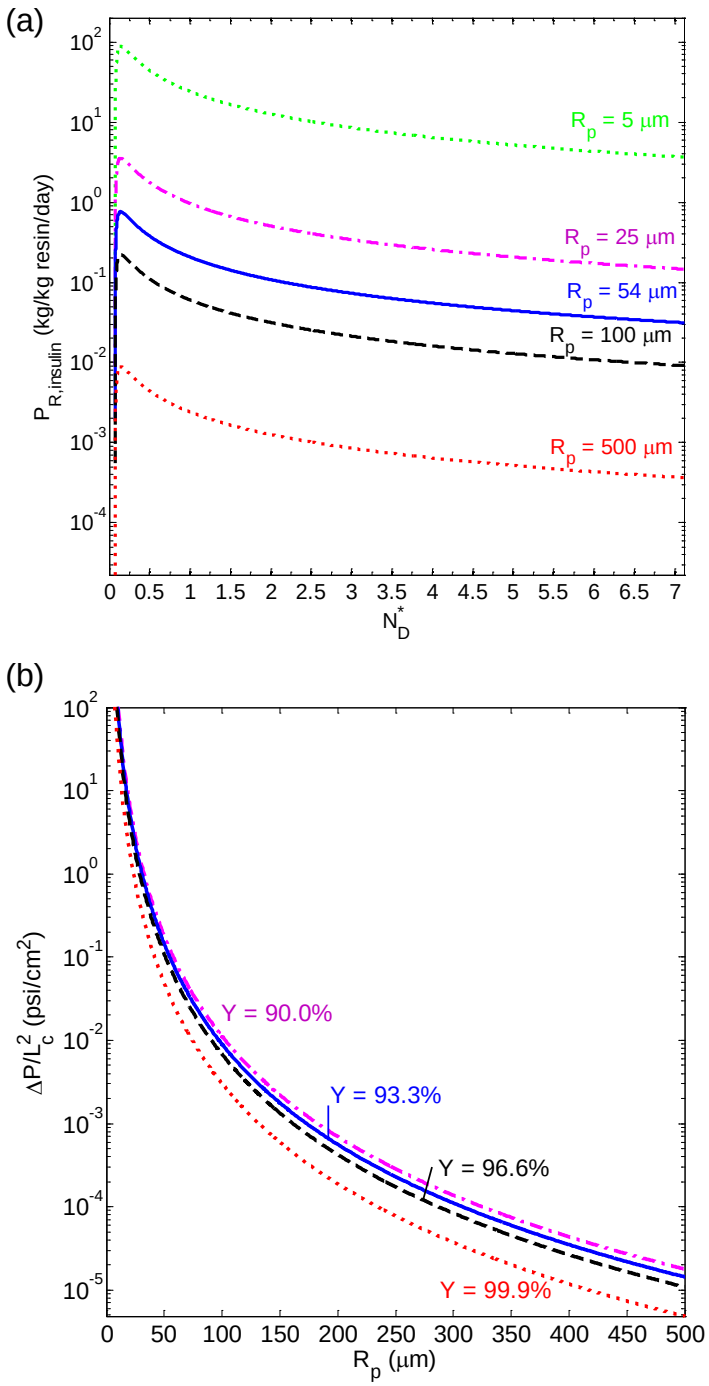

Figure 7.5. (a) Productivity at varying R_p and (b) Pressure drop per length^2 vs R_p at varying yields (fixed $N_D{}^* = N^*_{D,\max P_R} \sim 0.2$) – diffusion controlled.

7.4.3 Yield

The effect of yield on solvent consumption is examined in Figure 7.6a. Increasing the yield requirement increases the values of the four β terms in Eq. (3.27), resulting in the increase of the numerator and the decrease of the denominator. Thus, increasing yield results in increasing *D/F*. However, the increase in *D/F* is not very significant until yield is larger than 99%. The increase after 99% is more significant for small N_D^* (< 1). Increasing N_D^* reduces the dependence of *D/F* on yield. There is a sharp increase near 100% yield because significantly more solvent is required to confine the very low concentration portions of the waves in their respective zones.

The effect of yield on P_R is presented in Figure 7.6b. Increasing yield from 90% does not significantly change P_R until after yield exceeds 99%. From Eq. (3.29), it can be seen that increasing the values of the β's in the denominator decreases P_R, but the yield outside the brackets in the numerator mitigates this effect until the yields are very high. Increasing yield requirement means more separation between the solute bands, resulting in less column utilization or lower P_R. The productivity approaches zero near 100% yield because a very small feed flow rate is required for the separation. Increasing N_D^* decreases the dependence of P_R on yield.

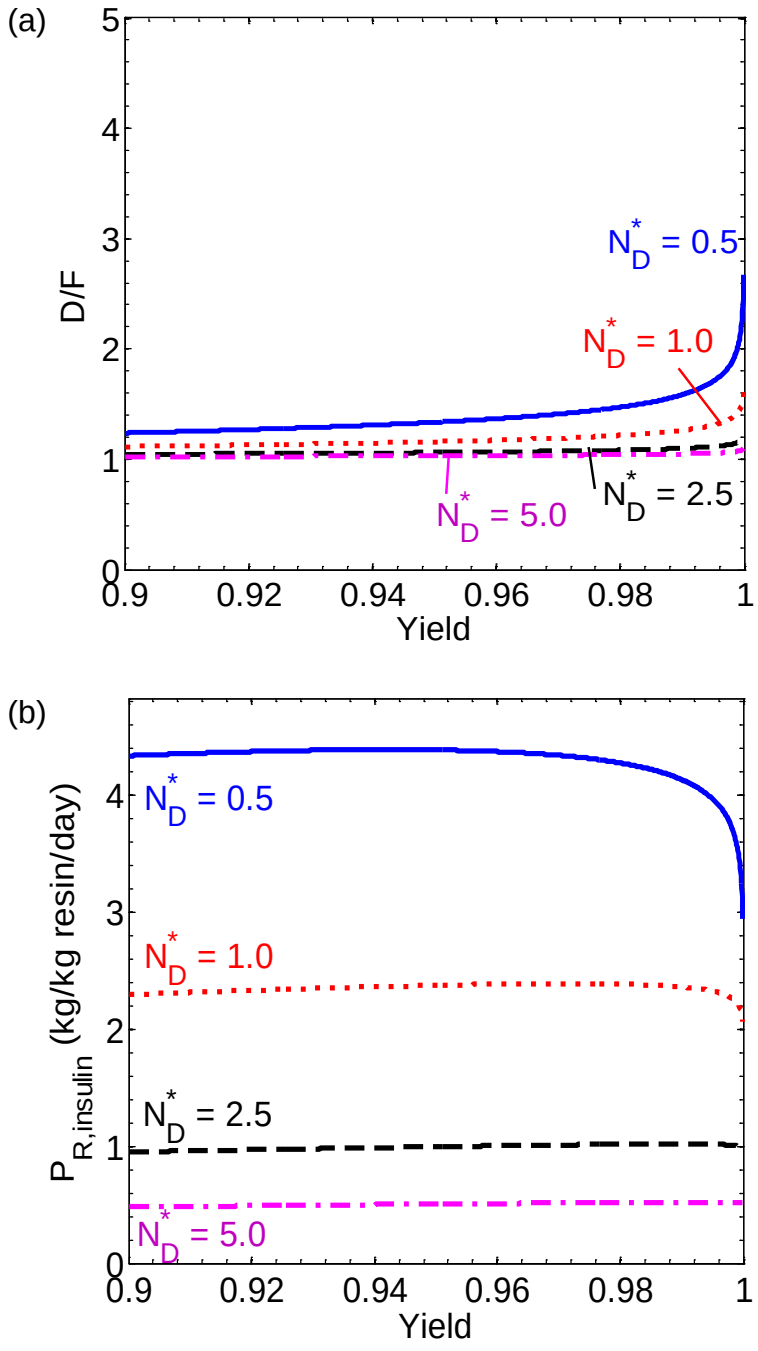

Figure 7.6. (a) *D/F* and (b) P_R vs. yield at various N_D^* - diffusion controlled, 3-3-3-3 configuration.

7.4.4 Retention Factors and Selectivity

Because N_D^* is dependent on selectivity and retention factors, $N_{D,1}$ was fixed at 6.5, which corresponds to the lowest cost design for Ring B (see Section 7.7). Solvent consumption is plotted against α in Figure 7.7a. Increasing α always decreases *D/F* because there is an increasing difference in wave velocities but there is little gain when α is larger than 1.5. There is a vertical asymptote at α equal to one because there would be no difference in the wave velocities of the two species and no separation could occur. The effect of the retention factors (δ) can also be seen in Figure 7.7a. The lines for δ_1 stop at different α's because there is a maximum δ_2 in SEC. When a solute accesses all the pore space, the maximum size-exclusion factor is one and the maximum δ is equal to the particle porosity if *DV* is negligible. The *D/F* values are higher for larger δ's because more solvent is needed for the solutes to diffuse out of the particles at the same α.

Increasing α always increases the P_R, as shown in Figure 7.7b. Increasing α is shown as increasing δ_2 for a fixed δ_1. The more the slow solute can access the pore volume, the more efficiently the sorbent particles are used. Therefore, a larger retention factor for the slow solute provides a higher productivity at the same selectivity. The P_R linearly increases with selectivity because the P_R for an ideal system is linearly dependent on selectivity, as are the correction terms for non-ideal SEC systems with negligible *DV*, Eq. (3.29a).

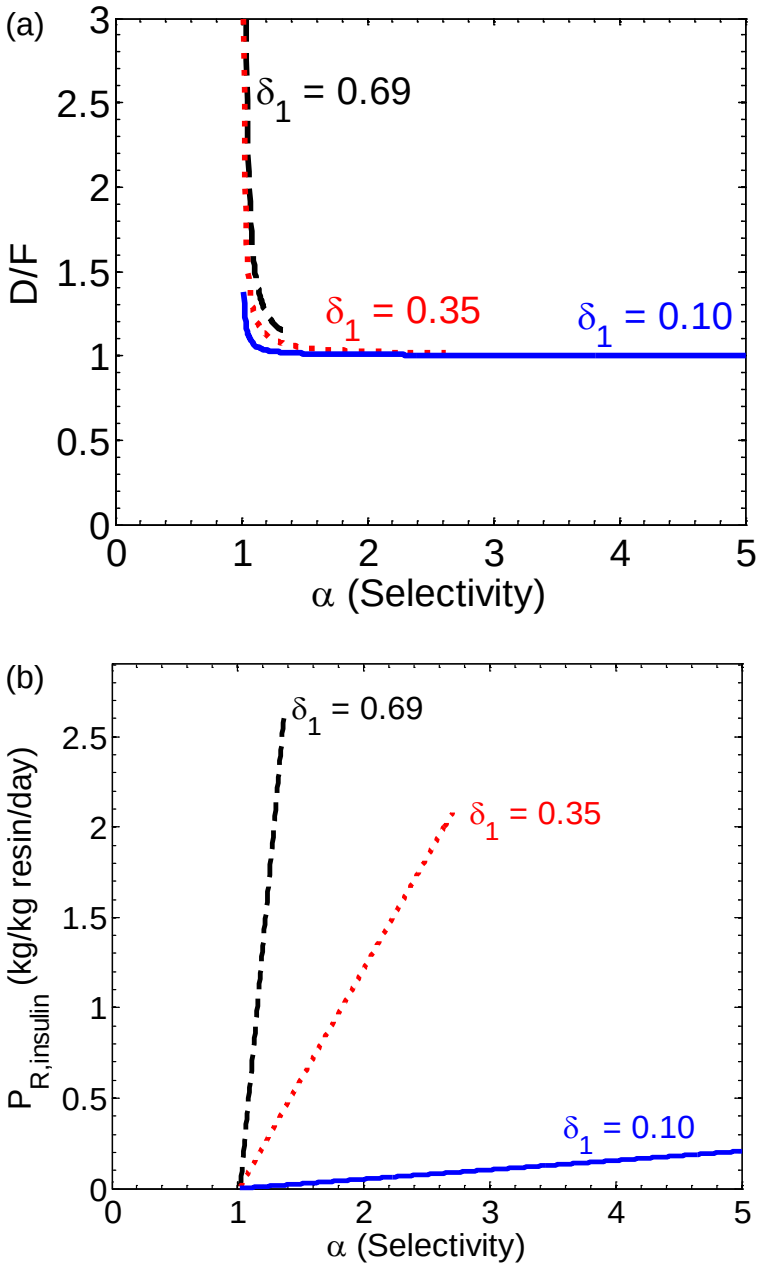

Figure 7.7. (a) *D/F* and (b) P_R vs. selectivity at a fixed N_D^* and various δ_1 – diffusion controlled, 3-3-3-3 configuration. Fixed $N_{D,1}$ = 6.5.

7.4.5 Dead Volume Effect on Retention Factors and Selectivity

Extra-column *DV* increases the retention factors and introduces dispersion effects. The dispersion can be plug flow (no dispersion), Taylor dispersion, or that of a completely stirred tank. Since they are equipment dependent, they are not considered in this study. Only the effect of *DV* on the retention factors, and subsequently selectivity, is discussed below.

Increasing *DV* increases the values of the retention factors (δ), Eq. (3.6). Since N_D^* is dependent on δ, Eq. (3.18), constant $N_{D,1}$ curves are shown in Figure 7.8. Dead volume can significantly increase *D/F*, Figure 7.8a. From Eq. (3.27), it is clear that increasing δ values increases *D/F* for diffusion controlled systems. However, the effect of *DV* can be significantly reduced at larger $N_{D,1}$. Because the difference in the retention factors is unaffected by *DV*, *D/F* is unaffected by *DV* at large $N_{D,1}$, Eq. (3.15). Dead volumes less than 2% ($DV < 0.02$) do not significantly increase *D/F* for this system.

Increasing the *DV* of the system reduces the selectivity, which in turn reduces the productivity, Figure 7.8b. It can be seen from Eq. (3.16) that increasing $N_{D,1}$ can reduce the impact of *DV* because the difference in retention factors is not affected by *DV*. However, the productivity also decreases with increasing $N_{D,1}$. Dead volumes less than 2% do not significantly affect the productivity of the SEC-SMB.

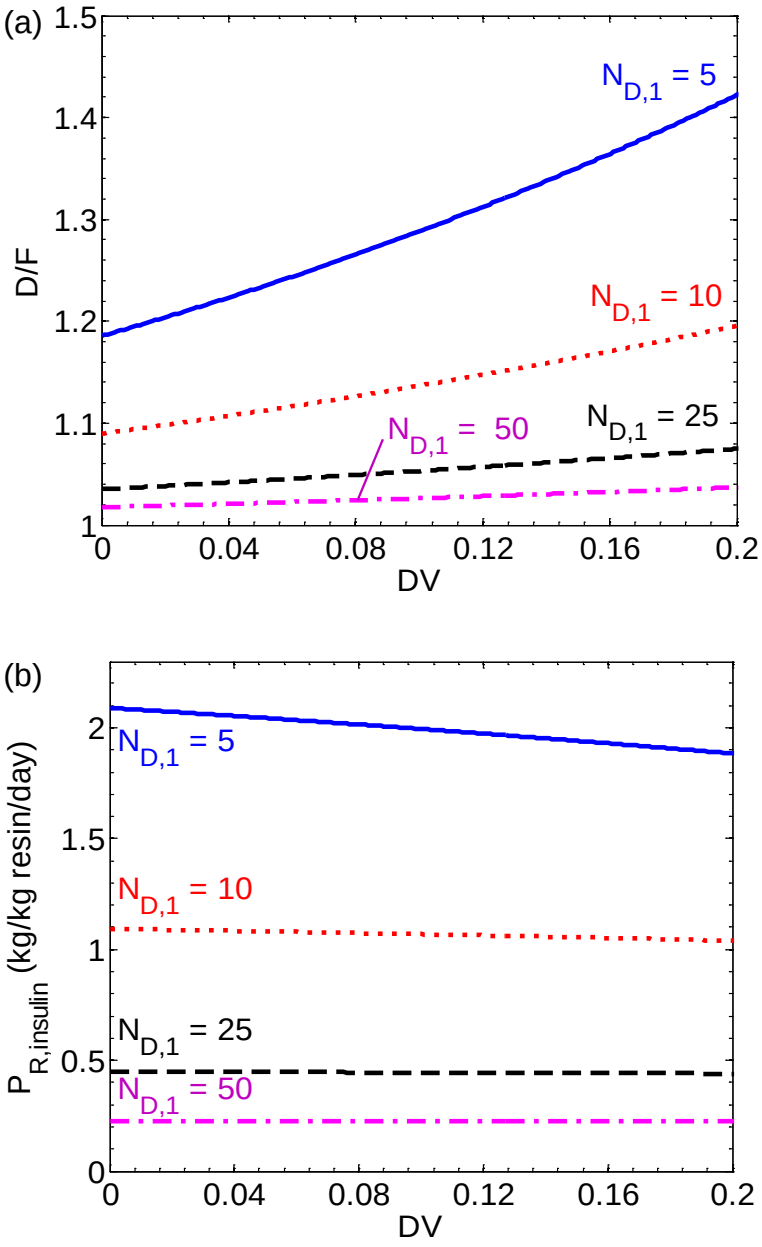

Figure 7.8. (a) *D/F* and (b) P_R vs. *DV* for various $N_{D,1}$ - diffusion controlled, 3-3-3-3 configuration.

7.4.6 Diffusivity Ratio

The effect of diffusivity ratio (γ) on *D/F* is explored in Figure 7.9a. As γ increases, *D/F* decreases when N_D^* is a fixed parameter (i.e. $N_{D,1}$ is fixed). Increasing γ with a fixed $N_{D,1}$ is equivalent to increasing $D_{p,2}$. By increasing the diffusivity of the slow solute, the concentration waves become sharper and thus require less solvent to prevent the waves from spreading into different zones. There is a minimum value of γ for the system to be feasible. For γ greater than three, *D/F* does not change significantly. The *D/F* dependence on γ is larger at low N_D^*, where diffusion effects are more significant.

The P_R curves always increase with increasing γ, until P_R reaches a plateau. The waves become sharper, resulting in increased column utilization or sorbent productivity, Figure 7.9b. There is a minimum γ for P_R to be positive. The P_R does not change significantly after γ exceeds 3. Increasing N_D^* reduces P_R, and also reduces the dependence of P_R on γ.

Figure 7.7 and Figure 7.9 show that large α and large γ both decrease *D/F* and increase P_R. A large ratio of γ/α can also decrease *D/F* and increase P_R, as shown in Eqs. (27) and (29a). If γ/α is small, increasing the length of Zones I and III can have a similar effect on *D/F* as increasing γ/α, Eq. (3.27). Increasing the length of Zone III also increases P_R, Eq. (3.29a).

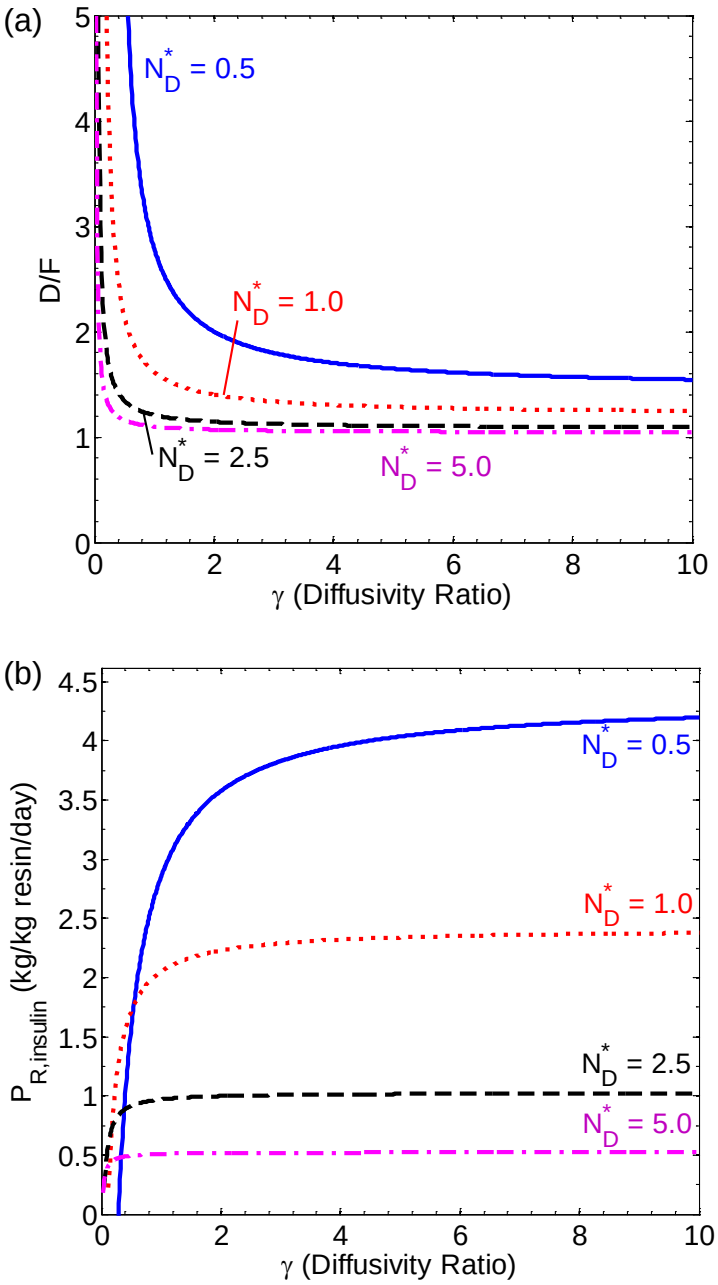

Figure 7.9. (a) *D/F* and (b) P_R vs. γ at various N_D^* - diffusion controlled, 3-3-3-3 configuration.

7.4.7 Phase Ratio

For diffusion controlled systems, D/F is independent of the phase ratio (ϕ), Eq. (3.27), because N_D^* is independent of ϕ, Table 3.1. The P_R is also independent of ϕ, Eq. (3.29).

7.5 Parametric Studies – Dispersion Controlled

As shown in Table 3.2, D/F, P_R, and $N_{\Delta P}$ are functions of Γ. To obtain values for Γ, axial dispersion coefficients were estimated using the Chung and Wen correlation for low Re, Eq. (36). For D/F, P_R, and pressure limit curves in this section, the values for α, δ, ϕ, and yields are reported in Table 7.2 and are fixed unless noted otherwise. For D/F curves, L_c and R_p are allowed to vary with changing P_{eb}^*. For P_R and pressure curves, the values of ε_b, N, $C_{F,i}$, ρ_p, and R_p, are given in Table 7.2, unless noted otherwise. The port velocity for P_R and pressure curves is fixed at 1 cm/min. For P_R curves, L_c varies with changing P_{eb}^*. For the pressure curves, μ and ΔP_{max} are fixed at the values reported in Table 7.2 and L_c is fixed at 13.5 cm.

7.5.1 P_{eb}^* and Column Configuration

The effect of P_{eb}^* on D/F is illustrated in Figure 7.10a. There is a minimum P_{eb}^* for the system to be feasible, as predicted by Eq. (35). The D/F decreases with increasing P_{eb}^* because axial dispersion effects decrease. These trends are supported by Eq. (34). The D/F does not change much after a P_{eb}^* of 50 ($L_c/R_p \sim 900$ for the given ϕ and δ, Eq. (37a)), when the dispersion effects start becoming negligible.

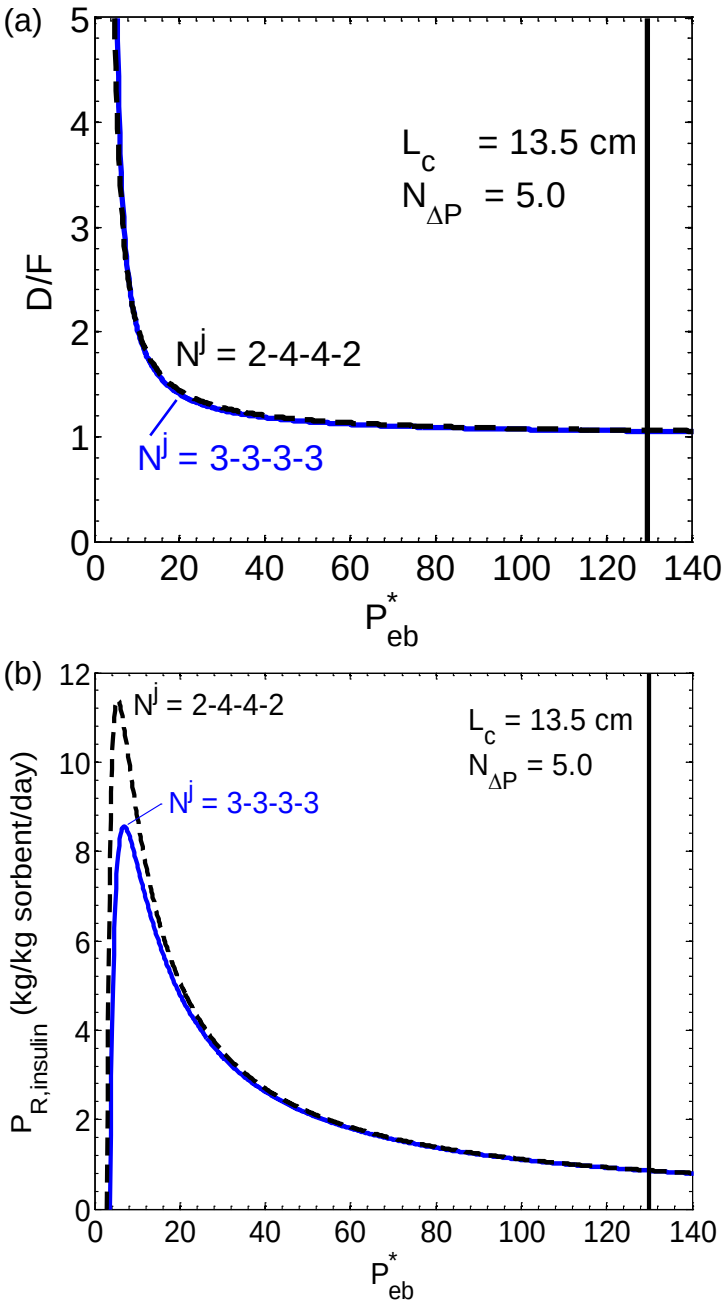

Figure 7.10. (a) *D/F* and (b) P_R vs P_{eb}^* for multiple column configurations at constant port velocity = 1 cm/min – dispersion controlled. Vertical line represents the maximum P_{eb}^* allowed by the pressure limitation.

Figure 7.10a also shows the effect of column configuration on *D/F*. From Eq. (34), it is apparent that increasing the zone length of any zone will decrease *D/F*. Since the Γ values for the four zones are not very different from each other, the column configuration for minimum *D/F* is an equal distribution (3-3-3-3). However, the *D/F* curve for the minimum *D/F* configuration is only slightly better than the *D/F* curve for the maximum P_R configuration (2-4-4-2).

For a fixed particle size, increasing P_{eb}^* is equivalent to increasing the column length. Because maximum pressure drop and port velocity are fixed, the maximum column length can be illustrated in Figure 7.10 as a vertical line. The vertical line represents the maximum P_{eb}^* allowed by the pressure limit. Values to the left of the line will satisfy the pressure limit.

The effect of P_{eb}^* on P_R is illustrated in Figure 7.10b and can be seen from Eq. (37). There is a minimum P_{eb}^* for the SMB to have a positive P_R, which is the same minimum P_{eb}^* for *D/F*. P_R increases with increasing P_{eb}^* rapidly at first, then peaks, and then slowly decreases. Increasing P_{eb}^* decreases the effects from axial dispersion. The maximum P_R occurs around a P_{eb}^* of 6. The effects of column configuration can also be seen in Figure 7.10b. Longer Zones II and III can increase P_R significantly, as expected from Eq. (39), but there is no effect at large P_{eb}^* (>50) because the dispersion effects become negligible.

7.5.2 Yield

The effect of yield requirement on *D/F* for dispersion controlled systems is shown in Figure 7.11a. Increasing yield requirement always increases *D/F* because of the extra solvent needed to confine the low concentration portions of the waves. This trend is similar to that for diffusion controlled systems. *D/F* does not change much until after yield exceeds 99%. There is a sharp increase near 100% yield because significantly more solvent is required to confine the very low concentration portions of the waves in their respective zones. Increasing P_{eb}^{*} decreases the effect of yield on *D/F* because dispersion effects decrease.

The effect of yield on P_R is shown in Figure 7.11b. Productivity does not significantly change with yield until it exceeds 99%. Increasing P_{eb}^{*} decreases the effect of yield on P_R, but also decreases P_R. To approach 100% yield, the feed flowrate must be significantly reduced, resulting in very small P_R.

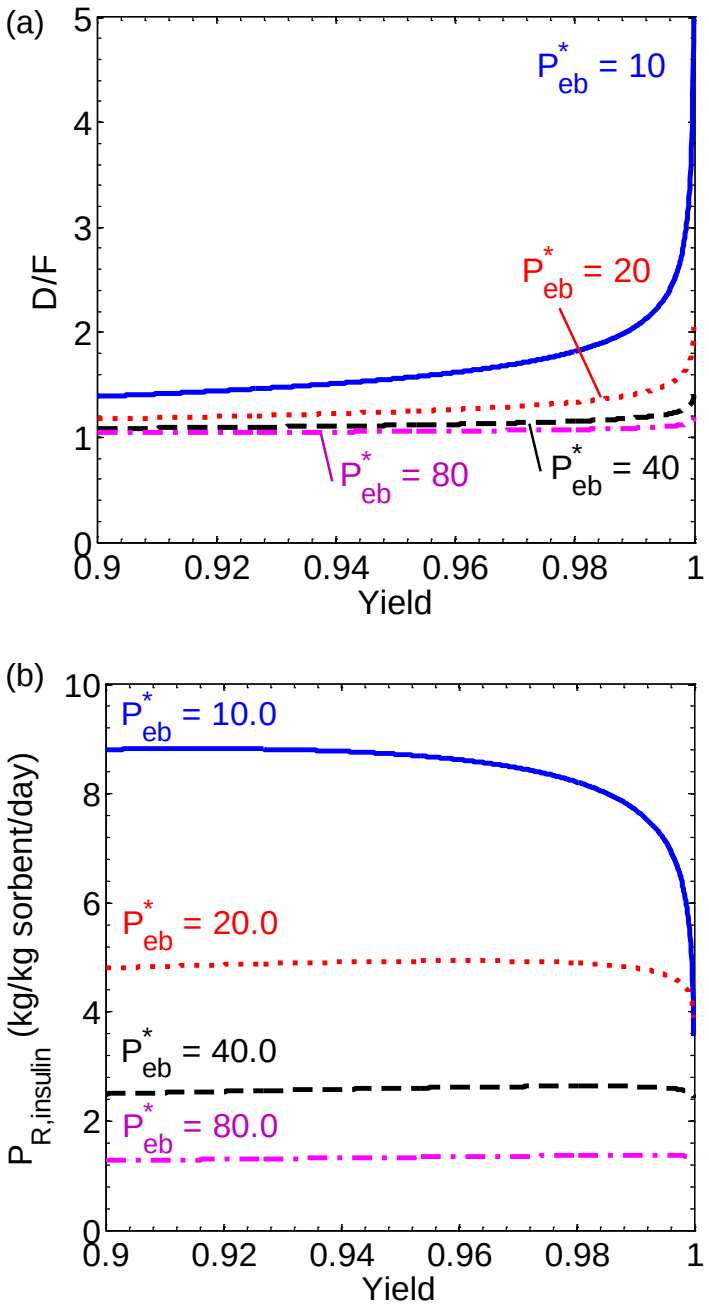

Figure 7.11. (a) *D/F* and (b) P_R^* vs yield at varying P_{eb}^*. Constant port velocity = 1 cm/min – dispersion controlled.

7.5.3 Retention Factors and Selectivity

Because P_{eb}^{*} is a function of retention factors and selectivity (Table 3.1), Figure 7.12 is generated using a constant Peclet number in Zone IV (P_{eb}^{IV} = 50). At very low selectivities (α~1), very large amounts of solvent are required to achieve separation, Figure 7.12a. Increasing α decreases the amount of solvent required for the separation because less solvent is needed to confine the concentration waves in their respective zones. Larger values of retention factors at the same α result in lower *D/F*. This result can be explained by Eq. (3.19) and Eq. (3.34) because increasing the retention factors increases P_{eb}^{*}, which decreases *D/F*. The lines for different retention factors end at different α's because of the limit on the maximum value of a retention factor in SEC.

The impact of α on P_R can be seen in Figure 7.12b. Productivity increases linearly with increasing α, Eq. (38a). Increasing δ_1, while maintaining the same α, results in a larger P_R because a larger amount of the pore phase of the sorbent particles is being accessed by the solutes, increasing the column utilization and productivity.

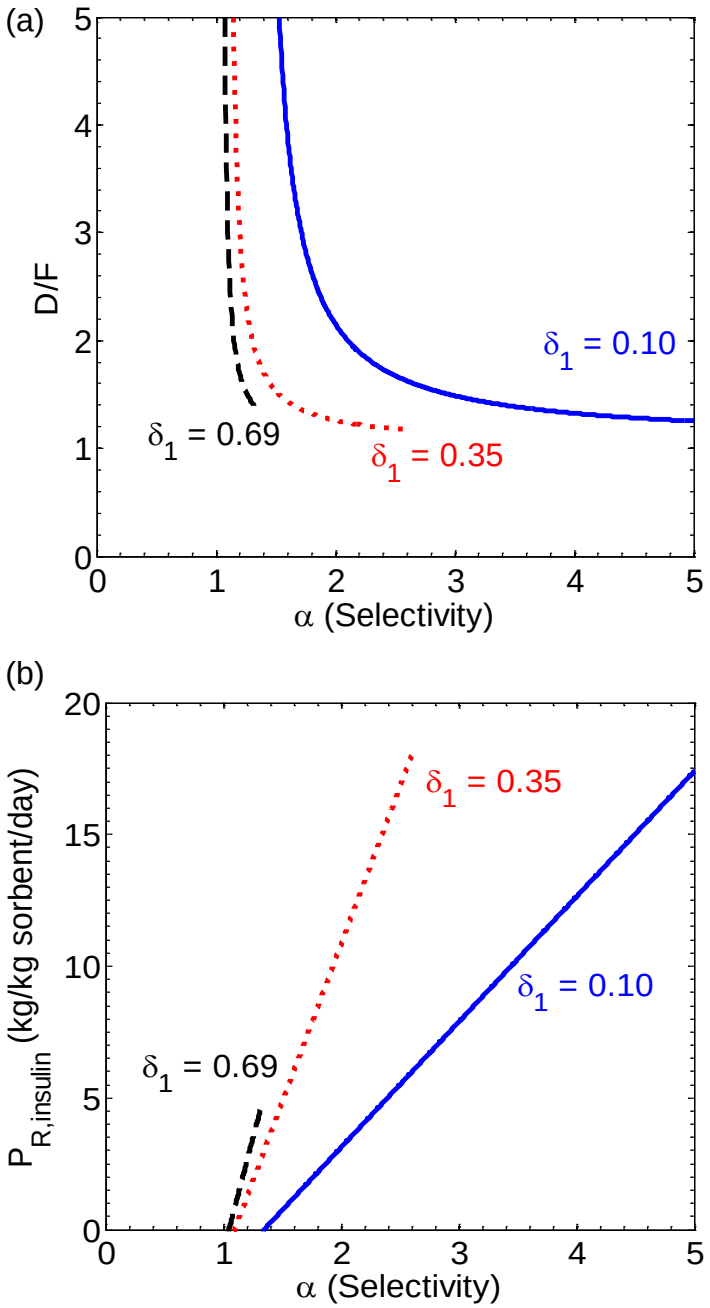

Figure 7.12. (a) *D/F* and (b) P_R vs selectivity at various values for δ_1. P_{eb}^{IV} fixed at 50 and port velocity fixed at 1 cm/min – dispersion controlled, 3-3-3-3 configuration.

7.5.4 Phase Ratio

The solvent consumption (D/F) as a function of P_{eb}^* is given in Eq. (34). For constant P_{eb}^*, D/F has only a weak dependence on ϕ because the axial dispersion coefficient ratios (I^j) are weak functions of ϕ, Eq. (A2.1). The phase ratio only affects D/F for low P_{eb}^* (<20), figure not shown. Increasing ϕ increases P_R for dispersion controlled systems, according to Eq. (38b). The term $(1 + \phi\delta_1)/\phi$ does not change significantly with increasing ϕ, but decreasing the ε_b in the denominator outside the brackets increases P_R, figure not shown.

7.6 Comparison of Diffusion Controlled and Dispersion Controlled Systems

Diffusion controlled systems and dispersion controlled systems are very similar in how D/F and P_R vary with the dimensionless groups. Increasing N_D^* (or P_{eb}^*) decreases D/F while P_R increases to a maximum and then decreases. Increasing α decreases D/F and increases P_R while increasing yield increases D/F and decreases P_R. Small retention factors favor low D/F and high P_R for diffusion controlled systems, whereas large retention factors are better for dispersion controlled systems. Increasing γ decreases D/F and increases P_R for diffusion controlled systems, but has no effect on dispersion controlled systems. Increasing ϕ increases P_R for dispersion controlled systems, but has no effect on D/F or P_R for diffusion controlled systems. Maximum P_R for diffusion controlled systems can be achieved when the diffusion time, step time, and pressure-limited convection time are matched. For dispersion controlled systems, the maximum P_R occurs when the axial dispersion time is about 10 times the step time and 50 times the convection time.

7.7 Cost Optimization of SEC-SMB for Insulin Purification

The production scale was chosen to be 5,000 kg insulin / year and the optimization results are reported in Table 7.3. Low pressure SMB (< 150 psi per zone) equipment was chosen because at this production scale, the equipment cost is dominating and high pressure equipment would be even more expensive. The sorbent was chosen to be the same as the sorbent used in the batch purification of insulin because the material properties are known and the performance of optimized SEC-SMB can be compared with that of batch SEC. For this particular sorbent, Sephadex G50, the maximum pressure drop per column is limited to 1.5 psi. The total dead volume was kept at 1.9% of the total packing volume because *DV* less than 2% does not significantly affect *D/F* or P_R, Figure 7.8. The yield specifications for both rings were set at 99% because Figure 7.6 shows that the yields do not significantly affect *D/F* or P_R unless they are specified over 99%. The potential impact of optimizing particle size on total cost is small (< 2%) for this sorbent, and will be discussed in the following section. For these reasons, four decision variables (Y_i, R_p, *DV*) were fixed, while the remaining 11 decision variables (L_c, N^j, ΔP_{max}, $u_0{}^j$, and ν) were optimized for minimum cost. Optimization of the 11 decision variables for one ring takes less than one minute on a laptop.

7.7.1 Ring B Cost Optimization

Ring B is diffusion controlled whereas both diffusion and dispersion effects are important in Ring A. For this reason, the optimization of Ring B is discussed first. Because the material properties are fixed, the total cost for Ring B can be plotted versus $N_D{}^*$ as a single 2-D curve, Figure 7.13. Cost functions for solvent, sorbent, and equipment are presented in Appendix A4.

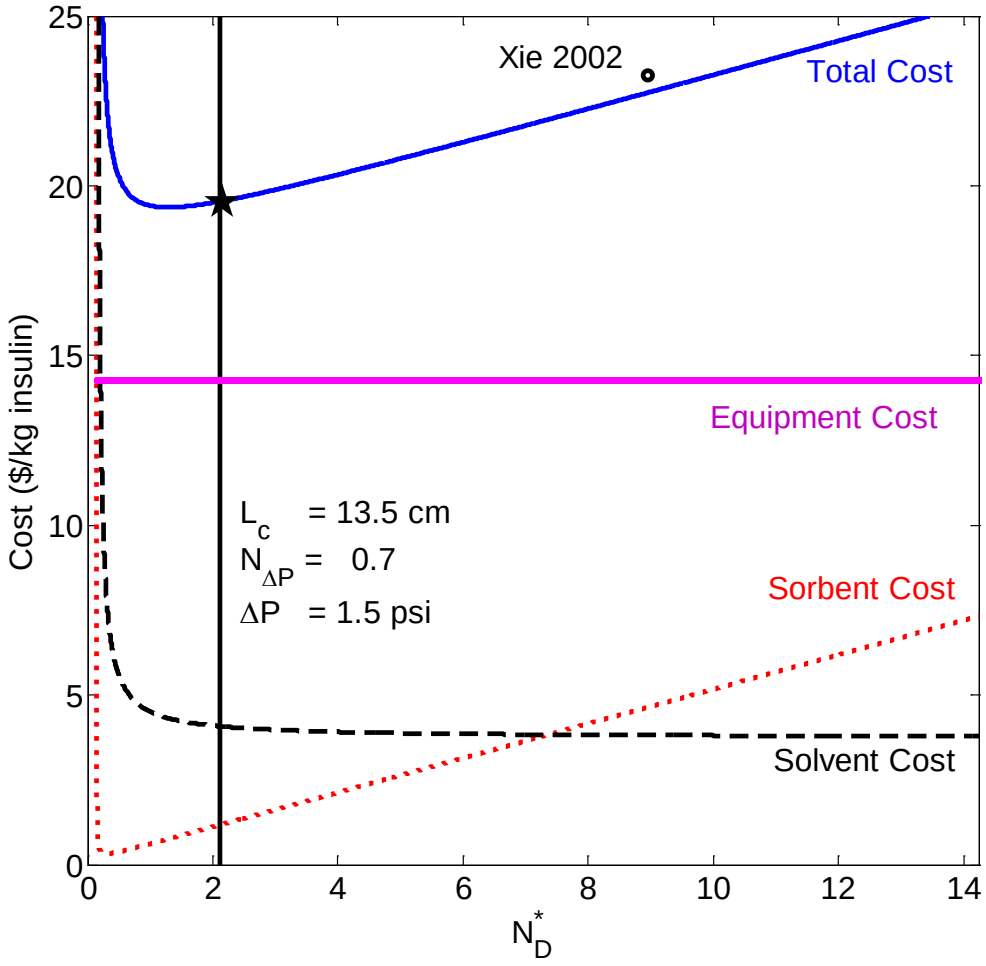

Figure 7.13. Estimates of total, resin, and solvent costs vs. N_D^* – diffusion controlled, 2-2-2-2 configuration. Black star indicates minimum achievable cost at pressure limit.

Unit equipment cost does not vary with N_D^* for fixed N^j and ΔP_{max}. At low N_D^* (<0.2, $N^*_{D,\max P_R}$), sorbent and solvent costs are high because *D/F* is large and productivity is low, Figure 7.3. The costs decrease with increasing N_D^* as *D/F* decreases and productivity increases. When N_D^* is larger than $N^*_{D,\max P_R}$, the sorbent cost increases with N_D^* because the productivity decreases. This increase in the sorbent cost causes a minimum in the total cost curve. This minimum, however, does not satisfy the pressure limit for this

system. As a result, the lowest cost design allowed by the pressure is at $N_D^* \sim 2$. At this N_D^*, column configuration has little effect on *D/F* or productivity, Figure 7.3. However, the equipment cost can be lowered by using fewer columns. Thus, the optimum column configuration is 2-2-2-2 if a minimum of two columns per zone is required.

If production scales are much larger than that of insulin, the unit equipment cost can be a small fraction of the total separation cost. In these cases, optimization of the material properties (especially R_p) and equipment parameters (L_c, ΔP_{max}) can significantly reduce the separation cost. For diffusion controlled systems, one can find the optimal combination of ($\Delta P_{max} R_p^4 / L_c^2$), using Eq. (30a), such that the minimum cost design is feasible. One can use $N^*_{D,\max P_R}$, Eq. (30a), in Eq. (32a) to obtain $N_{\Delta P,\text{diff},\max P_R}$. With ϕ and viscosity (μ), the value of ($\Delta P_{max} R_p^4 / L_c^2$) can be calculated. Because the value of N_D^* corresponding to the minimum cost design is always greater than, or equal to, $N^*_{D,\max P_R}$, designing $\Delta P_{max} R_p^4 / L_c^2$ for maximum P_R will always satisfy the pressure limit at the minimum cost design.

For dispersion controlled systems, Eq. (3.41) can be used to find the minimum $N_{\Delta P}$ at the P_{eb}^* value corresponding to the minimum cost design. The value of $N_{\Delta P}$ can then be used to find a value of ($\Delta P_{max} R_p^2 / L_c \nu$), which ensures that the minimum cost design satisfies the pressure limit. For systems in which both diffusion and dispersion effects are significant, Eq. (3.25) can be used in a similar manner.

The calculated cost of Ring B based on the experimental design reported by Xie et al., 2002 is about $6 higher than the minimum cost found in this study. Their operating conditions were based on SWD for a fixed column length, 13.7 cm, and 10 columns were

used instead eight columns, the optimum number of columns obtained from SSWD. The switching time was also longer than the optimum switching time, resulting in N_D^* = 8.9. The calculated cost falls close to the SSWD prediction for N_D^* = 8.9, Figure 7.13. The difference in total cost is mainly due to the difference in the total number of columns.

7.7.2 Ring A Cost Optimization

Because both diffusion and dispersion effects are important for Ring A, the total cost should be plotted against N_D^* and P_{eb}^* as a 3D surface. However, the total cost surface is concave up and cannot be easily viewed. As such, the inverse of the total cost is plotted against N_D^* and P_{eb}^* in Figure 7.14a. Since the z-axis is the inverse of total cost, the maximum point of the surface corresponds to the minimum cost design.

The grey surface represents the pressure limit and divides the cost surface into feasible and infeasible regions. N_D^* lower than the pressure surface and P_{eb}^* larger than the surface would violate the maximum pressure constraint. Because the system is limited by pressure, the achievable minimum cost point is N_D^* = 14.9 and P_{eb}^* = 560, which is marked on a contour plot of the surface, Figure 7.14b. The lines in Figure 7.14b represent constant total cost values projected onto the N_D^* and P_{eb}^* plane. The black dashed line is the pressure limit. The region below the black line is infeasible. A summary of the optimized costs and equipment parameters are shown in Table 7.3.

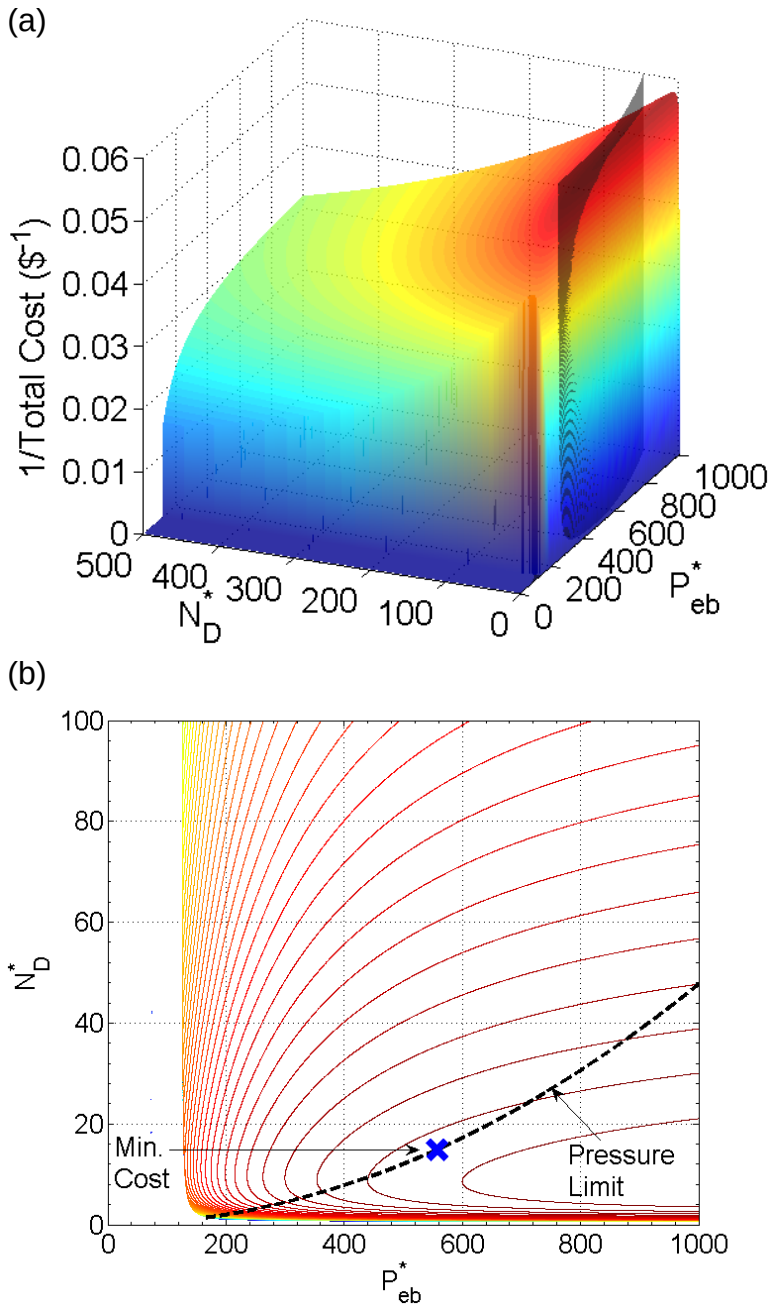

Figure 7.14. (a) Inverse of total cost curve vs. P_{eb}^* and N_D^* for Ring A. Pressure limit is indicated by the black surface and indicates the minimum N_D^* at each P_{eb}^* for the system to not exceed the maximum pressure. (b) Contour plot of (a). Black dashed line represents the maximum pressure limit. Regions below the black line are infeasible.

Table 7.3 compares batch SEC production of insulin and two different SEC-SMB systems based on the same sorbent. The SMB design of Xie in 2002 was based on the operating parameters from the SWD method for a fixed column length of 13.7 cm. A cost optimized SMB design for both Ring A and Ring B was found using the SSWD equations, Table 7.3. The cost optimized design reduced the overall separation cost by 16% from the design of Xie et al. Both SMBs are significantly lower in cost than the batch method. The optimized SMB reduces the solvent consumption from batch SEC by 66%, increases the productivity by 34 times, and reduces the cost by 62%.

7.7.3 Ring B Material Property and *DV* Sensitivity

The cost optimization shown in Table 7.3 is based on the material properties, pressure limit, and dead volume of the experimental system of Xie et al. Column length and configuration are optimized to reduce the unit separation cost. If the material properties, pressure limit, and dead volume are allowed to vary, the SSWD can further reduce the separation cost. The effects of changing each of the equipment parameters and material properties on solvent cost and sorbent cost are shown in Table 7.4.

Increasing the pressure limit from 1.5 to 50 psi per column moves the pressure limit line in Figure 7.13 to a lower N_D^*, allowing the system to be designed at the N_D^* corresponding to the global minimum cost. As a result, D/F decreases by 5% and P_R increases by 16%. The separation cost only reduces by 1% because the equipment cost is dominating at 83% of the total cost. Because the minimum cost N_D^* was already accessible at 50 psi per column, increasing the pressure limit to 75 psi per column does not change the value of N_D^* for minimum cost. Only the aspect ratio of the column increases (L_c increases, ID decreases). This change can be explained by the left-hand side of Eq. 32a.

Table 7.4. Effects of material properties, pressure limit, and dead volume on Ring B optimization.

Parameter Changed	New Parameter Values	*D/F*	Solvent Cost ($/kg insulin)	L_c (cm)	*ID* (cm)	P_R (kg insulin/ kg resin/ day)	Sorbent Cost ($/kg insulin)	Total Cost[e] ($/kg insulin)
Base Case (Table 5)		1.39	2.27	11.4	29.6	2.79	0.79	17.35
ΔP_{max} (psi)	50	1.32	2.16	61.5	11.9	3.23	0.68	17.13
	75	1.32	2.15	75.3	10.7	3.23	0.68	17.12
DV (% CV)	0	1.38	2.25	11.2	29.0	2.96	0.74	17.28
	10	1.46	2.38	11.9	31.9	2.33	0.95	17.62
ε_b	0.3	1.40	2.29	8.4	33.3	2.79	0.79	17.37
	0.4	1.40	2.28	14.8	26.8	2.85	0.77	17.34
ε_p	0.50	1.53	2.49	12.2	35.7	1.80	1.22	18.00
	0.95	1.38	2.25	11.4	29.1	2.91	0.76	17.30
γ	1	1.50	2.46	13.7	33.5	1.83	1.21	17.96
	100	1.37	2.24	10.9	28.8	3.11	0.71	17.24
$K_{se,1}$	0.010	1.07	1.74	8.3	12.0	23.33	0.09	16.12
	0.100	1.07	1.75	8.2	12.6	21.36	0.10	16.14
R_p (μm)	25	1.26	2.06	3.7	35.9	5.85	0.38	16.73
	100	1.61	2.63	29.9	26.8	1.31	1.68	18.61
ΔP_{max}, *DV*, ε_b, ε_p, γ, $K_{se,1}$, R_p	150, 0.0, 0.3, 0.95, 100, 0.01, 25	1.01	1.65	10.4	3.7	187.49	0.01	15.95

[e]The equipment cost does not change between cases.

As expected from Figure 7.8, decreasing the dead volume from 1.9% CV in the base case to zero has little effect on *D/F* or P_R, while increasing the dead volume to 10% CV increases *D/F* by 5% and decreases P_R by 16%.

The bed void fraction can only be varied from 0.3 to 0.4, and does not directly affect *D/F* (Eq. 21) or P_R for diffusion controlled systems Eq. (3.29b), as expected. However, it indirectly affects P_R because larger ε_b values result in longer columns for the same pressure drop, Eq. (3.24), which allows for a smaller N_D^* value, which results in slightly higher P_R (2%). However, the overall impact on *D/F* or P_R is relatively small for this system.

The particle porosity does not typically exceed 0.95. Increasing ε_p from 0.89 to 0.95 does not have much of an effect on *D/F* or P_R. However, decreasing ε_p to 0.5 reduces both the dimensionless diffusion rate, N_D^*, and the δ's, resulting in increasing *D/F* by 10%, Eq. (3.27), and decreasing P_R by 65%, Eq. (3.29b).

Increasing the diffusivity ratio from 7.2 to 100 does not significantly reduce *D/F*, Eq. (3.27), but increases P_R by 11%, Eq. (3.29b). Decreasing the diffusivity ratio to 1 increases *D/F* by 8% and decreases P_R by 34%, as expected from the trends shown in Figure 7.9.

Reducing the size-exclusion coefficient of insulin from 0.74 to 0.1 increases selectivity from 1.3 to 7.7, which reduces *D/F* by 23% and increases P_R by 676%, Eq. (3.27) and Eq. (3.29b), respectively. Further reduction of the size-exclusion coefficient of insulin to 0.01 increases the selectivity to ~23, does not further reduce *D/F* and further increases P_R by 9%.

Low pressure sorbents do not typically have radii much smaller than 25 microns, because smaller particles will require a packing length much shorter than 10 cm, as expected from Figure 7.5b. Decreasing the particle radius from 54 to 25 μm reduces *D/F* by 9% and increases P_R by 110%, Eqs. (15, 17). However, L_c is impractically small because

of the limited pressure drop of 1.5 psi per column. Increasing R_p to 100 μm increases *D/F* by 16% and decreases P_R by 53%, Eq. (3.15) and Eq. (3.17), respectively.

The result of combining all the hypothetical changes in the material properties and equipment parameters is shown in the last row of Table 7.4. The *D/F* approaches that of an ideal system, as a result of the high selectivity and zero *DV*. The P_R increases by 66 fold mainly because of the synergistic effects of reducing particle size, increasing selectivity, and increasing the pressure limit. The total cost approaches the lowest possible total cost for the given feed concentration, because the sorbent cost becomes negligible and the solvent cost approaches that of an ideal system. Further decrease in unit solvent cost is only possible if the feed concentration can be increased. Increasing feed concentration would also reduce the unit equipment cost because the production rate is increased using the same equipment. The results in Table 7.4 indicate that the factors with the largest impact on solvent and sorbent costs are particle size, selectivity, and pressure limit.

In this example, equipment cost is dominating (81-90%) because of the small production scale (5,000 kg/year). Optimization of the material properties and equipment parameters has limited impact on the total separation cost (8%). However, for other applications with much larger production scales, optimization of the material properties and equipment parameters can significantly reduce the total separation cost.

CHAPTER 8. CONCLUSIONS AND RECOMMENDATIONS

The separations developed in this dissertation achieved the goal of recovering valuable compounds (specifically polycarbonate and flame retardants) from electronic waste. Polycarbonates were recovered using a mixed-solvent extraction process. The flame retardants can be recovered from a side stream of the extraction process via SEC-SMB.

8.1 Polycarbonate Extraction

A room-temperature, sequential extraction process called SEPoR (Sequential Extraction for Polymer Recovery) was developed to recover polycarbonate. Two mixed solvents were used to recover polycarbonates with high yield (>95%) and a similar purity and molecular weight distribution as virgin polycarbonates. The compositions of the mixed-solvents were developed using Hansen solubility parameters, gradient polymer elution chromatography, and solubility tests. The estimated cost of recovery is less than 30% of the cost of producing virgin polycarbonates from petroleum. This method would potentially reduce raw materials from petroleum, use 84% less energy, reduce emission by 1-6 tons CO_2 per ton polycarbonates, and reduce polymer accumulation in landfills and associated environmental hazards. Although the specific example is focused on the recovery of polycarbonates from electronic waste, the method developed in this dissertation potentially can be applied for the recovery of many different polymers from various wastes.

8.2 SEC-SMB for Flame Retardant Recovery

A side steam from the SEPoR process contains valuable flame retardants in a mixture with SAN. SEC-SMB was used to separate FRs from SAN and achieved high purity with high yield. The results of these experiments show that intrinsic parameters estimated from single column experiments can have a small (a few %) errors. The operating flow rates and step time based on the estimated parameters can result in significant deviations of column profiles or product purities in long SMB operations. Pilot SMB experiments with 10 or more cycles are needed to detect any small errors. Comparison of VERSE simulated column profiles and effluent histories with the pilot SMB data can help obtain accurate parameters, which are needed for designing reliable SMBs for large-scale production. Fast startup methods based on SWD and VERSE effectively reduced the startup time for the SMB by more than 18 fold. Fourteen decision variables were optimized to obtain the lowest separation cost within one minute. The estimated separation cost for FR recovery by SEC-SMB is less than 3% of that for batch SEC and is less than 10% of the FR purchase price. The results of this work may help develop other SEC-SMB processes for recycling applications, which require high-purity products.

8.3 Speedy Standing Wave Design and Optimization for SEC-SMB

In order to design and optimize the SEC-SMB for FR recovery, the SWD equations were solved with dimensionless groups to produce analytical expressions for solvent consumption (D/F) and sorbent productivity (P_R). Solvent consumption and sorbent productivity are now explicitly related to the material properties, equipment parameters, and operating parameters. The sensitivity of solvent cost, sorbent cost, and total cost with respect to the material, equipment, and operating parameters was also elucidated.

The results of the parametric studies show that for diffusion controlled systems, one can reduce *D/F* and increase P_R by increasing selectivity (α), diffusivity ratio (γ), or γ/α. Decreasing retention factors (δ_i) reduces *D/F*, but also decreases P_R. The phase ratio (ϕ) does not affect *D/F* or P_R. When the yield specification is larger than 99%, *D/F* significantly increases and P_R significantly decreases. The key dimensionless group governing the operating parameters is N_D^*. There is a minimum value ($N_{D,min}^*$) required for the operation to be feasible. Increasing N_D^* will always reduce *D/F*, but the P_R peaks at about twice $N_{D,min}^*$, after which P_R decreases with increasing N_D^*. The column configuration (N^j) does not significantly affect *D/F*, but can significantly increase the peak P_R. Dead volume (*DV*) should be reduced to less than 2% of the total packing volume to minimize its impact on *D/F* and P_R. The competing effects of solvent consumption and P_R result in a cost minimum because solvent cost always decreases with N_D^* and sorbent cost increases when $N_D^* > N_{D,\max P_R}^*$. However, the cost minimum may not be achievable if the system has a pressure limit. The combination of ($\Delta P R_p^4/L_c^2$) which allows access to the cost minimum can be calculated from $N_{D,\max P_R}^*$, material properties (other than R_p), yields, column configuration, and viscosity. The corresponding $N_{\Delta P,diff}$ for maximum P_R is about 1 for the example system. Thus, the diffusion time, step time, and pressure-limited convection time are approximately equal at the maximum P_R.

For dispersion controlled systems, *D/F* can be reduced and P_R can be increased by increasing α and increasing retention factors. The dependence of *D/F* on retention factors is opposite to that of diffusion controlled systems. Increasing phase ratio does not significantly reduce *D/F*, but does increase P_R. The effects of yield specification on *D/F*

and P_R are similar to those for diffusion controlled systems. The key dimensionless group controlling the operating parameters is P_{eb}^*. The effects of P_{eb}^* on D/F and P_R are also similar to those of N_D^* for diffusion controlled systems. The column configuration and DV have similar effects on D/F and P_R as those of diffusion controlled systems. The value of ($\Delta P_{max} R_p^2/L_c$) can be found at the value of P_{eb}^* for minimum cost, such that the minimum cost design satisfies the pressure limit. The value of $P_{eb,\max P_R}^*$ can be calculated from yields, material properties, and column configuration. The maximum P_R occurs when the axial dispersion time is about 10 times the step time and about 50 times the pressure-limited convection time.

The recast SWD solutions of D/F and productivity can be used to optimize SMB designs. This method was demonstrated using insulin purification as an example and the optimal SMB design was compared to the industrial batch process. Optimization of 11 parameters (column length, column configuration, operating pressure, and operating parameters) reduces the solvent consumption from batch SEC by 66%, increases the sorbent productivity by 34 times, and reduces the total cost by 62%. If the material properties, pressure limit, and dead volume are allowed to change, solvent consumption can be further reduced by 28% and productivity can be further increased by 67 times. Since the equipment cost dominates (81% of total cost) at this relatively small production scale, optimization of the material properties and pressure limit only reduces the separation cost by 8%. Among the material properties, selectivity and particle size have the largest impact on solvent consumption and sorbent productivity. For applications with large production scales, the unit equipment cost is expected to be a small fraction of the total cost, and this

general optimization method is expected to significantly reduce solvent consumption, increase sorbent productivity, and reduce separation cost.

8.4 Looking Forward

There is still a great deal to learn about SMB systems and the power of the SSWD. The theory developed in this dissertation should be extended to more general cases so that SMBs for other applications can be quickly and easily designed and optimized. Some suggestions are:

1. Extend SSWD theory to include systems with linear adsorption isotherms.
2. Extend (1) to include systems with more than two components.
3. Extend SSWD theory to include systems with nonlinear adsorption isotherms (e.g. enantiomeric separations for pharmaceuticals).
4. Extend (3) to include systems with more than two components.
5. Extend SSWD theory to include thermal SMB systems (different temperatures in different zones).
6. Apply more sophisticated optimization techniques to SSWD for faster solutions.
7. Extend SSWD theory to different types of isotherms (e.g. Freundlich).

REFERENCES

REFERENCES

[1] C.M. Rochman, M.A. Browne, B.S. Halpern, B.T. Hentschel, E. Hoh, H.K. Karapanagioti, et al., Policy: Classify plastic waste as hazardous., Nature. 494 (2013) 169–71. doi:10.1038/494169a.

[2] K.L. Law, S. Morét-Ferguson, N.A. Maximenko, G. Proskurowski, E.E. Peacock, J. Hafner, et al., Plastic accumulation in the North Atlantic subtropical gyre., Science. 329 (2010) 1185–8. doi:10.1126/science.1192321.

[3] N.J. Themelis, C. Mussche, 2014 Energy and Economic Value of Municipal Solid Waste (MSW), Including Non-Recycled plastics (NRP), Currently Landfilled in the Fifty States, 2014.

[4] D. Lithner, A. Larsson, G. Dave, Environmental and health hazard ranking and assessment of plastic polymers based on chemical composition., Sci. Total Environ. 409 (2011) 3309–24. doi:10.1016/j.scitotenv.2011.04.038.

[5] T. Wakolbinger, F. Toyasaki, T. Nowak, A. Nagurney, When and for whom would e-waste be a treasure trove? Insights from a network equilibrium model of e-waste flows, Int. J. Prod. Econ. 154 (2014) 263–273. doi:10.1016/j.ijpe.2014.04.025.

[6] X. Yang, L. Sun, J. Xiang, S. Hu, S. Su, Pyrolysis and dehalogenation of plastics from waste electrical and electronic equipment (WEEE): a review., Waste Manag. 33 (2013) 462–73. doi:10.1016/j.wasman.2012.07.025.

[7] R. Rajarao, R. Ferreira, S.H.F. Sadi, R. Khanna, V. Sahajwalla, Synthesis of silicon carbide nanoparticles by using electronic waste as a carbon source, Mater. Lett. 120 (2014) 65–68. doi:10.1016/j.matlet.2014.01.018.

[8] B.H. Robinson, E-waste: an assessment of global production and environmental impacts., Sci. Total Environ. 408 (2009) 183–91. doi:10.1016/j.scitotenv.2009.09.044.

[9] S. Herat, P. Agamuthu, E-waste: a problem or an opportunity? Review of issues, challenges and solutions in Asian countries., Waste Manag. Res. 30 (2012) 1113–29. doi:10.1177/0734242X12453378.

[10] United States Environmental Protection Agency (U.S. EPA), Electronics Waste Management in the United States Through 2009, Washington, D.C., 2011. http://www.epa.gov/osw/conserve/materials/ecycling/docs/summarybaselinereport2011.pdf.

[11] R. Kahhat, J. Kim, M. Xu, B. Allenby, E. Williams, P. Zhang, Exploring e-waste management systems in the United States, Resour. Conserv. Recycl. 52 (2008) 955–964. doi:10.1016/j.resconrec.2008.03.002.

[12] S. Schwarzer, A.D. Bono, G. Giuliani, S. Kluser, P. Peduzzi, E-waste, the hidden side of IT equipment's manufacturing and use, 2005. http://archive-ouverte.unige.ch/unige:23132 (accessed August 7, 2014).

[13] J. Beigbeder, D. Perrin, J.-F. Mascaro, J.-M. Lopez-Cuesta, Study of the physico-chemical properties of recycled polymers from waste electrical and electronic equipment (WEEE) sorted by high resolution near infrared devices, Resour. Conserv. Recycl. 78 (2013) 105–114. doi:10.1016/j.resconrec.2013.07.006.

[14] M. Schuckert, Life cycle analysis: Getting the total picture on vehicle engineering alternatives, Automot. Eng. 104 (1996) 49–52.

[15] A. Sepúlveda, M. Schluep, F.G. Renaud, M. Streicher, R. Kuehr, C. Hagelüken, et al., A review of the environmental fate and effects of hazardous substances released from electrical and electronic equipments during recycling: Examples from China and India, Environ. Impact Assess. Rev. 30 (2010) 28–41. doi:10.1016/j.eiar.2009.04.001.

[16] L.N. Vandenberg, R. Hauser, M. Marcus, N. Olea, W. V Welshons, Human exposure to bisphenol A (BPA)., Reprod. Toxicol. 24 (2007) 139–77. doi:10.1016/j.reprotox.2007.07.010.

[17] E.T.H. Vink, S. Davies, J.J. Kolstad, The eco-profile for current Ingeo polylactide production, Ind. Biotechnol. 6 (2010) 212–224.

[18] G. Wu, J. Li, Z. Xu, Triboelectrostatic separation for granular plastic waste recycling: a review., Waste Manag. 33 (2013) 585–97. doi:10.1016/j.wasman.2012.10.014.

[19] D. Bright, S. Dashevsky, Resorcinol Bis (Diphenyl Phosphate), a Non-Halogen Flame-Retardant Additive, J. Vinyl Addit. Technol. 3 (1997) 170–174. http://onlinelibrary.wiley.com/doi/10.1002/vnl.10184/abstract (accessed May 28, 2014).

[20] A. Ballesteros-Gómez, S.H. Brandsma, J. de Boer, P.E.G. Leonards, Analysis of two alternative organophosphorus flame retardants in electronic and plastic consumer products: Resorcinol bis-(diphenylphosphate) (PBDPP) and bisphenol A bis (diphenylphosphate) (BPA-BDPP), Chemosphere. 116 (2014) 10–14. doi:10.1016/j.chemosphere.2013.12.099.

[21] I.C. Nnorom, O. Osibanjo, Sound management of brominated flame retarded (BFR) plastics from electronic wastes: State of the art and options in Nigeria, Resour. Conserv. Recycl. 52 (2008) 1362–1372. doi:10.1016/j.resconrec.2008.08.001.

[22] I. van der Veen, J. de Boer, Phosphorus flame retardants: Properties, production, environmental occurrence, toxicity and analysis, Chemosphere. 88 (2012) 1119–1153. doi:10.1016/j.chemosphere.2012.03.067.

[23] E.M. Reingruber, A. Chojnacka, E. Jellema, B. de Bruin, W. Buchberger, P.J. Schoenmakers, Chromatographic examination of the chemical composition and sequence distribution of copolymers from ethyl and benzyl diazoacetate., J. Chromatogr. A. 1255 (2012) 259–66. doi:10.1016/j.chroma.2012.02.059.

[24] E. Uliyanchenko, S. van der Wal, P.J. Schoenmakers, Challenges in polymer analysis by liquid chromatography, Polym. Chem. 3 (2012) 2313. doi:10.1039/c2py20274c.

[25] R. Guo, Z. Shi, X. Wang, A. Dong, J. Zhang, Separation and quantification of dead species in styrene RAFT polymerization by gradient polymer elution chromatography, Polym. Chem. 3 (2012) 1314. doi:10.1039/c2py20102j.

[26] E.P. Kroeff, R.A. Owens, E.L. Campbell, R.D. Johnson, H.I. Marks, Production scale purification of biosynthetic human insulin by reversed-phase high-performance liquid chromatography., J. Chromatogr. 461 (1989) 45–61. doi:10.1016/S0021-9673(00)94274-2.

[27] D. Broughton, C.G. Gerhold, Continuous sorption process employing fixed bed of sorbent and moving inlets and outlets, 2,985,589, 1961.

[28] D. Broughton, Molex: Case history of a process, Chem. Eng. Prog. 64 (1968) 60–65.

[29] D. Broughton, Production-scale adsorptive separations of liquid mixtures by simulated moving-bed technology, Sep. Sci. Technol. (1984) 37–41. http://www.tandfonline.com/doi/abs/10.1080/01496398408068590 (accessed July 29, 2013).

[30] L. Pais, J. Loureiro, A. Rodrigues, Separation of 1, 1′-bi-2-naphthol enantiomers by continuous chromatography in simulated moving bed, Chem. Eng. Sci. 52 (1997). http://www.sciencedirect.com/science/article/pii/ S0009250996003983 (accessed July 29, 2013).

[31] Y. Xie, S. Mun, J. Kim, N.-H.L. Wang, Standing wave design and experimental validation of a tandem simulated moving bed process for insulin purification., Biotechnol. Prog. 18 (2002) 1332–44. doi:10.1021/bp025547r.

[32] S. Mun, Y. Xie, J.-H. Kim, N.-H.L. Wang, Optimal Design of a Size-Exclusion Tandem Simulated Moving Bed for Insulin Purification, Ind. Eng. Chem. Res. 42 (2003) 1977–1993. doi:10.1021/ie020680+.

[33] J. Houwing, H.A.H. Billiet, L.A.M. van der Wielen, Mass-transfer effects during separation of proteins in SMB by size exclusion, AIChE J. 49 (2003) 1158–1167. doi:10.1002/aic.690490509.

[34] A. Geisser, T. Hendrich, G. Boehm, B. Stahl, Separation of lactose from human milk oligosaccharides with simulated moving bed chromatography., J. Chromatogr. A. 1092 (2005) 17–23. doi:10.1016/j.chroma.2005.03.061.

[35] M.-T. Liang, R.-C. Liang, Fractionation of polyethylene glycol particles by simulated moving bed with size-exclusion chromatography., J. Chromatogr. A. 1229 (2012) 107–12. doi:10.1016/j.chroma.2011.12.094.

[36] R. Rajarao, I. Mansuri, R. Dhunna, R. Khanna, V. Sahajwalla, Characterisation of gas evolution and char structural change during pyrolysis of waste CDs, J. Anal. Appl. Pyrolysis. 105 (2014) 14–22. doi:10.1016/j.jaap.2013.09.014.

[37] L. Mastny, CDs and DVDs, Worldwatch Inst. (2004) 7. http://www.worldwatch.org/system/files/GS0005.pdf.

[38] J. Guo, J. Guo, Z. Xu, Recycling of non-metallic fractions from waste printed circuit boards: a review., J. Hazard. Mater. 168 (2009) 567–90. doi:10.1016/j.jhazmat.2009.02.104.

[39] K. Hatakeyama, T. Kojima, T. Funazukuri, Chemical recycling of polycarbonate in dilute aqueous ammonia solution under hydrothermal conditions, J. Mater. Cycles Waste Manag. (2013). doi:10.1007/s10163-013-0151-8.

[40] D.S. Achilias, E.V. Antonakou, E. Koutsokosta, A.A. Lappas, Chemical recycling of polymers from waste electric and electronic equipment, J. Appl. Polym. Sci. 114 (2009) 212–221. doi:10.1002/app.30533.

[41] M. Goto, Chemical recycling of plastics using sub- and supercritical fluids, J. Supercrit. Fluids. 47 (2009) 500–507. doi:10.1016/j.supflu.2008.10.011.

[42] S.M. Al-Salem, P. Lettieri, J. Baeyens, Recycling and recovery routes of plastic solid waste (PSW): a review., Waste Manag. 29 (2009) 2625–43. doi:10.1016/j.wasman.2009.06.004.

[43] B. Baytekin, H.T. Baytekin, B. a. Grzybowski, Retrieving and converting energy from polymers: deployable technologies and emerging concepts, Energy Environ. Sci. 6 (2013) 3467. doi:10.1039/c3ee41360h.

[44] P. Bell, D. Zoller, Polycarbonate recovery from polymer blends by liquid chromatography, US 2012/0329977 A1, 2012.

[45] G. Varadarajan, J. King Jr, B. Idage, S. Sivaram, V. Ranade, Method for recycling aromatic polycarbonates, US6034142, 2000.

[46] M. García-López, I. Rodríguez, R. Cela, Evaluation of liquid-liquid microextraction using polypropylene microporous membranes for the determination of organophosphorus flame retardants and plasticizers in water samples, Anal. Chim. Acta. 625 (2008) 145–153. doi:10.1016/j.aca.2008.07.026.

[47] Z. Gao, Y. Deng, W. Yuan, H. He, S. Yang, C. Sun, Determination of organophosphorus flame retardants in fish by pressurized liquid extraction using aqueous solutions and solid-phase microextraction coupled with gas chromatography-flame photometric detector, J. Chromatogr. A. 1366 (2014) 31–37. doi:10.1016/j.chroma.2014.09.028.

[48] G.A. MacKay, R.M. Smith, Supercritical fluid extraction and chromatography–mass spectrometry of flame retardants from polyurethane foams, Analyst. 118 (1993) 741. doi:10.1039/an9931800741.

[49] S.H. Smith, L.T. Taylor, Extraction of various additives from polystyrene and their subsequent analysis, Chromatographia. 56 (2002) 165–169. doi:10.1007/BF02493206.

[50] Y. Ma, K. Cui, F. Zeng, J. Wen, H. Liu, F. Zhu, et al., Microwave-assisted extraction combined with gel permeation chromatography and silica gel cleanup followed by gas chromatography-mass spectrometry for the determination of organophosphorus flame retardants and plasticizers in biological samples, Anal. Chim. Acta. 786 (2013) 47–53. doi:10.1016/j.aca.2013.04.062.

[51] B. Kowalski, M. Mazur, The Simultaneous Determination of Six Flame Retardants in Water Samples Using SPE Pre-concentration and UHPLC-UV Method, Water, Air, Soil Pollut. 225 (2014). doi:10.1007/s11270-014-1866-4.

[52] M. García-López, I. Rodríguez, R. Cela, Pressurized liquid extraction of organophosphate triesters from sediment samples using aqueous solutions, J. Chromatogr. A. 1216 (2009) 6986–6993. doi:10.1016/j.chroma.2009.08.068.

[53] T. Kröber, M.W. Wolff, B. Hundt, a. Seidel-Morgenstern, U. Reichl, Continuous purification of influenza virus using simulated moving bed chromatography, J. Chromatogr. A. 1307 (2013) 99–110. doi:10.1016/j.chroma.2013.07.081.

[54] P. Nestola, R.J.S. Silva, C. Peixoto, P.M. Alves, M.J.T. Carrondo, J.P.B. Mota, Adenovirus purification by two-column, size-exclusion, simulated countercurrent chromatography, J. Chromatogr. A. 1347 (2014) 111–121. doi:10.1016/j.chroma.2014.04.079.

[55] M. Wellhoefer, W. Sprinzl, R. Hahn, A. Jungbauer, Continuous processing of recombinant proteins: Integration of refolding and purification using simulated moving bed size-exclusion chromatography with buffer recycling, J. Chromatogr. A. 1337 (2014) 48–56. doi:10.1016/j.chroma.2014.02.016.

[56] S. Mun, Y. Xie, N.-H.L. Wang, Residence time distribution in a size-exclusion SMB for insulin purification, AIChE J. 49 (2003) 2039–2058. doi:10.1002/aic.690490814.

[57] Y. Xie, S.-Y. Mun, N.-H.L. Wang, Startup and Shutdown Strategies of Simulated Moving Bed for Insulin Purification, Ind. Eng. Chem. Res. 42 (2003) 1414–1425. doi:10.1021/ie020674d.

[58] G. Biressi, O. Ludemann-Hombourger, M. Mazzotti, R.M. Nicoud, M. Morbidelli, Design and optimisation of a simulated moving bed unit: role of deviations from equilibrium theory., J. Chromatogr. A. 876 (2000) 3–15. http://www.ncbi.nlm.nih.gov/pubmed/10823498.

[59] Z. Ma, N.-H.L. Wang, Standing wave analysis of SMB chromatography: Linear systems, AIChE J. 43 (1997) 2488–2508. doi:10.1002/aic.690431012.

[60] B.J. Hritzko, Y. Xie, R.J. Wooley, N.-H.L. Wang, Standing-wave design of tandem SMB for linear multicomponent systems, AIChE J. 48 (2002) 2769–2787. doi:10.1002/aic.690481207.

[61] T. Mallmann, B.D. Burris, Z. Ma, N.H.L. Wang, Standing wave design of nonlinear SMB systems for fructose purification, AIChE J. 44 (1998) 2628–2646. doi:10.1002/aic.690441206.

[62] Y. Xie, C.A. Farrenburg, C.Y. Chin, S. Mun, N.-H.L. Wang, Design of SMB for a nonlinear amino acid system with mass-transfer effects, AIChE J. 49 (2003) 2850–2863. doi:10.1002/aic.690491117.

[63] K.B. Lee, S. Mun, F. Cauley, G.B. Cox, N.-H.L. Wang, Optimal Standing-Wave Design of Nonlinear Simulated Moving Bed Systems for Enantioseparation, Ind. Eng. Chem. Res. 45 (2006) 739–752. doi:10.1021/ie0504248.

[64] K.B. Lee, C.Y. Chin, Y. Xie, G.B. Cox, N.-H.L. Wang, Standing-Wave Design of a Simulated Moving Bed under a Pressure Limit for Enantioseparation of Phenylpropanolamine, Ind. Eng. Chem. Res. 44 (2005) 3249–3267. doi:10.1021/ie049413p.

[65] G. Paredes, M. Mazzotti, Optimization of simulated moving bed and column chromatography for a plasmid DNA purification step and for a chiral separation., J. Chromatogr. A. 1142 (2007) 56–68. doi:10.1016/j.chroma.2006.12.009.

[66] F.G. Cauley, S.F. Cauley, K.B. Lee, Y. Xie, N.-H.L. Wang, Standing Wave Annealing Technique: For the design and optimization of nonlinear simulated moving bed systems with significant mass-transfer effects, Ind. Eng. Chem. Res. 45 (2006) 8697–8712. doi:10.1021/ie060300a.

[67] F.G. Cauley, Y. Xie, N.-H.L. Wang, Optimization of SMB systems with linear adsorption isotherms by the Standing Wave Annealing Technique, Ind. Eng. Chem. Res. 43 (2004) 7588–7599. doi:10.1021/ie049842n.

[68] F.G. Cauley, S.F. Cauley, N.-H.L. Wang, Standing wave optimization of SMB using a hybrid simulated annealing and genetic algorithm (SAGA), Adsorption. 14 (2008) 665–678. doi:10.1007/s10450-008-9119-8.

[69] K.B. Lee, R.B. Kasat, G.B. Cox, N.-H.L. Wang, Simulated moving bed multiobjective optimization using standing wave design and genetic algorithm, AIChE J. 54 (2008) 2852–2871. doi:10.1002/aic.11604.

[70] B.A. Miller-Chou, J.L. Koenig, A review of polymer dissolution, Prog. Polym. Sci. 28 (2003) 1223–1270. doi:10.1016/S0079-6700(03)00045-5.

[71] C. Hansen, Tables A.1-A.2, in: Hansen Solubility Parameters A User's Handb., 2nd ed., CRC Press, Boca Raton, FL, 2007: pp. 345–505.

[72] A. Martin, P. Wu, A. Adjei, A. Beerbower, J.M. Prausnitz, Extended Hansen solubility approach: Naphthalene in individual solvents, J. Pharm. Sci. 70 (1981) 1260–1264. http://onlinelibrary.wiley.com/doi/10.1002/jps.2600701120/abstract (accessed December 18, 2014).

[73] K. Srinivas, J.W. King, J.K. Monrad, L.R. Howard, C.M. Hansen, Optimization of subcritical fluid extraction of bioactive compounds using Hansen solubility parameters., J. Food Sci. 74 (2009) E342–54. doi:10.1111/j.1750-3841.2009.01251.x.

[74] C.M. Hansen, On predicting environmental stress cracking in polymers, Polym. Degrad. Stab. 77 (2002) 43–53. doi:10.1016/S0141-3910(02)00078-2.

[75] L.F. Henry, Prediction and evaluation of the susceptibilities of glassy thermoplastics to environmental stress cracking, Polym. Eng. Sci. 14 (1974) 167–176. doi:10.1002/pen.760140304.

[76] L. Ling, P.L. Chung, A. Youker, D.C. Stepinski, G.F. Vandegrift, N.H.L. Wang, Capture chromatography for Mo-99 recovery from uranyl sulfate solutions: Minimum-column-volume design method, J. Chromatogr. A. 1309 (2013) 1–14. doi:10.1016/j.chroma.2013.08.023.

[77] S. Ergun, Fluid flow through packed columns, Chem. Eng. Prog. 48 (1952) 89–94.

[78] M.M. Awad, Hagen number versus bejan number, Therm. Sci. 17 (2013) 1245–1250. doi:10.2298/TSCI1304245A.

[79] S.F. Chung, C.Y. Wen, Longitudinal dispersion of liquid flowing through fixed and fluidized beds, AIChE J. 14 (1968) 857–866. doi:10.1002/aic.690140608.

[80] J. Bentley, S. Li, Y. Kawajiri, Experimental validation of optimized model-based startup acceleration strategies for simulated moving bed chromatography, Ind. Eng. Chem. Res. 53 (2014) 12063–12076. doi:10.1021/ie500714p.

[81] S. Li, Y. Kawajiri, J. Raisch, A. Seidel-Morgenstern, Optimization of startup and shutdown operation of simulated moving bed chromatographic processes, J. Chromatogr. A. 1218 (2011) 3876–3889. doi:10.1016/j.chroma.2011.04.051.

[82] C.N. Pomeranz, S. V Olesik, Separation of poly-3-hydroxyvalerate-co-3-hydroxybutyrate through gradient polymer elution chromatography., J. Chromatogr. A. 1218 (2011) 7943–7. doi:10.1016/j.chroma.2011.08.065.

[83] S.H. Kim, L. Haimovich-Caspi, L. Omer, C.-M. Yu, Y. Talmon, N.-H.L. Wang, et al., Stability and State of Aggregation of Aqueous Fibrinogen and Dipalmitoylphosphatidylcholine Lipid Vesicles, Langmuir. 23 (2007) 5657–5664. doi:10.1021/la0634701.

[84] J. Mackie, P. Meares, The diffusion of electrolytes in a cation-exchange resin membrane. I. Theoretical, Proc. R. Soc. London. 232 (1955) 498–509. http://rspa.royalsocietypublishing.org/content/232/1191/498.short (accessed December 15, 2014).

[85] L.J. Fetters, N. Hadjichristidis, J.S. Linder, J.W. Mays, Molecular weight dependance of hydrodynamic and thermodynamic properties for well-defined linear polymers in solution, J. Phys. Chem. Ref. Data. 23 (1994) 619–640. doi:10.1063/1.555949.

[86] J. Berninger, R. Whitley, A versatile model for simulation of reaction and nonequilibrium dynamics in multicomponent fixed-bed adsorption processes, Comput. Chem. …. 15 (1991) 749–768. http://www.sciencedirect.com/science/article/pii/009813549185020U (accessed October 23, 2014).

[87] Q. Yu, N.-H.L. Wang, Computer simulations of the dynamics of multicomponent ion exchange and adsorption in fixed beds—gradient-directed moving finite element method, Comput. Chem. Eng. 13 (1989) 915–926. doi:10.1016/0098-1354(89)85064-1.

[88] R.D. Whitley, K.E. Van Cott, N.H.L. Wang, Analysis of nonequilibrium adsorption/desorption kinetics and implications for analytical and preparative chromatography, Ind. Eng. Chem. Res. 32 (1993) 149–159. doi:10.1021/ie00013a020.

[89] R. Whitley, K. Van Cott, J.A. Berninger, N.-H.L. Wang, Effects of protein aggregation in isocratic nonlinear chromatography, AIChE J. 37 (1991) 555–568. http://onlinelibrary.wiley.com/doi/10.1002/aic.690370409/full (accessed July 28, 2013).

[90] R.D. Whitley, J. a Berninger, N. Rouhana, N.H. Wang, Nonlinear gradient isotherm parameter estimation for proteins with consideration of salt competition and multiple forms., Biotechnol. Prog. 7 (1991) 544–53. doi:10.1021/bp00012a010.

[91] K.E. Van Cott, R.D. Whitley, N.-H.L. Wang, Effects of temperature and flow rate on frontal and elution chromatography of aggregating systems, Sep. Technol. 1 (1991) 142–152. doi:10.1016/0956-9618(91)80009-O.

[92] R. Whitley, X. Zhang, N. Wang, Protein denaturation in nonlinear isocratic and gradient elution chromatography, AIChE J. 40 (1994). http://onlinelibrary.wiley.com/doi/10.1002/aic.690400617/abstract (accessed July 28, 2013).

[93] Z. Ma, R.D. Whitley, N.-H.L. Wang, Pore and surface diffusion in multicomponent adsorption and liquid chromatography systems, AIChE J. 42 (1996) 1244–1262. doi:10.1002/aic.690420507.

[94] M. V. Ernest, J.P. Bibler, R.D. Whitley, N.-H.L. Wang, Development of a Carousel Ion-Exchange Process for Removal of Cesium-137 from Alkaline Nuclear Waste, Ind. Eng. Chem. Res. 36 (1997) 2775–2788. doi:10.1021/ie960729+.

[95] B.J. Hritzko, D.D. Walker, N.-H.L. Wang, Design of a carousel process for cesium removal using crystalline silicotitanate, AIChE J. 46 (2000) 552–564. doi:10.1002/aic.690460314.

[96] J.-H. Koh, N.-H.L. Wang, P.C. Wankat, Ion Exchange of Phenylalanine in Fluidized/Expanded Beds, Ind. Eng. Chem. Res. 34 (1995) 2700–2711. doi:10.1021/ie00047a020.

[97] J.-H. Koh, P.C. Wankat, N.-H.L. Wang, Pore and Surface Diffusion and Bulk-Phase Mass Transfer in Packed and Fluidized Beds, Ind. Eng. Chem. Res. 37 (1998) 228–239. doi:10.1021/ie970337i.

[98] M. V. Ernest, R.D. Whitley, Z. Ma, N.-H.L. Wang, Effects of Mass Action Equilibria on Fixed-Bed Multicomponent Ion-Exchange Dynamics, Ind. Eng. Chem. Res. 36 (1997) 212–226. doi:10.1021/ie960167u.

[99] Y. Xie, E. Van de Sandt, T. de Weerd, N.H. Wang, Purification of adipoyl-7-amino-3-deacetoxycephalosporanic acid from fermentation broth using stepwise elution with a synergistically adsorbed modulator., J. Chromatogr. A. 908 (2001) 273–91. http://www.ncbi.nlm.nih.gov/pubmed/11218130.

[100] C.Y. Chin, N.-H.L. Wang, Simulated Moving Bed Technology for Biorefinery Applications, in: S. Ramaswamy, H.-J. Huang, B. V. Ramarao (Eds.), Sep. Purif. Technol. Biorefineries, Wiley, 2013: pp. 167–202.

[101] G.S. Weeden, N.H. Soepriatna, N.-H.L. Wang, Method for Efficient Recovery of High-Purity Polycarbonates from Electronic Waste, Environ. Sci. Technol. 49 (2015) 2425–2433. doi:10.1021/es5055786.

[102] E. Antoniou, E. Themistou, B. Sarkar, M. Tsianou, P. Alexandridis, Structure and dynamics of dextran in binary mixtures of a good and a bad solvent, Colloid Polym. Sci. 288 (2010) 1301–1312. doi:10.1007/s00396-010-2259-x.

[103] F. Machui, S. Langner, X. Zhu, S. Abbott, C.J. Brabec, Determination of the P3HT:PCBM solubility parameters via a binary solvent gradient method: Impact of solubility on the photovoltaic performance, Sol. Energy Mater. Sol. Cells. 100 (2012) 138–146. doi:10.1016/j.solmat.2012.01.005.

[104] E. Uliyanchenko, P.J.C.H. Cools, S. van der Wal, P.J. Schoenmakers, Comprehensive two-dimensional ultrahigh-pressure liquid chromatography for separations of polymers., Anal. Chem. 84 (2012) 7802–9. doi:10.1021/ac3011582.

[105] S. Moyses, J. Ness, G. Papakonstantopoulos, 2-D chromatography applied to the study of block copolymers synthesized by nitroxide-mediated controlled free-radical seeded emulsion polymerization., J. Sep. Sci. 33 (2010) 3511–8. doi:10.1002/jssc.201000524.

[106] S. Moyses, Two-dimensional chromatography applied to the study of the thermo-oxidative degradation of poly(styrene-b-butadiene) star block copolymers., J. Sep. Sci. 35 (2012) 1741–7. doi:10.1002/jssc.201200174.

[107] M. Kamlet, R. Taft, The solvatochromic comparison method. I. The beta-scale of solvent hydrogen-bond acceptor (HBA) basicities, J. Am. Chem. Soc. 98 (1976) 377–383. doi:10.1021/ja00418a009.

[108] T. Freier, C. Kunze, K. Schmitz, Solvent removal from solution-cast films of biodegradable polymers, J. Mater. Sci. Lett. 20 (2001) 1929–1931. http://www.springerlink.com/index/w3158q3n77k41178.pdf (accessed December 18, 2014).

[109] K. Komiya, S. Fukuoka, M. Aminaka, K. Hasegawa, H. Hachiya, H. Okamoto, et al., Green Chemistry, in: P.T. Anastas, T.C. Williamson (Eds.), New Process Prod. Polycarbonate Without Phosgene Methylene Chloride, American Chemical Society, Washington, DC, 1996: pp. 20–32. doi:10.1021/bk-1996-0626.

[110] T. König, K. Kohlgrüber, R. De Cleyn, Device and method for degassing solvent-containing polycarbonate solutions, US8383757 B2, 2013. http://www.google.com/patents/US8383757 (accessed December 18, 2014).

[111] Heathland Recyclables & Thermoplastic, PVC Recycling, (2009). http://www.heathland.nl/pvc-recycling.html.

[112] G.S. Weeden, L. Ling, N.H. Soepriatna, N.-H.L. Wang, Size-exclusion simulated moving bed for separating organophosphorus flame retardants from a polymer, J. Chromatogr. A. 1422 (2015) 99–116. doi:10.1016/j.chroma.2015.09.064.

[113] R.S. Spencer, J.L. Williams, Concentrated solution viscosity of polystyrene, J. Colloid Sci. 2 (1947) 117–129. doi:10.1016/0095-8522(47)90015-9.

[114] G.S. Weeden, N.-H.L. Wang, Speedy standing wave design of size-exclusion simulated moving bed: Solvent consumption and sorbent productivity related to material properties and design parameters, J. Chromatogr. A. 1418 (2015) 54–76. doi:10.1016/j.chroma.2015.08.042.

[115] D.A. Horneman, M. Wolbers, M. Zomerdijk, M. Ottens, J.T.F. Keurentjes, L.A.M. van der Wielen, Surfactant-aided size exclusion chromatography., J. Chromatogr. B. Analyt. Technol. Biomed. Life Sci. 807 (2004) 39–45. doi:10.1016/j.jchromb.2004.01.061.

APPENDICES

Appendix A Additional Equations

A1 – Equations Relating β_i^j to Yields and Zone Velocities

The equations for the β terms are given by Eq. (A1.1), which were derived from equations presented in Hritzko et al. [60].

$$\beta_2^I = \ln\left[\frac{Y_2}{(1-Y_2)}\frac{\left(\frac{u_0^{III}}{u_0^{IV}}-1\right)}{\left(1-\frac{u_0^{II}}{u_0^{I}}\right)}\right] \tag{A1.1a}$$

$$\beta_1^{II} = \ln\left\{\frac{\left(\frac{u_0^{I}}{u_0^{II}}-1\right)}{(1-Y_1)}\left[\frac{Y_1}{\left(1-\frac{u_0^{IV}}{u_0^{III}}\right)}-1\right]\right\} \tag{A1.1b}$$

$$\beta_2^{III} = \ln\left\{\frac{\left(1-\frac{u_0^{IV}}{u_0^{III}}\right)}{(1-Y_2)}\left[\frac{Y_2}{\left(\frac{u_0^{I}}{u_0^{II}}-1\right)}+1\right]\right\} \tag{A1.1c}$$

$$\beta_1^{IV} = \ln\left[\frac{Y_1}{(1-Y_1)}\frac{\left(1-\frac{u_0^{II}}{u_0^{I}}\right)}{\left(\frac{u_0^{III}}{u_0^{IV}}-1\right)}\right] \tag{A1.1d}$$

A2 – Expression of Γ^j Using the Chung and Wen Correlation for Low Re

The Chung and Wen correlation for low Re (Re < 10) (Eq. 34) was used to evaluate the ratios of axial dispersion coefficients (Γ^j) from Eq. (3.9). The resulting equations are rearranged to solve for Γ^j, Eq. (A2.1).

$$\Gamma^I = \frac{1+\phi\delta_2}{1+\phi\delta_1-\frac{\phi(\delta_2-\delta_1)}{P_{eb}^*}\left(\frac{\beta_1^{IV}}{N^{IV}}+\frac{\beta_2^{I}}{N^{I}}\right)} \tag{A2.1a}$$

$$\Gamma^{II} = \frac{1+\phi\delta_1}{1+\phi\delta_1-\frac{\phi(\delta_2-\delta_1)}{P_{eb}^*}\left(\frac{\beta_1^{IV}}{N^{IV}}+\frac{\beta_1^{II}}{N^{II}}\right)} \tag{A2.1b}$$

$$\Gamma^{III} = \frac{1+\phi\delta_2}{1+\phi\delta_1 - \frac{\phi(\delta_2-\delta_1)}{P^*_{eb}}\left(\frac{\beta_1^{IV}}{N^{IV}} - \frac{\beta_2^{III}}{N^{III}}\right)} \tag{A2.1c}$$

A3 – Expression for P_{eb}^* for Maximum Productivity in Dispersion Controlled Systems

The Peclet number for maximum productivity, $P^*_{eb,\max P_R}$, at a constant port velocity can be found by taking the partial derivative of Eq. (37b) with respect to P_{eb}^* and setting the resulting equation equal to zero. The expression that $P^*_{eb,\max P_R}$ must satisfy is given by Eq. (A3.1).

$$\frac{\frac{(1+\phi\delta_1)}{\phi(\delta_2-\delta_1)}\frac{\beta_1^{II}}{N^{II}}\left(\frac{(1+\phi\delta_1)}{\phi(\delta_2-\delta_1)}P^*_{eb} - \frac{\beta_1^{IV}}{N^{IV}}\right)}{\left(\frac{(1+\phi\delta_1)}{\phi(\delta_2-\delta_1)}P^*_{eb} - \frac{\beta_1^{II}}{N^{II}} - \frac{\beta_1^{IV}}{N^{IV}}\right)^2} + \frac{\frac{(1+\phi\delta_2)}{\phi(\delta_2-\delta_1)}\frac{\beta_2^{III}}{N^{III}}\left(\frac{(1+\phi\delta_1)}{\phi(\delta_2-\delta_1)}P^*_{eb} - \frac{\beta_1^{IV}}{N^{IV}}\right)}{\left(\frac{(1+\phi\delta_1)}{\phi(\delta_2-\delta_1)}P^*_{eb} + \frac{\beta_2^{III}}{N^{III}} - \frac{\beta_1^{IV}}{N^{IV}}\right)^2}$$

$$+ \frac{\frac{(1+\phi\delta_1)}{\phi(\delta_2-\delta_1)}\frac{\beta_1^{II}}{N^{II}}}{\frac{(1+\phi\delta_1)}{\phi(\delta_2-\delta_1)}P^*_{eb} - \frac{\beta_1^{II}}{N^{II}} - \frac{\beta_1^{IV}}{N^{IV}}} + \frac{\frac{(1+\phi\delta_2)}{\phi(\delta_2-\delta_1)}\frac{\beta_2^{III}}{N^{III}}}{\frac{(1+\phi\delta_1)}{\phi(\delta_2-\delta_1)}P^*_{eb} + \frac{\beta_2^{III}}{N^{III}} - \frac{\beta_1^{IV}}{N^{IV}}} = 1 \tag{A3.1a}$$

At a large P_{eb}^*, or a large number of columns in all zones, Eq. (A3.1a) simplifies to Eq. (A3.1b).

$$P^*_{eb,\max P_R} = \frac{2\beta_1^{II}}{N^{II}} + \frac{2(1+\phi\delta_2)}{(1+\phi\delta_1)}\frac{\beta_2^{III}}{N^{III}} \tag{A3.1b}$$

A4 – Cost Functions for Insulin Example

The total cost (TC) is defined as the sum of the Equipment Cost (EC), Resin Cost (RC), and Solvent Cost (SC), Eq. (A4.1).

$$TC = EC + RC + SC \tag{A4.1}$$

The purchase cost of the equipment is assumed to be \$400,000 plus \$10,000 per column with a depreciation time of seven years and 4% downtime for a production scale of 5,000 kg insulin per year. The unit equipment cost is given by Eq. (A4.2).

$$EC\ \left[\frac{\$}{kg_{insulin}}\right] = \frac{\left(400{,}000[\$]+10{,}000\left[\frac{\$}{column}\right]N[columns]\right)}{(7\ [years])(0.96)\left(5{,}000\left[\frac{kg_{insulin}}{year}\right]\right)} \quad \text{(A4.2)}$$

The purchase cost for the sorbent is assumed to be $150 per liter. The usable life of the sorbent is assumed to four years. The diameter of the columns is determined by the production rate and the zone velocities. The unit sorbent cost is given by Eq. (A4.3).

$$RC\ \left[\frac{\$}{kg_{insulin}}\right] = \frac{(Bed\ Vol)(1-\varepsilon_b)(\rho_{particle})(Resin\ price)}{(Resin\ Life)(Production)} = \frac{\left(\frac{NL_C\pi D^2}{4}[L]\right)(1-\varepsilon_b)\left(0.12\left[\frac{kg}{L}\right]\right)\left(3086.5\left[\frac{\$}{kg}\right]\right)}{(4\ [years])\left(5{,}000\left[\frac{kg_{insulin}}{year}\right]\right)} \quad \text{(A4.3)}$$

The purchase price of solvent is assumed to be $0.10 per liter. Assuming no recycle of the recycle, the unit solvent cost is given by Eq. (A4.4).

$$SC\ \left[\frac{\$}{kg_{insulin}}\right] = \frac{\left(1+\frac{D}{F}\right)(Solvent\ price)}{(Feed\ Conc.)(Yield)} = \frac{\left(1+\frac{D}{F}\right)(0.1\ [\$/L])\left(1{,}000\left[\frac{g_{insulin}}{kg_{insulin}}\right]\right)}{\left(Feed\ conc.\left[\frac{g_{insulin}}{L}\right]\right)(Yield)} \quad \text{(A4.4)}$$

Batch SEC equipment cost is assumed to be $100,000 per unit of 12 columns with the same depreciation rate, resin life, and utilization factor as that of the SEC-SMB.

A5 – Cost Optimization Algorithm

The algorithm that was used to determine the optimum column configuration, column length, zone velocities, and port velocity for minimum cost is shown in Figure A5.1. Material properties, yields, dead volume, pressure limit, feed concentration, packing density, fluid viscosity, and production scale were held constant. The total number of columns was varied from eight to twelve and each zone was constrained to have at least two columns. The number of columns in Zone IV was calculated from the column balance of the other zones and the total number of columns. N_D^* ranged from 0.02 to 100 and P_{eb}^* ranged from 5 to 1,000. The initial values of the variables were sent to the SSWD algorithm,

Figure A5.1b. This algorithm used an initial guess for β_i^j and Γ^j and then evaluated u_0^j/ν. The SSWD algorithm then calculated β_i^j and Γ^j from u_0^j/ν using Eq. (A1.1) and Eq. (A2.1), respectively. If the calculated values were not within a tolerance of 0.001 of the guessed values, then the u_0^j/ν calculations were repeated with the new values of β_i^j and Γ^j. Once the values were within the tolerance, L_c was calculated from P_{eb}^* using Eq. (3.38b) and ν was calculated from N_D^* using Eq. (3.8) and Eq. (3.18). After ν was calculated, the zone velocities could be calculated using Eq. (3.20). The solvent consumption and sorbent productivity were then calculated using Eq. (3.20) and Eq. (3.21), respectively. The total cost of the separation was then calculated using Eqs. (A4.1-A4.4). The pressure drop of the system was calculated from Eq. (3.22) and compared to the set pressure limit of 1.5 psi per column. If the calculated pressure exceeded the pressure limit, then the design was not considered feasible. After the pressure check, the Peclet number was incremented and the process repeated until it reached 1,000. Then N_D^* was incremented and the P_{eb}^*cycle was repeated. Once N_D^* reached a value of 100, the column configuration would change, and the N_D^* and P_{eb}^* cycles would repeat. After all the cycles were completed, the minimum cost was found from all the stored values and the associated cost, L_c, N^j, u_0^j, and ν were determined. This algorithm was implemented using MATLAB R2014a on a laptop computer with a total run time of less than one minute.

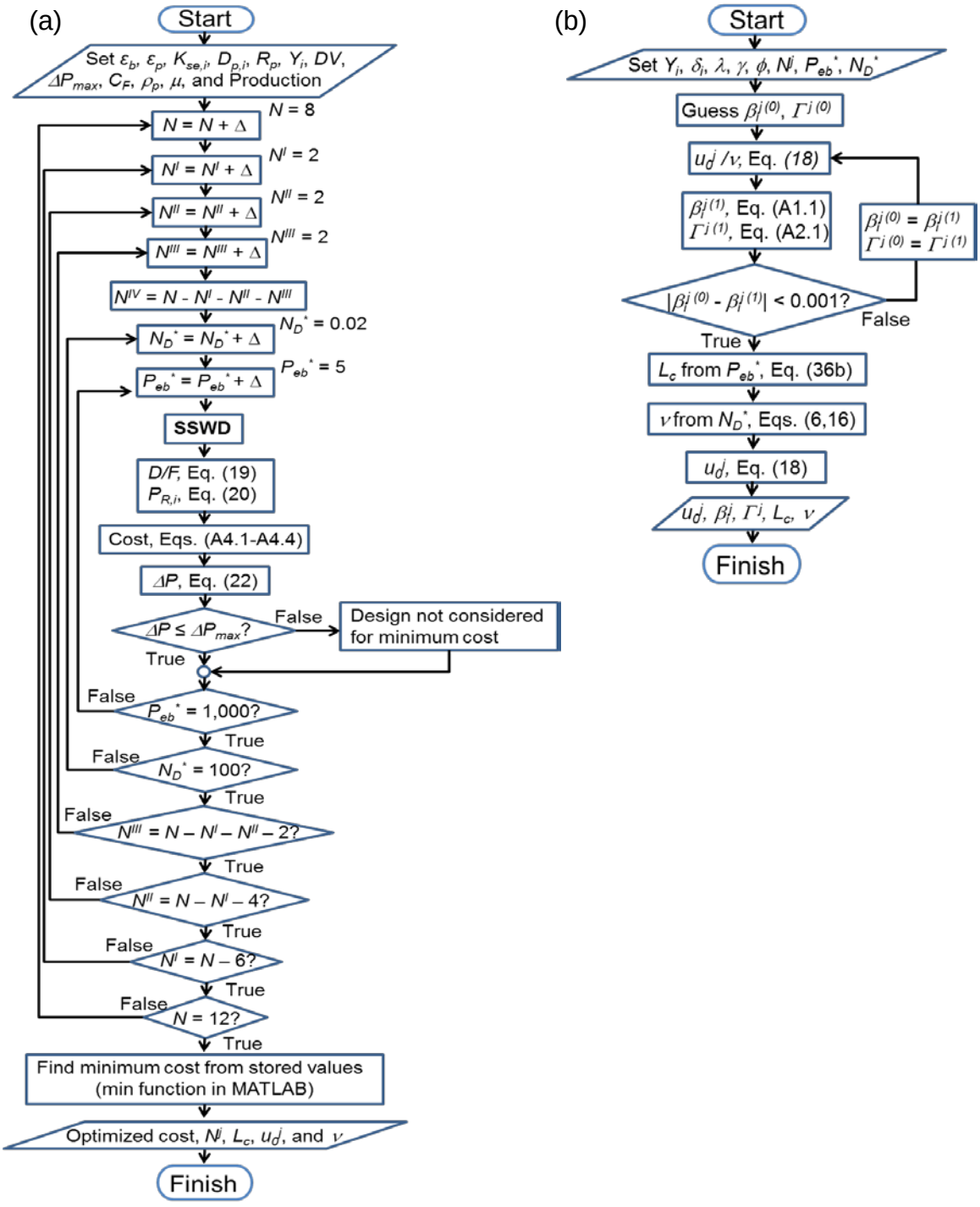

Figure A5.A.1. (a) algorithm for optimizing 10 decision variables (column configuration, column length, zone velocities, and port velocity) for minimum cost and (b) algorithm used by SSWD to determine column length, β_i^j, Γ^j, zone velocities and port velocity from given dimensionless groups.

Appendix B Parameters from Literature Cases

The expanded sets of parameters are shown in tables for Case 1 (Table B.1), Case 2 (Table B.2), and Case 3 (Table B.3).

Table B.1. Extended table of parameters for Case 1.

	1A	**1B**	**1C**
Authors		Liang and Liang	
Year		2012	
Component 1		20,000 MW PEG	
Component 2		1,500 MW PEG	
Design		Triangle	
ε_p		0.80	
ε_b		0.364	
$K_{se,1}$, $K_{se,2}$		0.38, 0.57	
δ_1, δ_2		0.30, 0.46	
$D_{p,1}$, $D_{p,2}$ (cm^2/min)		2.9 x 10^{-4}, 2.9 x 10^{-4}	
γ/α		0.66	
ϕ		1.74	
Configuration		2-2-2	
L_c (cm)		30	
Diameter (cm)		0.75	
DV		~ 0.00	
R_p (μm)		8.5	
$C_{F,1}$, $C_{F,2}$ (g/L)		1.9, 1.7	
Y_1, Y_2 (%)	65.5, 99.9	99.9, 99.9	99.9, 70.7
t_s (min)	20.5	21.5	22.5
Flowrates (mL/min)			
Desorbent		0.5	
Feed		0.045	
Extract		0.15	
Raffinate		0.395	
N_D^*	4,447	4,664	4,881
P_{eb}^* ($L_c/10\varepsilon_b R_p$)		1,751 (9,696)	

Table B.2. Extended table of parameters for Case 2.

	2A	**2B**	**2C**	**2D**	**2E**
Authors			Houwing et al.		
Year			2003		
Component 1			BSA		
Component 2			Myoglobin		
Design			Triangle		
ε_p			0.98		
ε_b			0.39		
$K_{se,1}$, $K_{se,2}$			0.65, 0.88		
δ_1, δ_2			0.73, 0.95		
$D_{p,1}$, $D_{p,2}$ (cm^2/min)			3.66×10^{-5}, 7.2×10^{-5}		
γ/α			1.50		
ϕ			1.56		
Configuration			2-2-2-2		
L_c (cm)			8.9		
Diameter (cm)			1.0		
DV			0.06		
R_p (μm)			100		
$C_{F,1}$, $C_{F,2}$ (g/L)			1.9, 1.7		
Y_1, Y_2 (%)	46.2, 90.0	60.5, 90.0	71.3, 82.5	86.7, 60.0	99.8, 40.5
t_s (min)	1.14	1.14	1.14	1.14	1.14
Flowrates (mL/min)					
Desorbent	2.58	2.65	2.69	2.65	2.65
Feed	0.15	0.15	0.15	0.15	0.15
Extract	1.49	1.35	1.12	0.90	0.67
Raffinate	1.23	1.46	1.72	1.91	2.13
N_D^*	0.11	0.11	0.11	0.11	0.11
P_{eb}^* ($L_c/10\varepsilon_b R_p$)			38.0 (228)		

Table B.3. Extended table of parameters for Case 3.

	Case 3*
Authors	Xie et al.
Year	2002
Component 1	Insulin
Component 2	$ZnCl_2$
Design	SWD
ε_p	0.89
ε_b	0.35
$K_{se,1}$, $K_{se,2}$	0.74, 0.99
δ_1, δ_2	0.69, 0.91
$D_{p,1}$, $D_{p,2}$ (cm^2/min)	2.29 x 10^{-5}, 1.65 x 10^{-4}
γ/α	5.46
ϕ	1.86
Configuration	2-3-3-2
L_c (cm)	13.7
Diameter (cm)	5.1
DV	0.02
R_p (μm)	54
$C_{F,1}$, $C_{F,2}$ (g/L)	69.5, 0.303
Y_1, Y_2 (%)	99.7, 99.0
t_s (min)	33.7
Flowrates (mL/min)	
Desorbent	1.35
Feed	1.10
Extract	1.17
Raffinate	1.29
N_D^*	8.9
P_{eb}^* ($L_c/10\varepsilon_b R_p$)	145 (725)

Appendix C Cost Functions and Optimization for FR SMB

The total cost function used in this work to estimate the separation cost for SEC-SMB is shown in Eq. (C.1).

$$Total\ Cost\ (TC) = Resin\ Cost\ (RC) + Solvent\ Cost(SC) + Equipment\ Cost(EC) \tag{C.1}$$

where all the costs have the units of $/kg FR.

The resin cost was calculated according to Eq. (C.2),

$$RC\ \left[\frac{\$}{kg_{FR}}\right] = \frac{(Vol.\ of\ resin)(Resin\ price)}{(Resin\ Life)(Production)} = \frac{\left(\frac{NL_C\pi(ID)^2}{4}[L\ CV]\right)\left(19\left[\frac{\$}{L\ CV}\right]\right)}{(10\ [years])\left(10{,}000{,}000\left[\frac{kg_{FR}}{year}\right]\right)} \tag{C.2}$$

where *N* is the total number of columns and *ID* is the column inner diameter.

The solvent cost was calculated according to Eq. (C.3),

$$SC\ \left[\frac{\$}{kg_{FR}}\right] = \frac{\left(\frac{D}{F}\right)[RR*recycle\ cost+(1-RR)*Solvent\ price]}{(Feed\ Conc.)(Yield)} = \frac{\left(\frac{D}{F}\right)(.99*.002+.01*1)[\$/L]\left(1{,}000\left[\frac{g_{FR}}{kg_{FR}}\right]\right)}{\left(C_F\left[\frac{g_{FR}}{L}\right]\right)(Yield)} \tag{C.3}$$

where *RR* is the recycle ratio of solvent.

The equipment cost was calculated according to Eq. (C.4).

$$EC\ \left[\frac{\$}{kg_{FR}}\right] = \frac{(SMB\ price)}{(Depreciation\ Time)(Utilization\ Factor)(Production)} = \frac{(3{,}000{,}000[\$])}{(7\ [years])(.96)\left(10{,}000{,}000\left[\frac{kg_{FR}}{year}\right]\right)} \tag{C.4}$$

The cost optimization algorithm that was used to determine the optimum yields, particle radius, column configuration, column length, zone velocities, and port velocity is shown in Figure C.1. Material properties (other than particle radius), dead volume, pressure limit, feed concentration, packing density, fluid viscosity, and production scale were held constant. The total number of columns was varied from eight to twelve and each zone was

constrained to have at least two columns. The number of columns in Zone IV was calculated from the column balance of the other zones and the total number of columns. N_D^* ranged from 0.1 to 20, P_{eb}^* ranged from 5 to 1,000, R_p ranged from 112 μm to 450 μm, and yields ranged from 0.990 to 0.999. The initial values of the variables were passed to the SSWD algorithm, Fig. C.1b, which used an initial guess for β_i^j and Γ^j and then evaluated u_0^j/ν. The SSWD algorithm then calculated β_i^j, and Γ^j from u_0^j/ν. If the calculated values were not within 0.001 of the guessed values, then the u_0^j/ν calculations were repeated with the calculated values of β_i^j and Γ^j. Once the values were within the tolerance, L_c was calculated from P_{eb}^* and ν was calculated from N_D^*. Once ν was calculated, the zone velocities were calculated. The solvent consumption and sorbent productivity were then calculated. The overall separation cost (total cost) was then calculated. The pressure drop of the system was calculated and compared to the set pressure limit of 100 psi per zone. If the calculated pressure exceeded the pressure limit, then the design was not considered feasible. After the pressure check, the Peclet number was increased and the process repeated until $P_{eb}^* = 1{,}000$. Then, N_D^* was increased and the P_{eb}^*cycle repeated. Once N_D^* reached a value of 20, the particle size increased and the N_D^* and P_{eb}^* cycles repeated. In similar fashions, all the cycles were repeated for varying column configuration and yield of each component. After all the cycles were completed, the minimum cost was found from all the stored values and the associated cost, Y_i, R_p, L_c, N^j, u_0^j, and ν were determined. This algorithm was implemented using MATLAB R2014a on a laptop computer with a total run time of less than one minute.

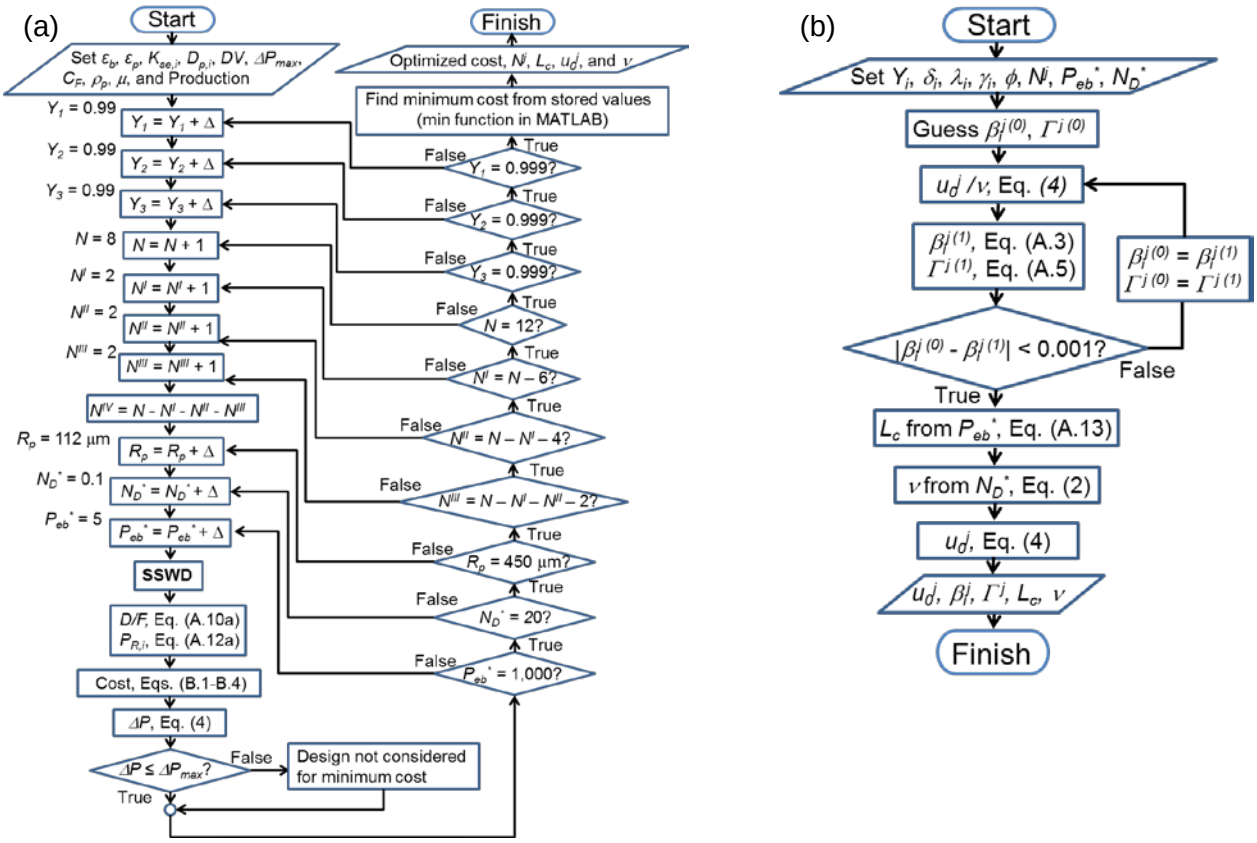

Figure C.1. (a) algorithm for optimizing 14 decision variables (yields, particle size, column configuration, column length, zone velocities, and port velocity) for minimum cost and (b) algorithm used by SSWD to determine column length, β_l^j, Γ^j, zone velocities, and port velocity from given dimensionless groups.

Appendix D Additional GPEC Results

The HSP screening gave a large number of promising solvent pairs (11 x 11), shown in Table D.1, and even a larger number of mixtures (10 or more compositions for each solvent pair), which were potentially feasible for separations. GPEC was used to find the specific compositions of the solvent pairs which were promising for extraction.

The first solvent pair tested was methanol and DCM. The Hansen parameters for DCM, methanol, PC, PS, and SAN are shown in Figure D.1a. The overlaid chromatograms of the pure standards using the methanol/DCM gradient are shown in Figure D.1b. The line between the methanol and DCM points passes through the SAN sphere first, then through the PC and PS spheres, indicating that the pair may not be able to separate PC from PS. This prediction is confirmed by the GPEC results. The methanol/DCM gradient effectively separates the flame retardants and SAN, but PS, PC, and BrPC all elute at the same composition. Since PS, PC, and BrPC all elute together, this solvent pair would not be useful to recover high-purity polycarbonates when the feed contains PS.

Table D.1. Tables of Hansen solubility parameters for (a) strong solvents for PC, (b) weak solvents for PC, and (c) polymers PC, PS, and SAN.

(a)

Chemical	Cost ($/kg)[b]	B.P. (°C)	(MPa$^{.5}$) δ_D	δ_P	δ_H	PC RED	PS RED	SAN RED
Dichloromethane (DCM)	0.50	40	18.2	6.3	6.1	0.17	0.66	0.54
1,2-Ethylene dichloride (EDC)	0.56	84	19.0	7.4	4.1	0.66	0.53	0.27
Chloroform ($CHCl_3$)	0.70	61	17.8	3.1	5.7	0.56	0.75	0.85
1,4-Dioxane (DIOX)	1.00	101	19.0	1.8	7.4	0.82	0.65	1.01
1,1,2,2-Tetrachloroethane (TCE)	1.00	147	18.8	5.1	5.3	0.41	0.56	0.57
Aniline (ANI)	1.60	184	19.4	5.1	10.2	0.78	0.65	0.96
Cyclohexanone (CyHEX)	1.90	156	17.8	6.3	5.1	0.35	0.71	0.53
Carbon tetrachloride (CCl_4)	2.00	77	17.8	0.0	0.6	1.57	0.89	1.17
Tetrahydrofuran (THF)	2.50	66	16.8	5.7	8.0	0.51	0.91	0.89
Benzaldehyde (BENZ)	2.50	178	19.4	7.4	5.3	0.62	0.48	0.36
Dibromomethane (DBM)	5.00	97	17.8	6.4	7.0	0.14	0.74	0.65

(b)

Chemical	Cost ($/kg)[b]	B.P. (°C)	(MPa$^{.5}$) δ_D	δ_P	δ_H	PC RED	PS RED	SAN RED
Methanol (MeOH)	0.35	65	15.1	12.3	22.3	3.22	1.89	2.41
Ethanol (EtOH)	0.60	78	15.8	8.8	19.4	2.48	1.59	2.02
Isopropyl alcohol (IPA)	0.66	83	16.0	6.8	17.4	2.06	1.43	1.82
Acetone (ACE)	0.70	56	15.5	10.4	7.0	1.25	1.15	0.95
Methyl ethyl ketone (MEK)	0.70	80	16.0	9.0	5.1	1.00	1.03	0.75
Acetonitrile (ACN)	0.71	82	15.3	18.0	6.1	2.43	1.47	1.36
Toluene (TOL)	0.85	111	18.0	1.4	2.0	1.21	0.78	0.97
Acetaldehyde (AceAl)	0.90	20	14.7	12.5	7.9	1.73	1.34	1.20
Benzene (BEN)	1.03	80	18.4	0.0	2.0	1.40	0.78	1.11
n-hexane (HEX)	1.28	68	14.9	0.0	0.0	2.02	1.29	1.50
n-heptane (HEP)	1.40	99	15.3	0.0	0.0	1.94	1.24	1.44

(C)

Polymer	(MPa$^{.5}$) δ_D	δ_P	δ_H	R_0
PC	18.1	5.9	6.9	5.5
PS	22.3	5.8	4.3	12.7
SAN	19.1	9.5	3.1	8.7

(a)

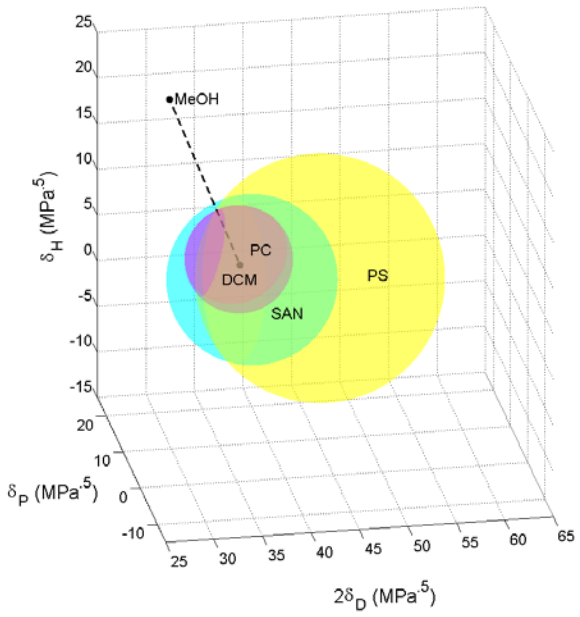

(b)

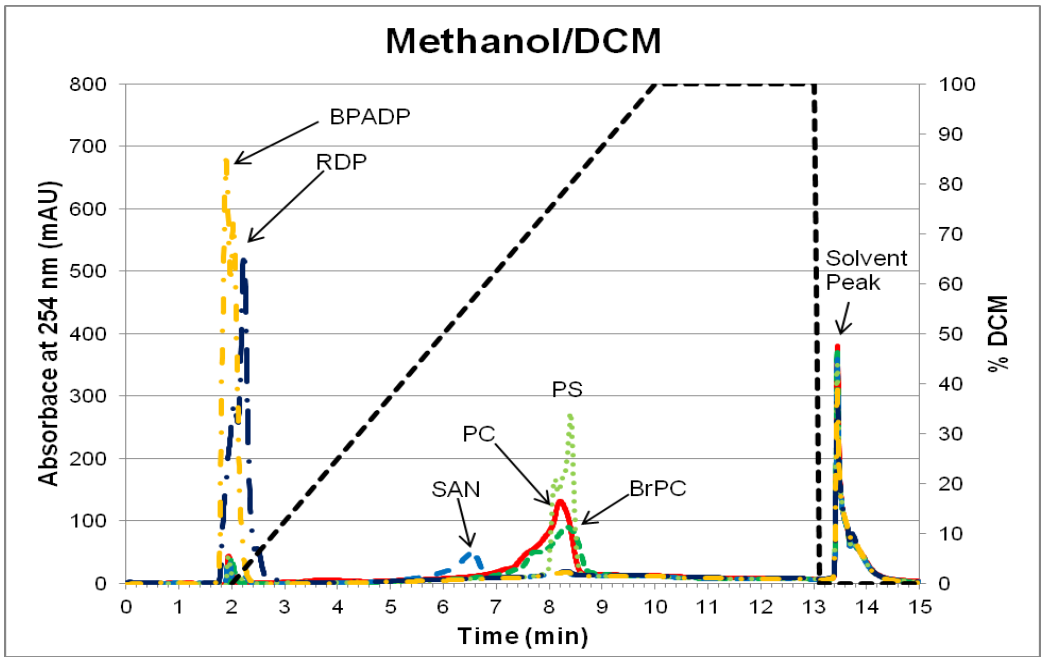

Figure D.1. (a) Hansen solubility parameter space with PC, PS, and SAN solubility spheres plotted with methanol and DCM gradient as a dashed line. (b) Composite chromatogram of the six major components (each chromatogram overlaid over the other). Note that the polystyrene (PS), brominated polycarbonate (BrPC), and non-brominated polycarbonate (PC) peaks are all on top of one another.

The next solvent pair tested was n-hexane and THF. The Hansen parameters for n-hexane, THF, PC, PS, and SAN are shown in Figure D.2a. The overlaid chromatograms of the pure standards using the n-hexane/THF gradient are shown in Figure D.2b. Figure D.2a predicts that the gradient from n-hexane to THF will dissolve PS first, then SAN, and then PC. The combination of n-hexane and THF separates PS and the flame retardants from the polycarbonates effectively. PC splits into two peaks based on MW. The first peak is comprised of low MW PC and the second peak is comprised of relatively high MW PC. SAN is not completely separated from the low MW PC. To recover high-purity PC, some yield must be lost to effectively remove the SAN in this case.

(a)

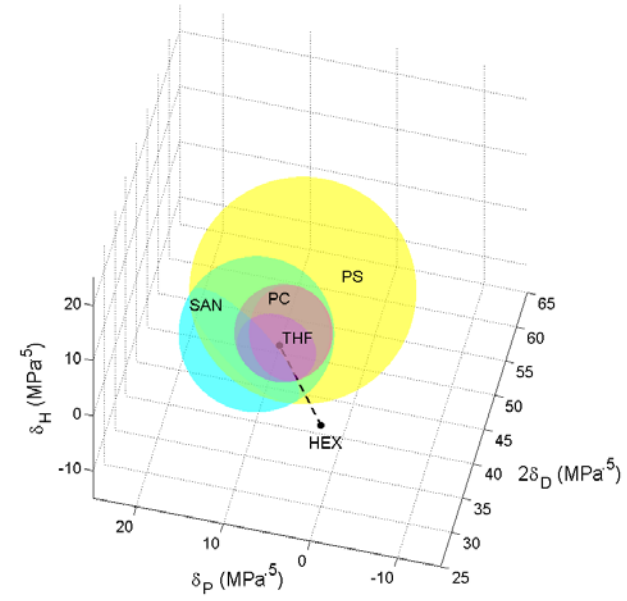

(b)

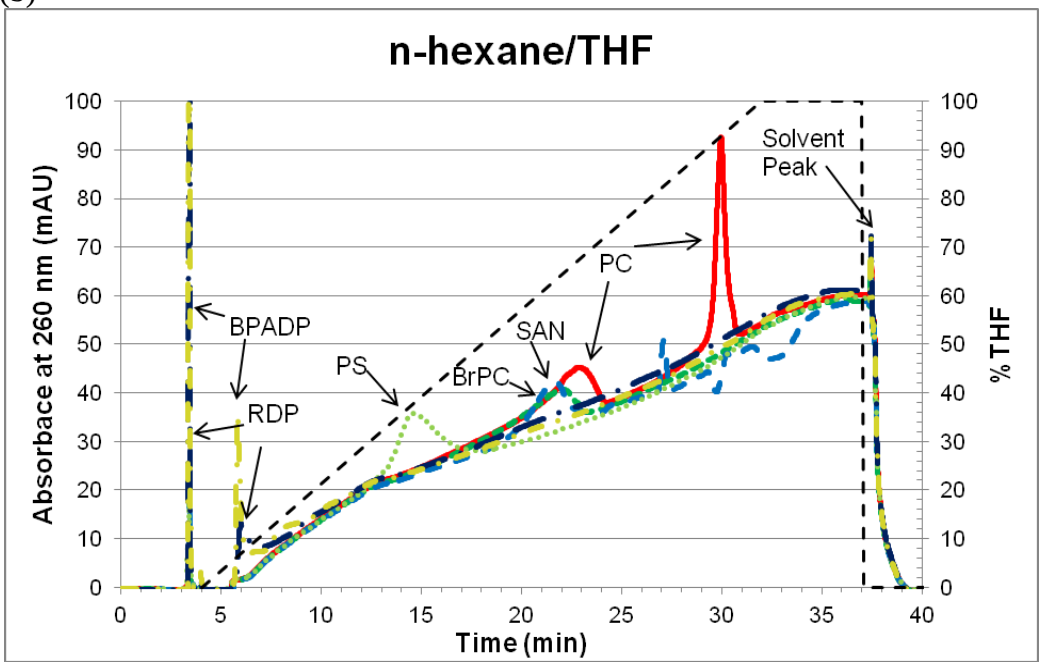

Figure D.2. (a) Hansen solubility parameter space with PC, PS, and SAN solubility spheres plotted with n-hexane and THF gradient as a dashed line. (b) Composite chromatogram of all six components. Note the early exit of PS due to its non-polar nature. SAN, PC, and BrPC all exit at the same time. The gradient is shown by the black dashed line.

The next solvent pair tested was IPA and THF. The Hansen parameters for IPA, THF, PC, PS, and SAN are shown in Figure D.3a. The overlaid chromatograms of the pure standards using the IPA/THF gradient are shown in Figure D.3b. Figure D.3a predicts that the IPA/THF gradient will dissolve SAN first, then PS, then PC. The GPEC results disagree with the predictions of which solvent compositions would dissolve which polymers. This is most likely due to hydrogen bond formation between solvent molecules, which is not accounted for in Hansen's parameters. A solvent mixture of 30% IPA 70% THF can effectively separate the polycarbonates from the other components in Figure D.3. If there are any insoluble impurities, then a second extraction step using 100% THF would dissolve the polycarbonates and the insolubles can then be removed by filtration. There will be some yield loss due to the overlap of the low MW peak with SAN and PS.

(a)

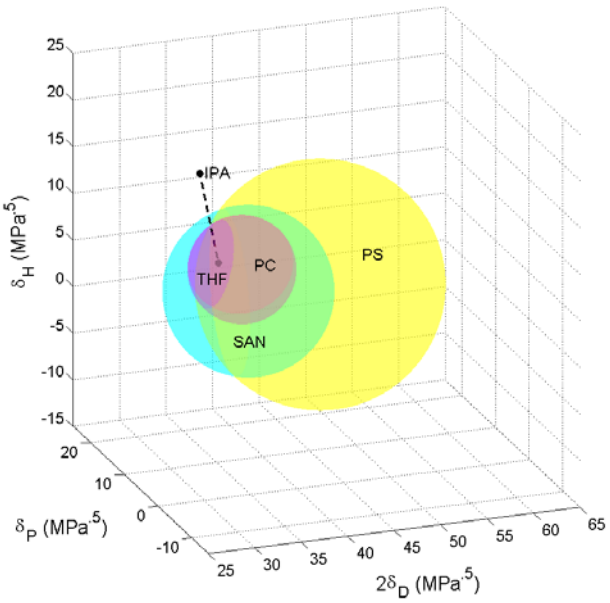

(b)

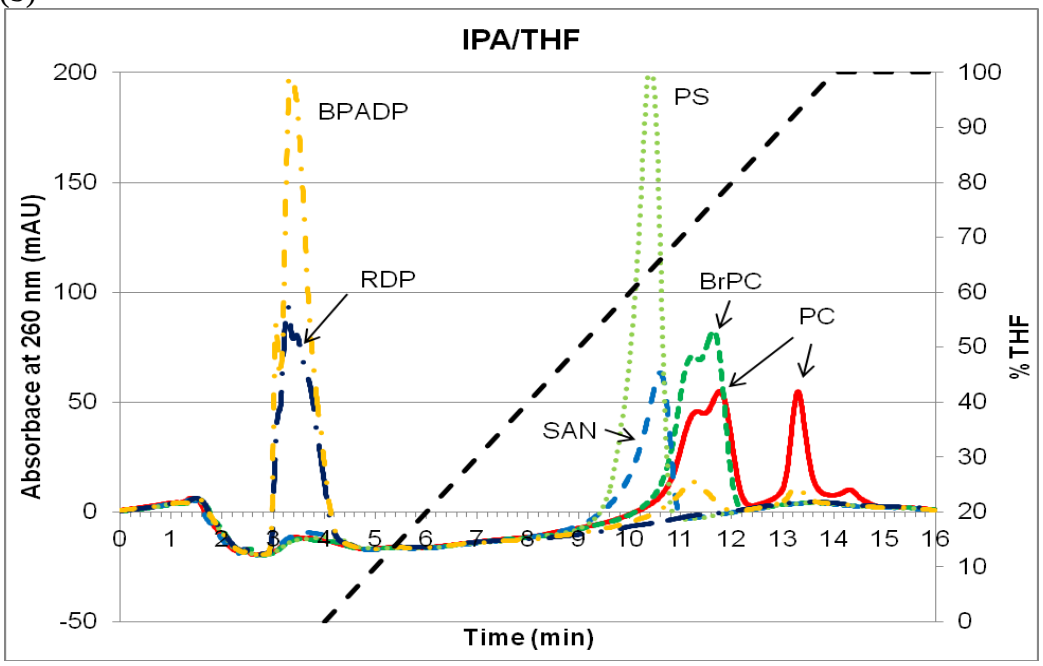

Figure D.3. (a) Hansen solubility parameter space with PC, PS, and SAN solubility spheres plotted with IPA and THF gradient as a dashed line. (b) Composite chromatogram of all six components. There is no separation between RDP and BPADP, PS and SAN co-elute, as do PC and BrPC.

The next solvent pair tested was ACN and THF. The Hansen parameters for ACN, THF, PC, PS, and SAN are shown in Figure D.4a. The overlaid chromatograms of the pure standards using the ACN/THF linear gradient are shown in Figure D.4b. Figure D.4a predicts that SAN will dissolve first, then PC, then PS. These predictions are confirmed by the GPEC results. This solvent pair can effectively separate the polycarbonates from the other components but would require three extractions. The first extraction step would be at 30% THF to remove the flame retardants and SAN. The second extraction step would be at 50% THF to remove the low MW PC and BrPC. The third extraction step would remove PS by using 62% THF, and the remaining solid would be the high MW PC. If there are insolubles, the solid can be dissolved in 100% THF to remove the rest of the PC and the insolubles can be removed. However, THF is a relatively expensive chemical and has multiple safety and environmental concerns so it is not a desirable solvent to use on a plant scale for a product which is about $2.50/kg.

(a)

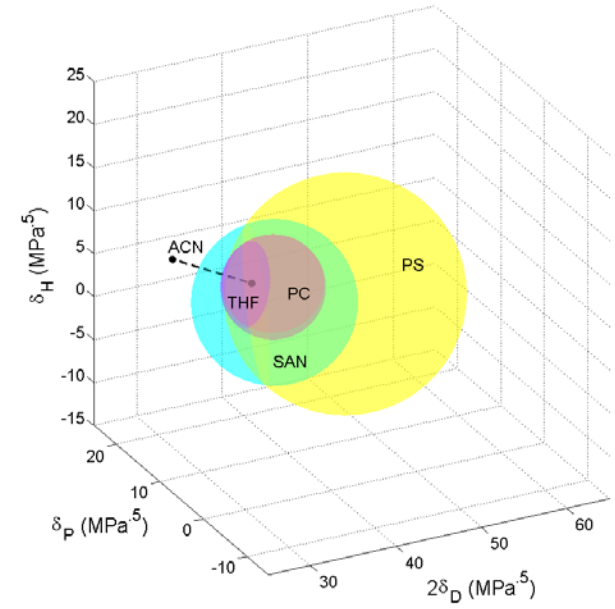

(b)

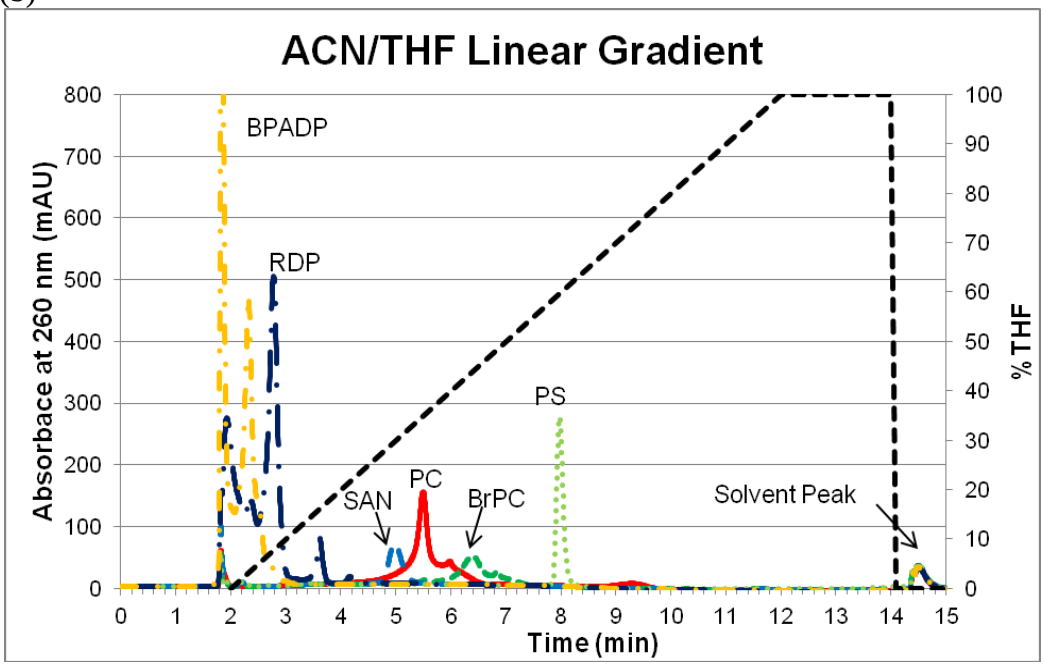

Figure D.4. (a) Hansen solubility parameter space with PC, PS, and SAN solubility spheres plotted with ACN and THF gradient as a dashed line. (b) Composite chromatogram of all six components. Note that the polystyrene peak (PS) is well-resolved. The rest of the peaks may be resolvable by modifying the gradient.

Appendix E Additional PC Analysis and Trommel Crude

E1 – SABIC PC Analysis

The PC in the liquid from the second extraction step of Experiment 5 was precipitated via addition of acetone. The solid PC was filtered from the solution, dried, and weighed. Part of the solid product was sent to SABIC for further analysis. The solid was analyzed using Fourier Transform Infrared Spectroscopy (FTIR) to determine PC purity and Gel Permeation Chromatography (GPC) to determine the MW distribution. The results of the FTIR and GPC are shown in Figure E.1 and Figure E.2, respectively. The sample was >99% PC with no detectable traces of BrPC and the MW distribution of the sample was very similar to the MW distribution of virgin PC with the exception that a small amount of the very low MW PC was lost, most likely in the first extraction step.

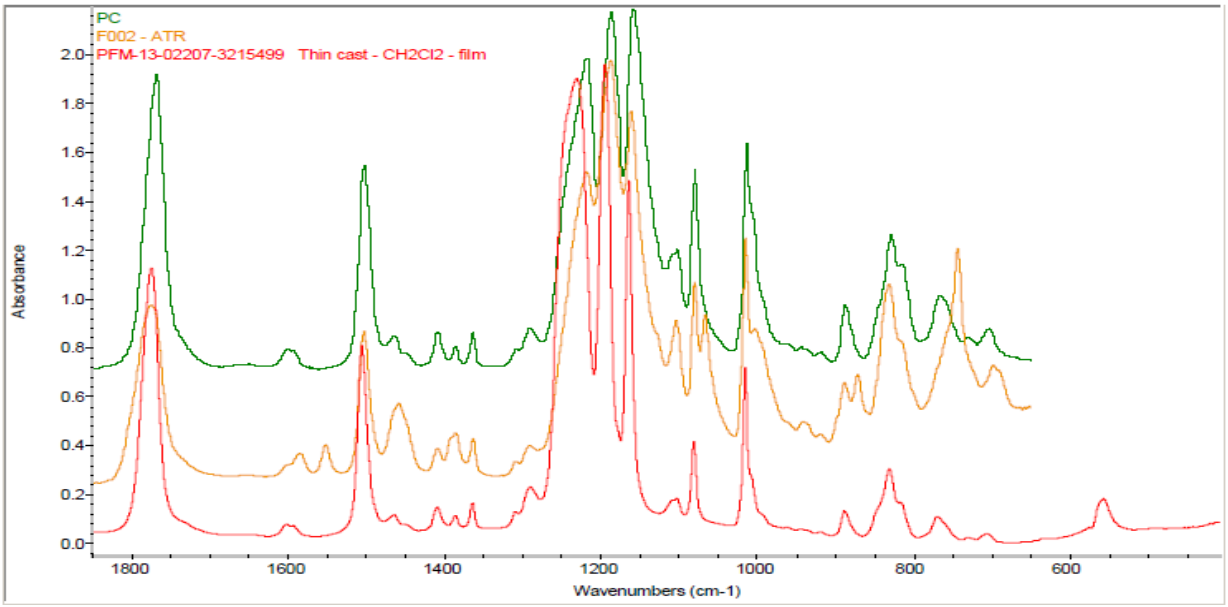

Figure E.1. FTIR analysis of PC product performed by Dr. David Zoller at SABIC-IP. Green curve is a PC reference (PC), yellow curve is a BrPC reference (F002-ATR), and the red curve is the PC product curve. FTIR confirms that the product is PC with BrPC below detection limits.

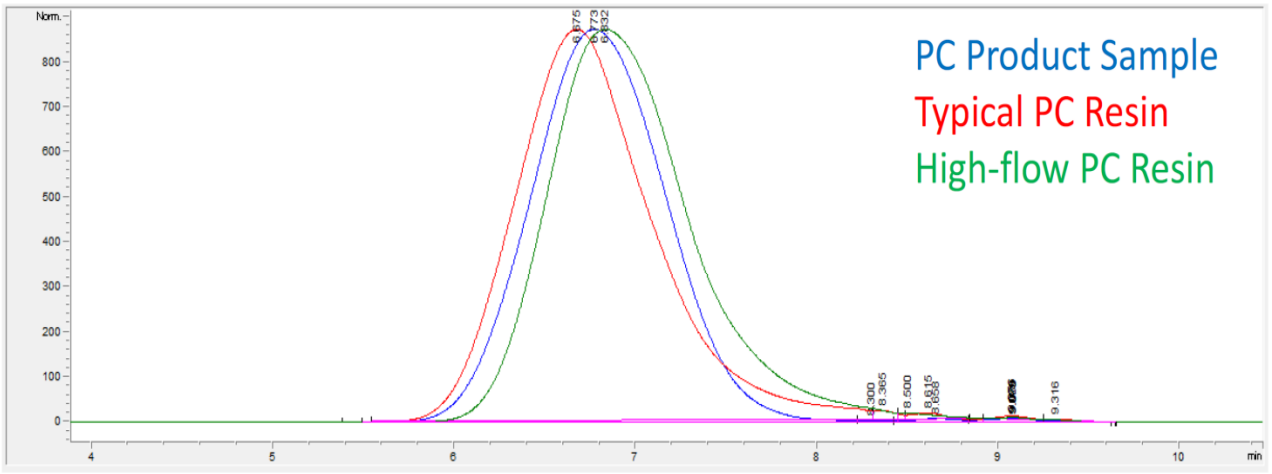

Figure E.2. GPC of PC product sample performed by Dr. David Zoller at SABIC-IP. GPC supports hypothesis that some low MW PC is lost during Extraction 1.

E2 – PC Extraction Summaries

The overall mass balances for the extraction process are shown in Table E.1 and a summary of experiments is presented in Table E.2. The purity, yield, and solvent consumption are listed for multiple experiments. Larger yields were achieved with smaller scales due to easier filtration using filter paper. The larger scale experiments ran into problems with the filter paper clogging and solvent evaporation, which lead to lower yields. The purities have been fairly constant within the limits of the detection method. The second filtration step was replaced with centrifugation to increase the yield to 95% for the larger scale experiment. Solvent consumption will be a major cost at industrial scales, so reducing the amount of solvent used was a priority. Solvent consumption was reduced to about 23 kg solvent /kg PC with no appreciable loss in purity or yield.

Table E.1. Overall mass balances for the PC extraction process from crude waste.

Stream	Phase	Amount of Polymers Relative to Feed (g)	Solvent (ACE/ DCM) (vol.%)	Composition (Mass Fraction of Polymers)				
				PC	BrPC	SAN	RDP, BPADP	ABS + others
Crude	Solid	1.00	-	0.57	0.02	0.10	0.06	0.25
E1	Liquid	0.17	50/50	0.05	0	0.60	0.35	0
F1	Solid	0.83	-	-	-	-	-	-
E2	Liquid	0.58	0/100	0.98	0.02	0	0	0
F2	Solid	0.25	-	0	0	0	0	1

The Trommel crude contains more impurities, including some unknown polymers and dyes. The HPLC chromatogram of the Trommel crude dissolved in DCM is shown in Figure E.3 while the composition of the solid crude is shown in Table E.3. The Trommel crude is only about 19% PC with 41% PS and 29% SAN. It was subjected to the same procedure as the crude from computer housings, but resulted in a lower purity and a lower yield. Filtration and centrifugation were extremely difficult for the first extraction step in 50/50 (vol.%) ACE/DCM because of gel formation. The gel would prevent fluid from passing through the filter paper and it was denser than the mixed-solvent, so it could not be separated from the solids with centrifugation. This gel layer appears to be caused by aggregation of PS, which was not present in the crude from computer housings, with SAN. PS was expected to completely dissolve since the concentration of PS was below the wt.% used for the visual dissolution tests.

Table E.2. Purity, yield, and solvent consumption over multiple experiments.

Exp.	Feed Mass (g)	Polymer Conc. (wt.%)[c]		Final PC Product Purity[d] (%)	Overall PC Yield (%)	Overall Solvent Consumption (g solvent/ g PC)[e]	Comments
		Step 1	Step 2				
1	0.28	6.6	6.2	98.7	98.0	>100	Solvent use too high
2	0.74	17.2	10.9	98.7	92.5	>100	Some product loss due to filtration Solvent use too high
3	30.0	9.7	10.0	98.6	71.0	64.3	First filtration had large yield loss Solvent use too high
4	15.2	25.4	15.1	96.9	64.1	30.1	First filtration improved, second filtration had large yield loss
5	15.1	24.8	10.1	97.5	95.6	22.7[f]	Replaced second filtration with centrifugation. PC precipitated by ACE addition. Product filtered from solution.
6[h]	31.4	10.8	3.6	95.0[g]	93.1	69.3	First extraction step uses pure DCM PC precipitated by ACE addition to reach 50/50 ACE/DCM (vol.%)

[c] Polymer concentration of the solution (i.e. mass of polymers divided by the sum of the mass of polymers and the mass of solvent)
[d] Only impurity is BrPC – determined by HPLC
[e] Includes solvent used for washing solid between extraction steps and after precipitation
[f] Amount of solvent used to precipitate PC added 7.1 g/g PC to the total solvent used
[g] Balance is about 4% BrPC and 1% PS
[h] Trommel crude

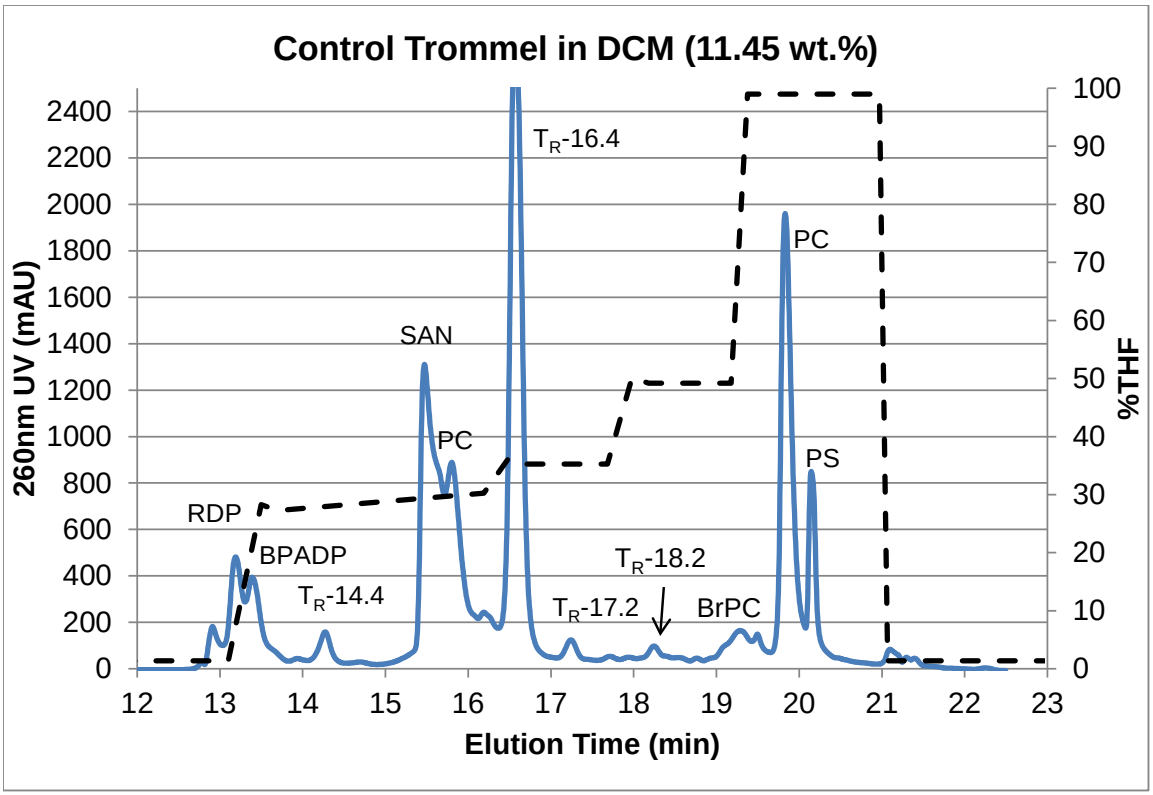

Figure E.3. HPLC chromatogram of 11.45 wt% (if all solid dissolved) Trommel dissolved in DCM.

To alleviate these handling issues, the Trommel crude was first dissolved in DCM. The small amount (< 3%) of ABS and other insolubles was removed by centrifugation. The solvent composition of the liquid was then changed by adding ACE to reach a 50/50 (vol.%) ACE/DCM mixture. PC precipitates in the new solvent composition leaving the rest of the polymers and impurities in solution. The HPLC chromatogram of the liquid after this precipitation step is shown in Figure E.4. All the impurities are present in the solution and only some low MW PC did not precipitate.

Table E.3. Polymer composition of Trommel crude determined by ACN/THF HPLC analysis of Trommel crude dissolved in DCM.

Component	Retention Time (min)	Wt.% in Solid[n]
RDP	13.2	3.3
BPADP	13.4	3.8
T_R-14.4	14.4	-
SAN	15.5	29.3
PC (Low MW)	15.8	6.4
T_R-16.4	16.6	-
T_R-17.2	17.2	-
T_R-18.2	18.2	-
BrPC	19.2	1.0
PC (High MW)	19.8	12.8
PS	20.1	40.8
ABS + Other Insolubles	-	2.6

[n]Assuming the unknown impurities have negligible contribution to the mass of the solid

The PC product is recovered by filtration and then washed with 50/50 (vol.%) ACE/DCM to remove interparticle fluid. The PC product was then dissolved in DCM and analyzed by HPLC. The chromatogram of the PC product is shown in Figure E.5. The product was 99% PC and BrPC, with about 93% yield. The low MW PC that remained in the 50/50 (vol.%) ACE/DCM mixture is responsible for the yield loss. The mass balance for the Trommel is shown in Table E.4. It may be possible to increase PC yield by increasing the ACE vol.% of the mixed solvent during precipitation to lower the solubility of the low MW PC. PS must still have sufficient solubility in the new mixture to avoid co-precipitation with PC.

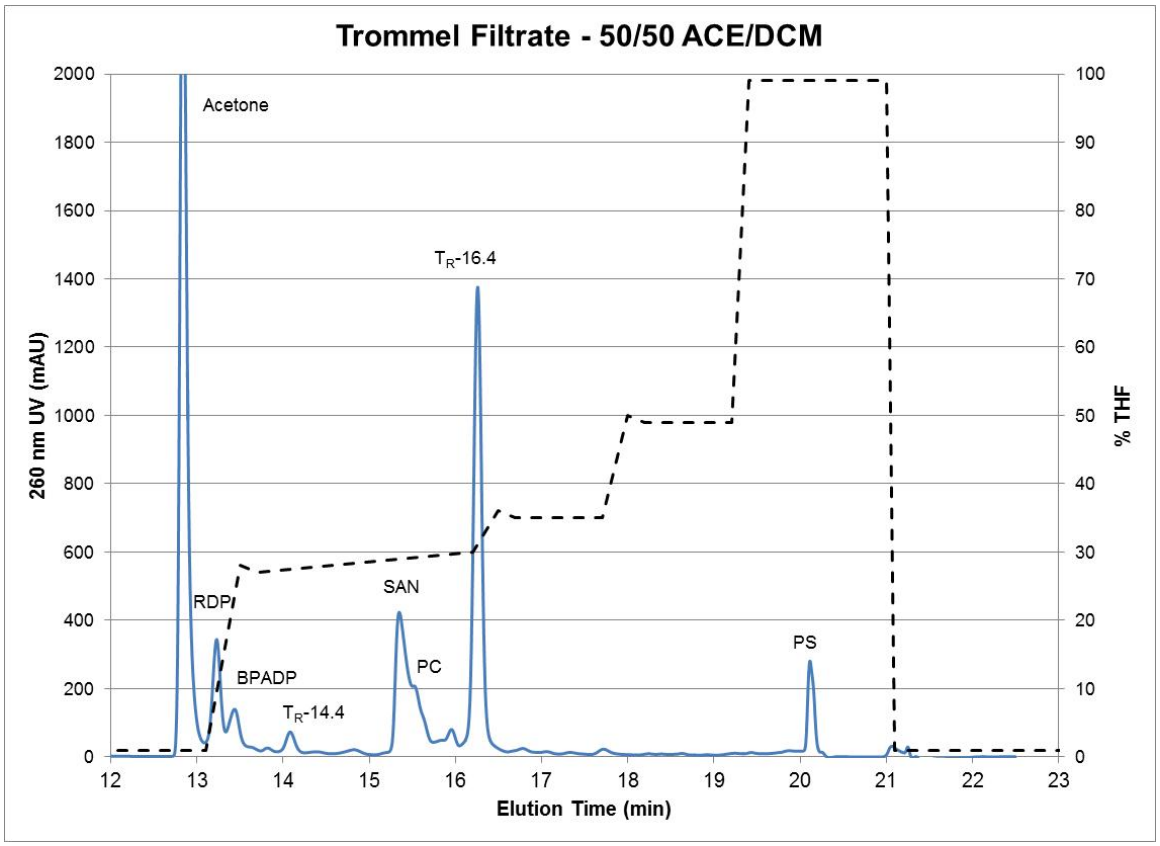

Figure E.4. HPLC chromatogram of filtrate from PC precipitation step to recover PC from the Trommel crude (3.6 wt.% if all polymers were still dissolved).

The feed cost of the Trommel crude would be about three times higher than the crude from computer housings because the PC content of the Trommel crude is about three times less than the PC content of the crude from computer housings. The solvent use and energy consumption per kg PC product would also be much higher than for the crude from computer housings for the same reason, which is why the total cost for PC recovery from Trommel crude is about $4.23 per kg PC.

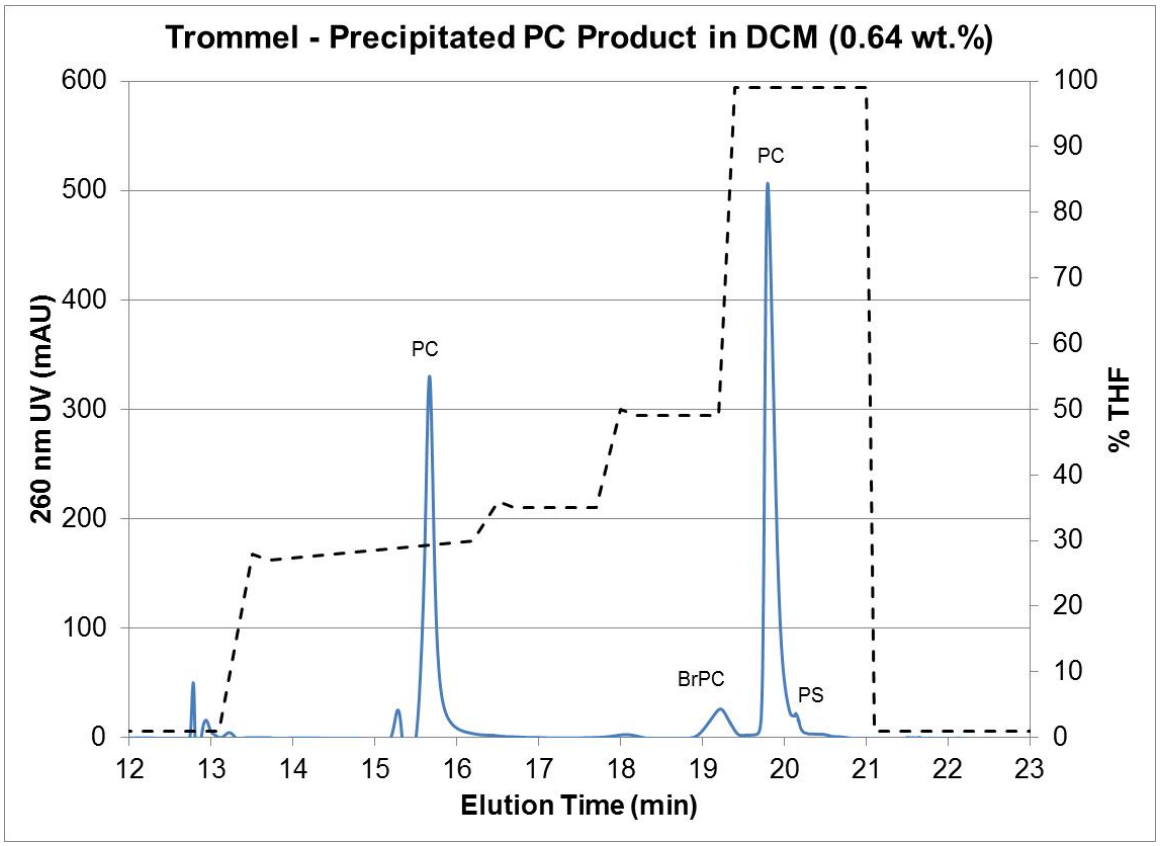

Figure E.5. HPLC chromatogram of precipitated PC product from Trommel crude (0.64 wt.% in DCM).

Table E.4. Overall mass balances for the PC extraction process from Trommel crude.

Stream	Phase	Amount of Polymers Relative to Feed (g)	Solvent (ACE/ DCM) (vol.%)	Composition (Mass Fraction of Polymers)					
				PC	BrPC	SAN	RDP, BPADP	PS	ABS + others
Trommel	Solid	1.00	-	0.19	0.01	0.29	0.07	0.41	0.03
E1	Liquid	0.97	0/100	0.20	0.01	0.30	0.07	0.42	0
F1	Solid	0.03	-	0	0	0	0	0	1
E2	Liquid	0.78	50/50	0.01	0	0.37	0.09	0.53	0
F2	Solid	0.19	-	0.95	0.04	0	0	0.01	0

The SEPoR process has been shown to effectively recover PC with high purity from wastes with varying PC contents (19-57 wt.%). Assuming the equipment cost, feed cost, and total mass of solvent used in the process are independent of PC content, the PC content at which the estimated cost of the SEPoR process is equal to the purchase price of PC ($2.5 per kg) is about 32 wt.%. If the feed cost ($0.36 per kg crude) were reduced, then using the SEPoR process on even lower PC content wastes could be economically feasible

VITA

VITA

George S. Weeden Jr. was born on September 14, 1988 in Joliet, Illinois to George and JoEllen Weeden. He has one younger sister, Emily. He grew up in a small town called Manhattan and then moved to a slightly bigger town (Lowell, Indiana). He graduated from Lowell High School in 2007, the year of the James Bond themed proms, and entered Purdue University in the Fall of the same year. He graduated from Purdue with a Bachelor of Science degree in chemical engineering on Friday May 13, 2011. He immediately entered Purdue again for his graduate studies in chemical engineering. He is interested in the design and optimization of separations processes, especially at large scales. He received a Doctor of Philosophy from Purdue University on another Friday the 13th, this time in May of 2016.